Development and Application of Whole Cell and Intact Outer-Membrane Environments for Double Electron-Electron Resonance on Membrane Proteins

Arthur Kaz Sikora
New York, New York

B.S., University of Washington, 2011

A Thesis presented to the Graduate Faculty
of the University of Virginia in Candidacy for the Degree of
Doctor of Philosophy

Department of Chemistry

University of Virginia
August 2016

_____

_____

_____

_____

Abstract

In order to fully understand the function of a protein its native environment must be taken into account. Native membranes contain many unique features inaccessible in reconstituted systems that may greatly influence membrane protein function. Despite its importance, an unrealized goal in structural biology is the determination of structure and conformational change at high resolution for membrane proteins within the cellular environment.

BtuB, the *Escherichia coli* outer membrane TonB-dependent cyanocobalamin transporter has been widely studied but its transport mechanism is not fully understood. TonB dependent transporters are essential for the success of many pathogenic bacteria, making these interesting targets for new antibiotics. These proteins are a family of outer membrane β-barrels that Gram-negative bacteria use to transport essential nutrients such as vitamin B12 or iron. Although high-resolution crystal structures have been obtained for many of these proteins, the mechanism of substrate transport is still unclear. The outer membrane environment is low in free reactive cysteines and thus provides low background signal for Double Electron-Electron Resonance (DEER) measurements

DEER is a well-established technique to follow conformational changes in purified membrane protein complexes. This work details the development of DEER in whole living cells and intact outer membranes. Our approach avoids detergent extraction, purification and reconstitution usually required for these systems. With this approach structure, function, conformational changes and molecular interactions of outer membrane proteins can be studied at high resolution in the cellular environment. We then observe and

characterize conformational changes in the second extracellular loop of BtuB upon ligand binding and compare the DEER data with high-resolution crystal structures. These comparisons reveal that ligand binding in whole cells is reflective of previous studies done in reconstituted systems.

Finally using the native-system DEER technique we show that signaling also occurs from the periplasmic to the extracellular surface in BtuB. The binding of a TonB fragment to the periplasmic interface alters the second extracellular loop to create a more open loop configuration, and it diminishes the affinity of BtuB for substrate. This work demonstrates that the Ton box and the extracellular substrate binding site are allosterically coupled in BtuB, a feature that appears to be critical to the TonB-dependent transport mechanism.

TABLE OF CONTENTS

List of Figures

List of Tables

Abbreviations

A	normalized amplitude
AEBSF	4-(2-Aminoethyl) benzenesulfonyl fluoride hydrochloride
ATP	adenosine triphosphate
B_{12}	vitamin B12 same as cyanocobalamin
Ca^{2+}	calcium ions
CD	circular dichroism
CDT	1,1′-carbonyl-di-(1,2,4-triazole)
CE	cell envelope
CM	cytoplasmic membrane
CNCbl	cyanocobalamin same as vitamin B12
CW	continuous wave
DEER	double electron electron resonance
DFT	density functional theory
DLPC	1,2-diauroyl-*sn*-glycero-3-phosphocholine
DMSO	dimethyl sulfoxide
DNA	deoxyribonucleic acid
DSB	disulfide bond formation
E. Coli	*escherichia coli*
EDTA	ethylenediaminetetraaetic acid
EM	electron microscopy
EPR	electron paramagnetic resonance
FRET	fluorescence resonance energy transfer

GHz	gigahertz
HPLC	high performance liquid chromatography
KDa	Kilo Dalton
LC-MS	liquid chromatography – mass spectrometry
LEM	linear extrapolation model
LPS	lipopolysaccharide
MALDI-ToF	matrix-assisted laser desorption/ionization time of flight
MD	molecular dynamics
mG	milli Gauss
mT	milli Tesla
MOMD	microscopic order macroscopic disorder model
MTSL	S-(1-oxyl-2,2,5,5-tetramethyl-2,5-dihydro-1H-pyrrol-3-yl)methyl methanesulfonothioate
NMR	nuclear magnetic resonance spectroscopy
OG	*n*-octyl-β-D-glucopyranoside
OM	outer membrane
PDB	protein data bank
PL	phospholipids
PMF	proton motive force
POPC	1-Palmitoyl-2-oleoylphosphatidylcholine
RMSD	root mean squared deviation
RNA	ribonucleic acid
RP	reverse phase

RT	room temperature
SDSL-EPR	site-directed spin labeling electron paramagnetic resonance
S/N	signal to noise
ssNMR	solid state nuclear magnetic resonance spectroscopy
TBDTs	tonB-dependent transporters
τ_c	correlation time
TEMPO	(2,2,6,6-Tetramethylpiperidin-1-yl)oxyl spin label
Tm	phase memory time
TPOA	2,2,5,5-tetramethyl-pyrroline-1-oxyl-3-carboxylic acid amide spin label
UFF	universal force field
W	watt
WT	wild-type

Acknowledgments

The best way to describe my journey as a graduate student is unexpected. I have always loved science but never thought I would be a chemist. I have always had aspirations of teaching but am shocked by the instructional and pedagogical experiences I have experienced during graduate school. As I reflect on my time I am very happy to have chosen this path and can't wait to see what my future will bring.

I want to first thank my research mentor, Dr. David Cafiso. He always had time to listen and never ran out of interesting directions to take my project next. I am very thankful to the members of the Cafiso lab, both past and present. This lab has always been supportive of me, coming to my practice talks and editing my posters and abstracts and never shying away from discussions of EPR theory or instrument procedure. I also credit my sanity and happiness to my friends in other labs, sometimes a wine tasting or lunch break where science talk is forbidden turns out to be the best medicine.

I want to especially thank my longtime girlfriend and recent fiancé Sara Blankenship. She is an invaluable source of knowledge and inspiration both in the lab and at home. I know I have been really lucky to have someone at home who can not only understand what I do every day but help me solve problems and achieve my goals.

I am very grateful for the collaborations I have been lucky enough to participate in. I know this work would be very different if I had not started working with Dr. Benesh Joseph on whole cell DEER. His ideas and directions have proved invaluable towards the

design and success of many experiments. I also appreciate the wisdom and expertise of Dr. Robert Nakamoto who was always passionate about my protein and had great ideas and experiments from the physiological side of BtuB research.

Outside the lab I own my success to many wonderful people both at UVa and outside it. My family has been wonderful through this journey, always being there to hear about life in Virginia and making me feel welcome at home anytime I can get away.

I want to also acknowledge Dr. Kenneth Elzinga for helping mentor me towards professorship. His advice and guidance was crucial to filling the gaps that have made me successful thus far. I am grateful that I will be able to seek his wisdom for many years to come. Last but not least I want to acknowledge the center for teaching excellence at UVa and Dr. Michael Palmer and Dorothe Bach for providing me with many amazing teaching opportunities and for editing and discussion teaching materials with them.

I know that my journey forward will be full of new unexpected twist and amazing surprises and I can wait to get started.

Chapter 1: Introduction

1.1 Significance

Proteins are arguably the most important class of macromolecules; they perform a range of diverse functions and are responsible for all the reactions that make life possible. Due to their importance, proteins have been widely studied, and many protein-related breakthroughs have won Nobel prizes. One major subfield of proteomics that has been poorly represented in literature is membrane proteins. One third of cellular proteins are thought to represent membrane proteins.[1] Membrane proteins are thought to be the target of over 60% of all pharmaceutical drugs.[2] However, only 1.5% of the structures deposited into the protein data bank represent membrane proteins. Since the first membrane protein sturcture was deposited in 1985, 518 unique membrane protein sturctures have been deposited. This growth, while promising, has been much slower than predicited as recently as 2005.[3]

One hurdle to better understanding of the structure and mechanisms of action of membrane proteins is the complex membrane itself. This poorly understood environment is very dynamic and heterogeneous, showing domains and charged regions similar to those found in the most complex proteins.[4] The function of membrane proteins has been proven to be greatly affected by lipid composition and membrane curvature.[5,6]

In order to properly study membrane proteins, both the protein and lipid have to be taken into account. Finding techniques that are able to accurately examine the protein in detail without being severely impacted by the membrane has been a very large challenge. The

two most commonly used techniques for the structural characterization of soluble proteins, X-ray crystallography and Nuclear Magnetic Resonance Spectroscopy (NMR), have been known to struggle with reconstituted proteins. X-ray crystallography has long been the most utilized method of obtaining protein structures, but these structures suffer from X-ray damage and limited solvent choice. Furthermore, limited conformers and tricky ligand refinement procedures limit the completeness of this technique.[7,8] NMR has filled in some of the gaps left by X-ray crystallography but struggles with large membrane proteins due to overlapping peaks requiring complex peak assignment procedures and reduced data quality due to rapid sample relaxation.[9]

1.2 Cell Membranes and membrane proteins

The membrane is the medium or solution in which membrane proteins exist. The little work that has been done to understand lipid-protein interactions has been largely driven by crystal structures. Furthermore, it is known that soluble proteins are greatly affected by the solvent and understanding solvent-protein effects has been the topic of many studies.[10,11] It is no surprise then that the composition and curvature of the membrane environment has long been implicated as very important to proper protein function.[12] The lipid environment can affect proteins in two different ways. The first would involve lipid based modulation of the character of the membrane as a whole; this tuning might produce the right membrane physical parameters for membrane protein function. The second way lipids might modify proteins is through a direct lipid-protein contact or binding. Both interactions are likely play a critical role in proper protein dynamics and 3D fold. The cellular membrane is very

complex and heterogeneous, whether it's a cytoplasmic membrane of a eukaryotic cell, the inner or outer membranes of *E. Coli*.

Gram negative bacteria have two membranes, the cytoplasmic membrane (CM) and the outermembrane (OM) (Figure 1.1). These two membranes are separated by a 15-20 nm aqueous space called the periplasm. The periplasm contains peptidoglycan as well as a diverse complement of proteins that protect the cell from lysis and increase cell rigidity.[13] The OM also provides the bacterium with resistance to many components of the host immune system, such as lysozyme and leukocyte proteins, as well as digestive enzymes and bile salts.[14] The outer leaflet of the OM is dominated by lipopolysaccharide. These lipids possess a long string of sugars that form a very effective barrier to small hydrophobic molecules.[15,16] The OM is the main reason that these families of bacteria are able to colonize harsh environments; the antibiotic resistant nature of this barrier further enhances the efficacy of these pathogens.

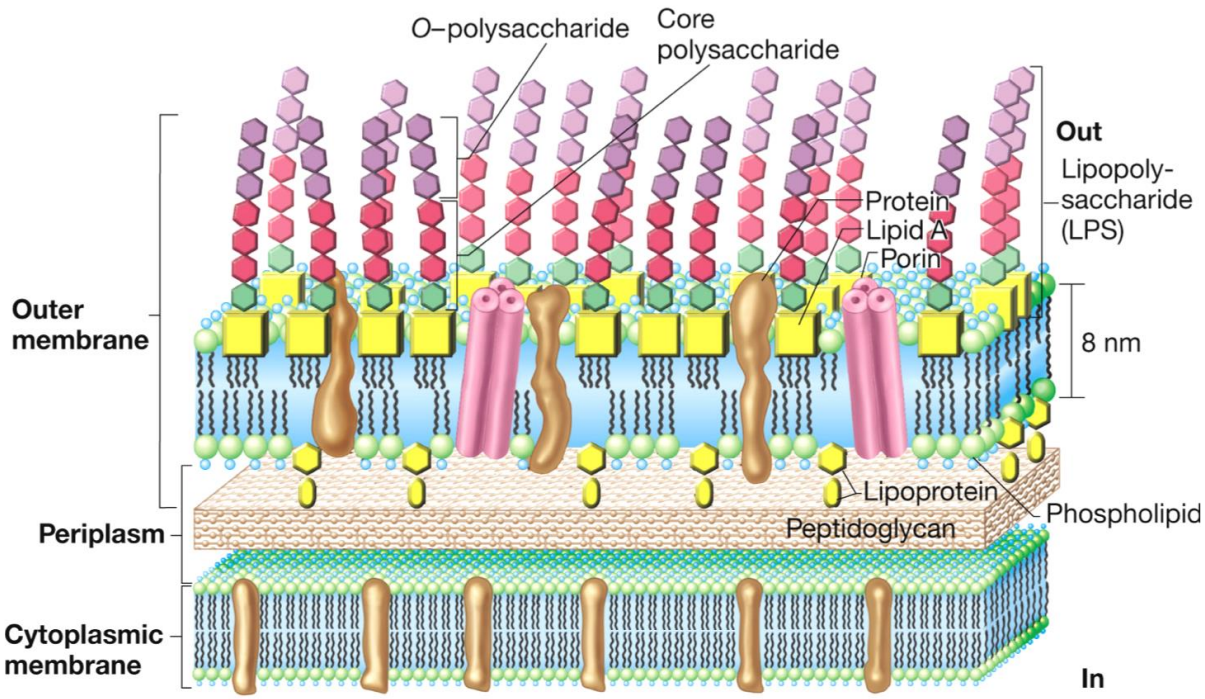

Figure 1.1: The membranes of a gram negative bacterial cell. Here the outer membrane is shown in great detail populated with membrane proteins and large amounts of lipopolysaccharide (LPS). Figure taken from Poinsot *el al* (2012).[16]

Cell membranes are comprised of lipids that vary in chain length, charge and head group hydrophobicity. Cells contain hundreds of different lipid species that are usually grouped by head group and chain differences. In phospholipids, the polar head group at the sn-3 position of the glycerol defines the type of lipid. Some examples include phosphatidylcholine, inositol, serine, ethanolamine or simply unmodified, phosphatidic acid.[17,18] Beyond the approximately 1000 lipid species that have been discovered in cell membranes, computer models have shown that tens of thousands of combinations are possible.[19] This lipid diversity and large size make these membrane systems very difficult to study using most techniques. Biological membranes are complex, they function much the same as two dimensional fluids would. These amphipathic barriers host a high density of proteins and carbohydrates and are very heterogeneous on various time and length scales.[20] Many studies have been performed to show how specific and important protein

lipid interactions are. Based on lipid mobility measurements lipids were foundto exchange from the protein surface to the bulk lipid in fluid bilayers at a rate of 10^7 s^{-1}, indicating these proteins exhibit transient interactions with many lipids. Interactions on longer timescales have also been observed.[21] The transmembrane flux of a fluorescent dye in lipid vesicles has been shown to increase when concentrations of phosphatidylglycerol, phosphatidic acid or cardiolipin increase due to a direct hydrogen bond formation and not curvature changes.[22,23] The anionic lipid phosphatidic acid has been shown to form stable micro domains around the nicotinic acetylcholine receptor.[24-26]

The outer membrane specific lipid LPS (Figure 1.2) are described as heat resistant, endotoxic components of Gram-negative bacterial cell walls that consist of conserved and highly variable regions.[27,28] Modifications to LPS such as O-glycosylation have been shown to modulate the activity of a major auto lysin in species of lactic acid bacteria.[29] Immunological studies of *H. pylori* show that LPS lipid A molecules mimic host cell antigens and thus keep the pathogen invisible to immune cells.[30] There are also many proteins that are soluble but possess known lipid binding or associating domains. Lipid anchored proteins found in the cytosol have lipid attachment moieties and can sometimes partition into bilayers.[31-33] These studies leave the question of how these interactions take place at the lipid-protein interface. Is it simply a non-specific van der Waals interaction or one of that involves specific charges? Questions like this mirror ones that are seen in soluble proteins, where solvent choice and solute concentration has been shown to be quintessential.[34]

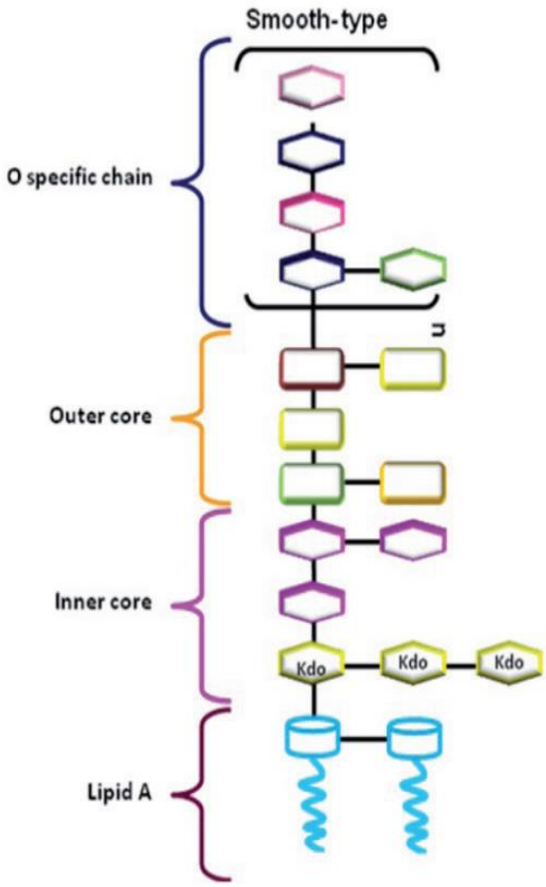

Figure 1.2: Lipopolysaccharide molecule. LPS is a lipid molecule specific to the outer membrane of Gram negative bacteria and undoubtedly plays a big role in function of the proteins that reside there. Figure taken from Reyes *et al* (2012).[29]

Currently we are only beginning to understand membrane protein function, and understanding that function in the context of the lipid environment is a key aspect of our current studies. Crystal structures of membrane proteins have been achieved but of the over 75,000 crystal structures only 1635 are of membrane proteins.[3] This is particularly troublesome as an estimated 20-30% of all genes in genomes code for transmembrane proteins.[33] These membrane protein crystals are almost all in detergent; while most detergents are mild and allow for some protein function, not much is known about the perturbation this non-native solvent produces. Crystallography can only provide limited information on dynamics or structural fluctuations and thus often provides just a starting

point for deeper studies into protein function. NMR has been used to study lipids and proteins but due to the large size of the membrane protein complex it is frequently poorly suited to study them together. The rare studies that have been done still require a detergent based environment which may obscure contributions from membrane-protein interactions.[36,37]

In silico studies have made substantial progress toward better understanding of lipids and membranes as well as protein movements within these environments.[38] This powerful technique has been applied to outer membranes and β barrels, and in many ways, these simulations have guided direct experimental work.[37] Computer based modeling does suffer from short simulation times and force field design problems. Other techniques attempting to shed light of this problem include time-resolved fluorescence microscopy[40-42] and 2D Infared spectroscopy.[43-45]

EPR is uniquely positioned to study these systems because the timescales of protein backbone motion and sidechain rotation are well within the EPR timescale. In fact, EPR is able to access time scales that represent the vast majority of lipid-protein interactions.[46] Currently, a major hurdle in EPR is the transition from detergents and lipids into native membranes and whole cells. This problem is mainly due to the large amount of free cysteines on proteins that can be labeled in heterogeneous systems.

Recent advances have resulted in the development of in lipid mimetic environments such as bicells, nanodiscs and lipid cubic phases.[47-49] In spite of this, the gold standard remains the intact membrane and whole cell. There is no substitute of the kind of lipid diversity and protein density seen in these in-vivo systems.

1.3 TonB dependent transporters (TBDTs)

Iron is an essential metal that is at the core of many metabolic processes, and bacteria all use a similar active transport system for the uptake of iron.[50] This method of iron uptake involves a family of outer membranes proteins that couple to and require the inner membrane protein TonB. They are, therefore, termed TonB-dependent transporters (TBDTs). The expression levels of many proteins involved in iron uptake are regulated by the external iron concentration.[51] Other TBDTs such as the receptor for cyanocobalamin (CN-Cbl), BtuB, also appear to be regulated by the concentration of substrate.[52] Based on sequence homology, over 98 TBDT proteins have been found across multiple gram negative bacterial species. The 45 crystal structures of this family that exist represent 12 structurally similar proteins.[53] Most of these proteins transport iron chelating molecules but cobalt and nickel chelators, carbohydrates and copper complexes are also among the known substrates for this diverse class of outer membrane proteins.[54]

The TBDT family is comprised of selective outer membrane pores that transport large, scarce, and important molecules that are very tightly controlled by host organisms. [55-57] In the cytoplasmic membrane active transporters employ ion gradients or adenosine triphosphate (ATP) hydrolysis. The OM does not have an energy source, so in order to achieve selective uni-directional transport, the electrochemical potential of protons or proton motive force (PMF) from the inner membrane is transduced by the periplasm spanning inner membrane bound protein TonB. This protein also interacts with the inner membrane proteins ExbB and ExbD (Figure 1.3). These two proteins are essential for

transport and are thought to harvest the PMF from the CM and use it to drive the energy dependent TonB cycling steps.

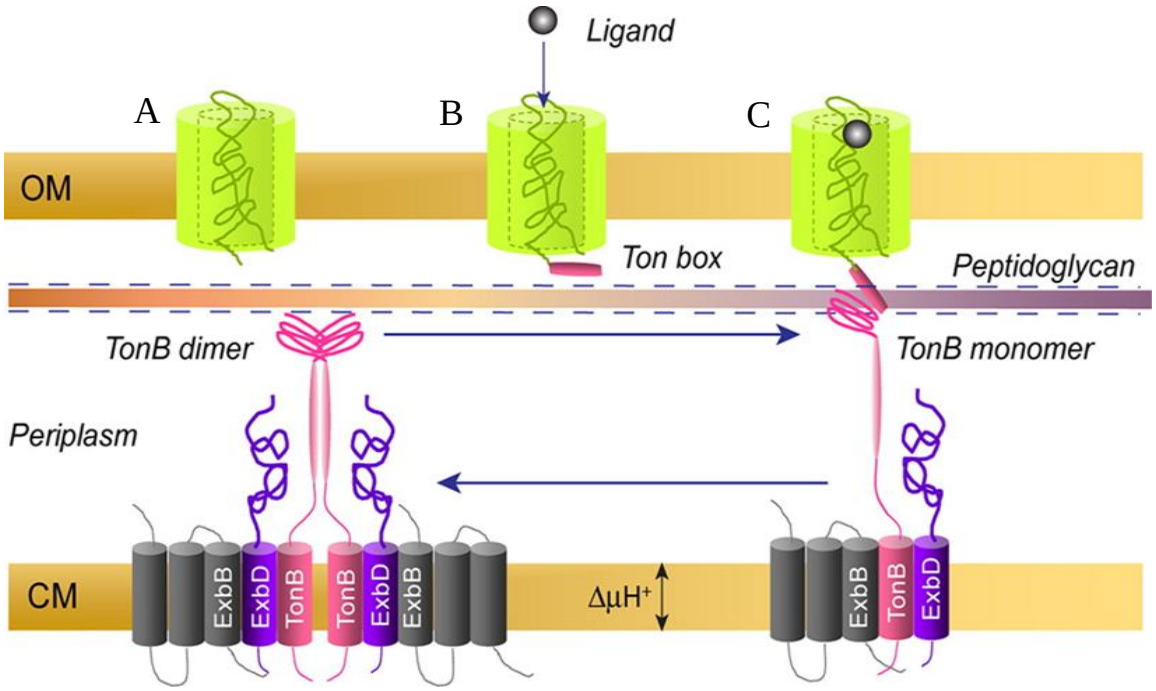

Figure 1.3 TonB Dependent Transport system and proposed transport cycle. Figure adapted from Freed *et al.* (2013).[58]A) TonB is driven into a dimeric state by the proton motive force transduced through the inner membrane proteins ExbB and ExbD. B) This kinetically trapped state associates with the peptidoglycan layer.[59] When substrate binds and the Ton Box is presented C) TonB binds to the green beta barrel as a monomer and is then able to provide energy for transport of the ligand.

All TDBT proteins are comprised of three domains; the 22-stranded β-barrel, a hatch or plug domain, and the TonB interacting domain or Ton Box. Each transporter in this family has outer loops of varying lengths. These loops may be used to help bind and draw substrates to the transporter interface. They then may close over the barrel during transport allowing for unidirectional transport. The hatch domain is 130-150 resides in length comprised of both α-sheets and β-sheets. The motions of this plug have long been a source

of study. In order for the large metal complexes like cyanocobalamin to pass through the barrel, the plug domain has to create a pore or dissociate from the barrel. An analysis of water molecules at the interface of the barrel and plug has revealed a highly solvated plug. This has been shown to be true for BtuB, FhuA, FecA and FepA.[57] The mechanism of this pore formation is not fully known but has been hypothesized to either include a transient rearrangement or partial unfolding. The Ton box is a highly conserved N-terminal sequence found in this family of transporters. The consensus sequence of the ton box is D/ETXXVXA, where X is a small hydrophobic residue.[56] Studies of many members of the TBDT family directly show that TonB does in fact bind to the Ton box.[60-62]

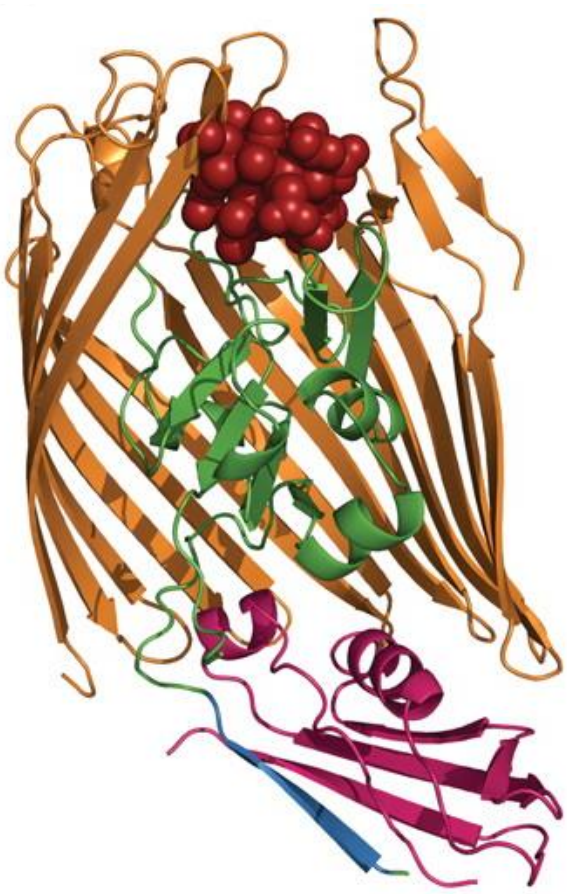

Figure 1.4 Crystal structure of BtuB co-crystalized with the C-terminal portion of TonB. The protein is oriented like it would be in the outer membrane with the bound vitamin B_{12} (cyanocobalamin) shown as red spheres. The β-barrel of BtuB (residues 138-594) is shown in orange, the hatch or plug domain is in green (residues 14-137) and the Ton box in blue (6-13). The first 5 residues did not crystallize due to fast motions of this segment. The TonB C-terminal domain (residues 153 to 233) is shown in magenta. Figure taken from Shultis *et al*. (2006).[61]

TonB is a 239-residue periplasm spanning protein that is anchored in the inner membrane and is comprised of three domains. The first 32 resides comprise a cytoplasmic helical transmembrane anchor. This segment is likely responsible for TonB responses to PMF via the essential residues Ser16 and His20, probably through its interactions with ExbB and ExbD. The interactions with ExbB and ExbD are likely not controlled by ionization changes in H20 of TonB, because the His20N mutant is still viable.[63] This 33 residue

segment can be modeled as an α-helix. The next domain is responsible for TonB rigidity and allows for easy transit through the periplasm. It consists of a 36 residue proline rich linker comprising of $(EP)_6$ and $(KP)_6$ repeats, followed by another extended region spanning residues 103-149. EPR and circular dichroism (CD) studies have shown this whole domain exists in an extended polyproline H helix.[64] Polyproline helices are used by many proteins and are the ideal structure to provide a rigid structure to TonB so that it might transit the periplasm.[65] Residues 150-239 make up the C-terminal domain that is responsible for association with the β-barrel transporters. Crystal structures of this domain have been obtained using X-ray crystallography[66] and NMR spectroscopy.[67] These structures are identical to a root mean squared deviation (RMSD) of 0.9Å, both show three stranded antiparallel β-sheet and two α-helices. There is controversial evidence about a dimeric form of the fragment, specifically a 4th β-strand (β4) that seems to induce dimerization in the NMR structure at high concentrations. Bioinformatic studies of bacterial genomes have shown the β4 is not present in most TonB proteins.[66] EPR distance measurements have shown that monomeric TonB is required for the high affinity transporter-TonB complex.[59]

The cytoplasmic membrane proteins ExbB and ExbD are 244 residues and 141 residues, respectively. While neither protein has been crystallized, protein topological experiments indicate they are both globular and α-helical.[69,70] In cells, the ratio of the protein complex is 1 TonB, 2ExbD, 7 ExbB.[71] The exact roles for ExbB and ExbD are unknown but they are required to transfer the PMF to TonB in a cyclical manner.[72,73] Furthermore ExbB has been shown to be responsible for PMF dependent changes in TonB,[72] and ExbD may act as a regulator, preventing transport related movements when a PMF is not present.[74]

Another theory postulates that in the absence of PMF, ExbD and TonB exist as homodimers stabilized by ExbB tetramers. When the PMF appears, TonB ExbD heterodimers transmit the energy for transport.[75]

This work details the design and utilization of native environments, whole cells and intact outermembranes, for the study of membrane proteins. A new technique, double electron electron resonance (DEER) with two protein bound spin labels in the whole cell environment is introduced in Chapter 3. This technique is proven to be a viable way of obtaining intraprotein distances using the BtuB protein, and the distances obtained closely resemble previous work in reconstituted systems. The main advantage of whole cells lies in the lipid and protein diversity that may contribute towards the full understanding of membrane protein structure and function. Chapter 4 shows that we are able to obtain the first data on protein conformational changes in the whole cell environment with DEER. This chapter describes more potential uses for the whole cell DEER technique and increases its appeal for future studies. In Chapter 5 we describe work that utilizes native systems in the study of the BtuB transport cycle. The binding of TonB to the periplasmic side of the BtuB protein causes a reduction in the transporter's affinity for its substrate. We are able to measure this change in affinity and show that TonB binding does not produce this effect in mutants which are transport deficient due to a ton box mutation. Finally, we present a study of BtuB hatch domain stability in Chapter 6. The hatch must reorganize during transport so the large substrate has room to pass through the transporter. We use urea denaturation to examine the energetics of unfolding the along the hatch domain of BtuB.

1.4 References

1. Wallin, E. & von Heijne, G. Genome-wide analysis of integral membrane proteins from eubacterial, archaen and eukaryotic organisms. *Protein Science.* **7**, 1029-38 (1998).

2. Bakheet, T. M. & Doig, A. J. Properties and identification of human protein drug targets. *Bioinformatics.* **4**, 451-7 (2009).

3. Jayasinghe, S., Hristova, K. & White S.H. MPtopo: A database of membrane protein topology. *Protein Science.* **10**, 455-8 (2000).

4. Engelman, D. M. Membranes are more than fluid. *Nature.* **438**, 578-80 (2005).

5. Jensen, M. O. & O. G. Mouritsen. Lipids do influence protein function the hydrophobic matching hypothesis revisited. *Biochim. Biophys. Acta.* **1666**, 205-26 (2004).

6. Cantor, R. S. Lipid composition and the lateral pressure profile in bilayers. *Biophys. J.* **76**, 2625-39 (1999).

7. Prive, G. G. Detergents for the stabilization and crystallization of membrane proteins. *Methods.* **41**,388-97 (2007).

8. Acharya, K. R. & Lloyd M. D. The advantages and limitations of protein crystal structures. *Trends Pharmacol Sci.* **26**, 10-14 (2005).

9. Yu, T., Raschle, T., Hiller S. & Wagner G. Solution NMR spectroscopic characterization of human VDAC-2 in detergent micelles and lipid nanodiscs. *Biochim. Biophys. Acta.* **1818**, 1562-69 (2012).

10. Cacace, M. G., Landau, E. M. & Ramsden, J. J. The Hofmeister series: salt and solvent effects on interfacial phenomena. *Q. Rev. Biophys.* **30**, 241-77 (1997).

11. Lazaridis, T. & Varsace, R. The treatment of solvent in multiscale biophysical modeling. *Isr. J. Chem.* **54**, 1074-83 (2014).

12. Lee, A. Biological membranes: the importance of molecular detail. *Trends Biochem Sci.* **36**, 493-500 (2011).

13. Graham, L.L., Harris, R., Villiger, W. & Beveridge, T.J. Freeze-substitution of gram-negative eubacteria: general cell morphology and envelope profiles. *J. Bacteriol.* **173**, 1623-33 (1991).

14. Nikaido, H. & Vaara, M. Molecular-Basis of Bacterial Outer-Membrane Permeability. *Microbiological Reviews.* **49**, 1-32 (1985).

15. Plesiat, P. & Nikaido, H. Outer membranes of gram-negative bacteria are permeable to steroid probes. *Molecular Microbiology.* **6**, 1323-33 (1992).

16. Poinsot, V., Carpéné M. A. & Couderc F. Coupled Mass Spectrometric Strategies for the Determination of Carbohydrates at Very Low Concentrations: The Case of Polysaccharides Involved in the Molecular Dialogue Between Plants and Rhizobia *Complex world of polysacarides* Edited by Desiree Nedra Karunaratne (2012).

17. Shevchenko, A., & Simons, K. Lipidomics: coming to grips with lipid diversity. *Nat. Rev. Mol. Cell. Biol.* **11**, 593-98 (2010).

18. Wenk, M. Lipiomics: new tools and applications. *Cell.* **143**, 888-95 (2010).

19. Yetukuri, L., Ekroos, K., Vidal-Puig, A., & Oresic, M. Informatics and computational strategies for the study of lipids. *Mol Biosyst.* **4**, 121-27 (2008).

20. Smith, A. Lipid-protein interactions in biological membranes: A dynamic perspective. *Biochim Biopshys. Acta.* **1818**, 172-77 (2012).

21. East, J., Melville D., & Lee, A. Exchange rates and numbers of annular lipids for the calcium and magnesium ion dependent adenosine triphosphate. *Biochem*. **24**, 2615-23 (1985).

22. Powl, A., East, J., & Lee, A. Anionic phospholipids affect the rate and extent of flux through the mechanosensitive channel of large conductance MscL. *Biochem,* **47**, 4317-28 (2008).

23. Powl, A., East, J., & Lee, A. Importance of direct interactions with lipids for the function of the mechanosensitive channel MscL. *Biochem,* **47**, 12175-84 (2008).

24. Dickey, A., & Faller, A. Behavioral differences between phosphatidic acid and phosphatidylcholine in the presence of the nicotinic acetylcholine receptor. *Biophys J.* **95**, 5637-47 (2008).

25. daCosta, C. J., Wagg, I. D., McKay, M. E. & Baenziger, J. E. Phosphatidic acid and phosphatidylserine have distinct structural and functional interactions with the nicotinic acetylcholine receptor. *J. Biol. Chem.* **15**, 14967-74 (2004).

26. Cheng, M. H., Liu, L. T., Saladino, A. C., Xu, Y. & Tang, P. Molecular dynamics simulations of ternary membrane mixture: phosphatidylcholine, phospharidic acd and cholesterol. *J. Phys. Chem. B.* **51**, 14186-92 (2007).

27. Chapot-Chartier, M. & Kulakauskas, S. Cell wall structure and function in lactic acid bacteria. *Microbial Cell Factories.* **13**, 59-82 (2014).

28. Rietschel, E. T., Kirikae, T., Schade, F.U., Mamat, U., Schmidt. G., Loppnow. H., Ulmer, A.J., Zähringer, U., Seydel. U. & Di Padova. F. Bacterial endotoxin: molecular relationships of structure to activity and function. *FASEB J.* **8**, 217-25 (1994).

29. Reyes, R. E., González, C. R., Jiménez, R. C., Herrera, M. R. & Andrade A. A. Mechanisms of O-Antigen Structural Variation of Bacterial Lipopolysaccharide (LPS) *Complex world of polysacarides.* Edited by Desiree Nedra Karunaratne (2012).

30. Chmiela, M., Miszczyk, E. & Rudnicka, K. Structural modifications of Helicobacter pylori lipopolysaccharide: An idea for how to live in peace. *World. J. Gastroenterol.* **20**, 9882-97 (2014).

31. Resh, M. Trafficking and signaling by fatty-acylated and prenylated proteins. *Nat. Chem. Biol.* **2**, 584-90 (2006).

32. Resh, M. Membrane targeting of lipid medified signal transduction proteins. *Sub cell. Biochem.* **37**, 217-32 (2004).

33. Lauwers, E., Goodchild, R. & Verstreken, P. Membrane lipid in presynaptic function and disease. *Neuron.* **90**, 11-25 (2016).

34. Zhang, Y. & Cremer P. Chemistry of Hofmeister anions and osmolytes. *Annu. Rev. Phys. Chem.* **61**, 63-83 (2010).

35. Krogh, A., Larsson, B., von Heijne, G. & Sonnhammer, L. Predicting transmembrane protein topology with a hidden Markov method: application to complete genomes. *J. Mol. Biol.* **305**, 567-80 (2001).

36. Bienvenue, A., Bloom, M., Davis, J. & Devaux, P. Evidence for protein-associated lipids from deuterium nuclear magnetic resonance studies of rhodopsin dimyristolphosphatidylcholine recombinations. *J. Biol. Chem.* **257**, 3032-38 (1982).

37. Fox, A. D., Larsson, P., Lo, H. R., Kroncke, H. B., Kasson, P. & Columbus, L. Structure of the Neisserial Outer Membrane Protein Opa60: Loop Flexibility Essential to Resceptor Recognition and Bacterial Engulfment. *JACS*. **28**, 9938-46 (2014).

38. Parkin, J., Chavent, M. & Khalid, S. Molecular simulations of gram-negative bacterial membranes: a vignette of some recent successes. *Biophys J.* **109**, 461-8 (2015).

39. Wu, E., Fleming, P., Yeorn, M., Widmalm, G., Klaudei, J., Fleming, K., & Im, W. *E. coli* outermembrane and interactions with OmpLA. *Biophys J.* **106**, 2493-502 (2014).

40. Klar, T., Jakobs, S., Dyba, M., Egner, A., & Hell, S. Fluorescence microscopy with diffraction resolution barrier broken by stimulated emission. *Proc. Natl. Acad. Sci. U.S.A.* **97**, 8206-10 (2000).

41. Rust, M., Bates, M., & Zhuang, X. Sub-diffraction-limit imaging by stochastic optical reconstruction microscopy (STORM). *Nat. Methods.* **3**, 793-6 (2006).

42. Hess, S., Girirajan, T., & Mason, M. Ultra-high resolution imaging by fluorescence photoactivation localization spectroscopy. *Biophys J.* **91**, 4258-72 (2006).

43. Kim, Y., & Hochstrasser, R. Applications of 2D IR spectroscopy to peptides, proteins, and hydrogen-bond dynamics. *J. Phys. Chem. B.* **113**, 8231-51 (2009).

44. Zheng, J., Kwak, K., Asbury, J., Chen, X., Piletic, I., & Fayer, M. Ultrafast dynamics of the solute-solvent complexation observed at thermal equilibrium in real time. *Science.* **309**, 1338-43 (2005).

45. Fecko, C., Eaves, J., Loparo, J., Tokmakoff, A., & Geissler, P. Ultrafast hydrogen-bond dynamics in the infrared spectroscopy of water. *Science.* **301**, 1698-1702 (2003).

46. Borbat, P., Costa-Filho, A., Earle, K., Moscicki J., & Freed, J. Electron spin resonance in studies of membranes and proteins. *Science* **291**, 266-269 (2001).

47. Bayburt, T., & Sligar, S. Membrane protein assembly in nanodics. *FEBS letters.* **584**, 1721-27 (2010).

48. Caffrey, M. Crystalizing membrane proteins for structure determination: use of lipidic mesophases. *Annu. Rev. Biophys.* **38**, 29-51 (2009).

49. Faham, S., & Bowie, J. Bicelle crystallization: a new method for crystallizing membrane proteins yields a monomeric bacteriorhodopsin structure. *J. Mol. Biol.* **316**, 1-6 (2002).

50. Krewulak, K. & Vogel H. Structural biology of bacterial iron uptake. *Biochim Biopshys. Acta.* **1778**, 1781-1804 (2008).

51. Bagg, A. & Neilands J. Ferric uptake regulation protein acts as a repressor, employing iron (II) as a cofactor to bind the operator of an iron transport operon in *Escherichia Coli*. *Biochemistry*. **26**, 5471-77 (1987).

52. Kadner, R. Repression of synthesis of the vitamin B12 receptor in *Escherichia Coli*. *J. Bacteriol.* **136**, 1050-57 (1978).

53. Noinaj, N., Guillier, M., Barnard ,T. & Buchanan S. TonB-Dependent Transporters: Regulation, Structure and Function. *Annu. Rev. Microbiol.* **64**, 43-60 (2010).

54. Schauer, K., Rodionov, D. & deReuse, H. New Substrates for TonB-Dependent Transport: do we only see the 'Tip of the iceberg'? *Trends Biochem.* **33**, 330-38 (2008).

55. Postle, K. & Kadner, R. Touch and go: Tying TonB to transport. *Mol. Microbiol.* **49**, 869-82 (2003).

56. Krewulak K & Vogel H. TonB or not TonB: is that the question? *Biochem Cell Biol* **89**, 87-97 (2011).

57. Chimento, D., Kadner, R. & Wiener M. Comparative structural analysis of TonB-dependent outer membrane transporters: implications for the transport cycle. *Proteins*: *Struct, Funct, Bioinf* **59**, 240-51 (2005).

58. Freed, D.M., Lukasik, S.M., Sikora, A., Mokdad, A., & Cafiso D.S. Monomeric TonB and the ton box are required for the formation of a high-affinity transporter-TonB complex. *Biochemistry.* **52**, 2638-48 (2013).

59. Kaserer, W., Jiang, X., Xiao, Q., Scott, D., Bauler, M., Copeland, D., Newton, S. M. & Klebba, P. E. Insight from TonB hybrid proteins into the mechanism of iron transport through the outer membrane. *J. Bacteriol.* **190**, 4001-16 (2008.

60. Fanucci, G. E., Coggshall, K. A., Cadieux, N., Kim, M., Kadner, R. J. & Cafiso D. S. Substrate-induced conformational changes of the periplasmic N-terminus of an outer-membrane transporter by site-directed spin labeling. *Biochemistry*. **42**, 1391-1400 (2003).

61. Shultis, D.D., Purdy, M.D., Banchs, C.N. & Wiener, M.C. Outer membrane active transport: structure of the BtuB:TonB complex. *Science.* **312**, 1396-9 (2006).

62. Pawelek, P.D., Croteau, N., Ng-Thow-Hing, C., Khursigara, C. M., Moiseeva, N., Allaire, M. & Coulton, J. W. Structure of TonB in complex with FhuA, E-coli outer membrane receptor. *Science.* **312**, 1399-1402 (2006).

63. Swayne, C. & Postle, K. Taking the Escherichia coli TonB transmembrane domain "offline"? Nonprotonatable Asn substitutes fully for TonB His20. *J. Bacteriol.* **193**, 3693-701 (2011).

64. Kohler, S.D., Weber, A., Howard, S.P., Welte, W. & Drescher, M. The proline-rich domain of TonB possesses an extended polyproline II-like conformation of sufficient length to span the periplasm of Gram-negative bacteria. *Protein Science.* **19**, 625-630 (2010).

65. Adzhuber, A.A., Sternberg, J., & Makarov, A.A. Polyproline-II Helix in Proteins: Structure and Function. *J. Mol. Biol.* **12**, 2100-32 (2013).

66. Kodding, J., Killig, F., Polzer, P., Howard, S.P., Diederichs, K., & Welte, W. Crystal structure of a 92-residue C-terminal fragment of TonB from *Escherichia coli* reveals significant conformational changes compared to structures of smaller TonB fragments. *J. Biol. Chem.* **280**, 3022-28 (2005).

67. Peacock, S.R., Weljie, A.M., Howard, P.S., Price, F.D., & Vogel, H.J. The solution structure of the C-terminal domain of TonB and interaction studies with TonB box peptides. *J. Mol. Biol.* **345**, 1185-97 (2005).

68. Chu, B.C., Peacock, R.S., & Vogel, H.J. Bioinformatic analysis of the TonB protein family. *Biometals*. **20**, 467-483 (2007).

69. Kampfenkel, K. & Braun, V. Membrane topology of the Escherichia coli ExbD protein. *J. Bacteriol.* **174**, 5485-7 (1992).

70. Kampfenkel, K. & Braun, V. Topology of the ExbB protein in the cytoplasmic membrane of Escherichia coli. *JBC* **268**, 6050-7 (1993).

71. Higgs, P.I., Larsen, R.A. & Postle, K. Quantification of known components of the Escherichia coli TonB energy transduction system: TonB, ExbB, ExbD and FepA. *Molecular Microbiology* **44**, 271-81 (2002).

72. Larsen, R.A., Thomas, M.G. & Postle, K. Protonmotive force, ExbB and ligand-bound FepA drive conformational changes in TonB. *Molecular Microbiology* **31**, 1809-1824 (1999).

73. Ollis, A.A., Manning, M., Held, K.G. & Postle, K. Cytoplasmic membrane protonmotive force energizes periplasmic interactions between ExbD and TonB. *Molecular Microbiology* **73**, 466-481 (2009).

74. Ollis, A.A., & Postle, K. The same periplasmic ExbD residues mediate in vivo interactions between ExbD homodimers and ExbD-TonB heterodimers. *Journal of Bacteriology* **193**, 6852-63 (2011).

75. Gresock, M. G., Kastead, K. A. & Postle, K. From Homodimer to Heterodimer and Back: Elucidating the TonB Energy Transduction Cycle *J. Bacteriol.* **21**, 3433-45 (2015).

Chapter 2: Electron Paramagnetic Resonance (EPR)

2.1 Electron Paramagnetic resonance Theory[1,2]

Electron Paramagnetic Resonance (EPR) spectroscopy is a magnetic resonance technique that detects unpaired electrons. Free electrons can be found in many natural compounds, most notably metal binding proteins and free radicals. Free electrons are short lived but are very important in many enzymatic processes such as photosynthesis, catalysis and oxidation, to name a few. In site-directed spin labeling electron paramagnetic resonance (SDSL-EPR), an organic stable free-radical called a nitroxide is incorporated into a protein though site directed mutagenesis and reaction with a target residue. The following EPR theory will be presented in the context of these nitroxides, although many concepts are general and may be applied to any unpaired electron.

2.1.1 Zeeman Interactions

The spin magnetic moment can be described by its relation to spin angular momentum S:

$$\mu = -g\beta S \tag{2.1.1}$$

where g is the g factor for an unpaired electron and β is the Bohr magneton. The g factor is a measure of the magnetic moment of a particle (section 2.2). For a lone electron the g factor has been shown to be 2.0023. The Bohr magneton is represented as:

$$\beta = \frac{e\hbar}{2mc} \tag{2.1.2}$$

In equation 2.1.2 e is the charge of the electron and m is its mass. ħ is Planck's constant divided by 2π and c is the speed of light.

A signal is produced during an EPR experiment when transitions occur between quantized Zeeman energy levels in the presence of an applied magnetic field. These quantized energy levels are a result of the interaction between the spin magnetic moment μ and the magnetic field B and can be expressed by the following Hamiltonian operator:

$$H = -\mu \cdot B \tag{2.1.3}$$

Substituting μ from equation 2.1.1 into 2.1.3 we get

$$H = g\beta S \cdot B \tag{2.1.4}$$

The quantized angular momentum is taken along the z direction, thus the Hamiltonian in the z direction is:

$$H = g\beta S_z \cdot B_z \tag{2.1.5}$$

The electron spin angular momentum in the z direction is expressed by the operator S_z. Since the system is comprised of only a free electron the eigenvalues for the Hamiltonian are $m_s \pm ½$. Making the energies of the system:

$$E = \pm ½ g\beta B \tag{2.1.6}$$

And the difference between the energy levels

$$\Delta E = g\beta B \tag{2.1.7}$$

Expressing this according to the Bohr condition, $\Delta E=h\nu$ the expression becomes:

$$h\nu = g\beta B \tag{2.1.8}$$

The frequency at which the electron spin μ precesses about H is known as the Larmor frequency and can be expressed in terms of electron gyromagnetic ratio γ_e and the angular frequency ω:

$$\omega = \gamma_e B \tag{2.1.9}$$

Where $\omega = 2\pi\nu$ and $\gamma_e = g\beta/\hbar$. When the Larmor frequency is met the Zeeman transitions are observed in the resulting EPR signal.

The g-factor for a free electron is known with a great deal of accuracy, it has a value of 2.0023193043622. There is a deviation that occurs when the free electron is stabilized into a radical. This change is due to the unpaired electron interacting with local magnetic fields produced by other atoms. The new B_{eff} felt by the electron is:

$$B_{eff} = B(1 - \sigma) \tag{2.1.10}$$

Here σ represents the local field contributions. So the resonance condition becomes

$$h\nu = g\beta B(1 - \sigma) \tag{2.1.11}$$

This quantity $g(1 - \sigma)$ can simply be expressed as g, the nitroxide g factor. The local magnetic field contribution can be positive or negative.

2.1.2 Nitroxide Hyperfine Interactions

A simple unpaired electron would produce only one transition but this unpaired electron is localized onto the 2p π orbital of the nitrogen atom. Due to the fact that the lone electron is on this nitrogen a hyperfine interaction between the electron and nucleus produces three transitions. This nitrogen nucleus has a spin of 1, this results in the spin quantum numbers m_I are 1, 0 and -1. And transitions at each represented by ΔE_1, ΔE_0, and ΔE_{-1} as shown in Figure 2.1. These three transitions result in a spectrum as seen in figure 2.1.1 b. The electron-nuclear interaction stems from two sources. The first is the Fermi contact which arises from an isotropic interaction. The second interaction is anisotropic magnetic dipole-dipole. Both of these terms are combined into the hyperfine tensor **A**, however the dipolar component dominates this interaction. The relationship of **S** and **I**, the electron and nuclear spin angular momentum respectively, in this hyperfine interaction is represented by the Hamiltonian:

$$H = \mathbf{S} \cdot \mathbf{A} \cdot \mathbf{I} \qquad (2.1.12)$$

Adding this hyperfine interaction to the original electron spin Hamiltonian:

$$H = g\beta S \cdot B + \mathbf{S} \cdot \mathbf{A} \cdot \mathbf{I} \qquad (2.1.13)$$

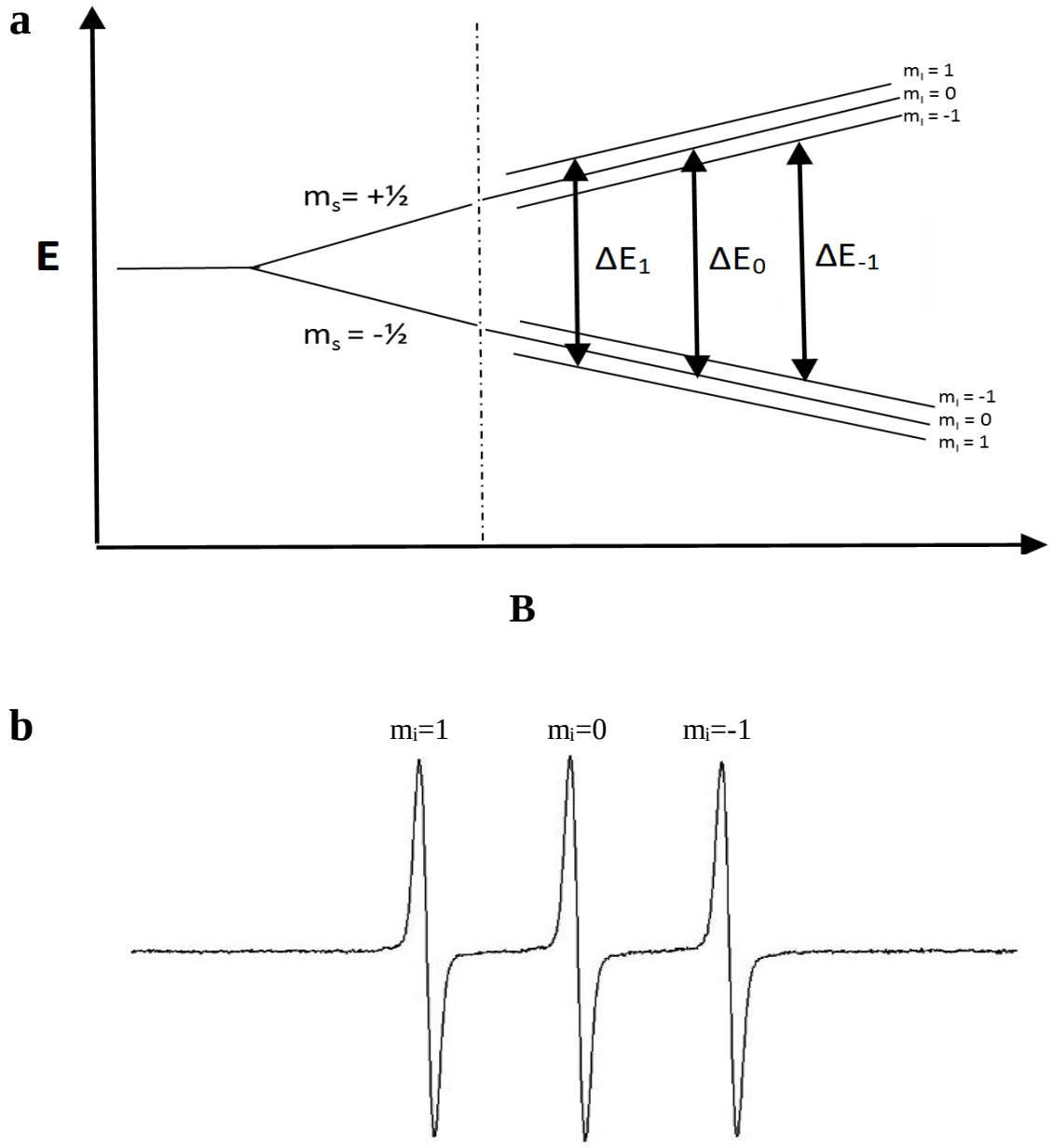

Figure 2.1 Nitrogen Hyperfine Interaction. **a)** The electron magnetic moment interacts with the nitrogen nuclear magnetic moment results in the hyperfine interaction. This interaction results in three transitions, one for each nuclear quantum number m_i= 1, 0, -1. **b)** Each transition ΔE_1, ΔE_0, ΔE_{-1} can be detected and when converted to the first derivative results in a characteristic CW-EPR lineshape

2.1.3 Spin magnetic frame[3-5]

The EPR spectrum is highly dependent on the orientation of the spin label in the magnetic field. This results in spectral anisotropy in both the Zeeman and hyperfine tensors. Each tensor, **g** and **A** respectively are represented by a 3 by 3 matrix that is diagonal in the magnetic frame (Figure 2.2). These tensors are highly dependent on environment of the electron therefore, **A** and **g** tensors for a given spin label and environment can only be accurately determined using multiple EPR frequencies and/or extensive simulations.[6] For the spin label, S-(1-oxyl-2,2,5,5-tetramethyl-2,5-dihydro-1H-pyrrol-3-yl) methyl methanesulfonothioate (MTSL R1), in solvent exposed sites the magnetic parameters are: $\mathbf{g_{xx}}$ = 2.0089, $\mathbf{g_{yy}}$ = 2.0050, and $\mathbf{g_{zz}}$ = 2.0023 and A_{xx} = 6.2, A_{yy} = 5.9 and A_{zz} = 37.[5,7]

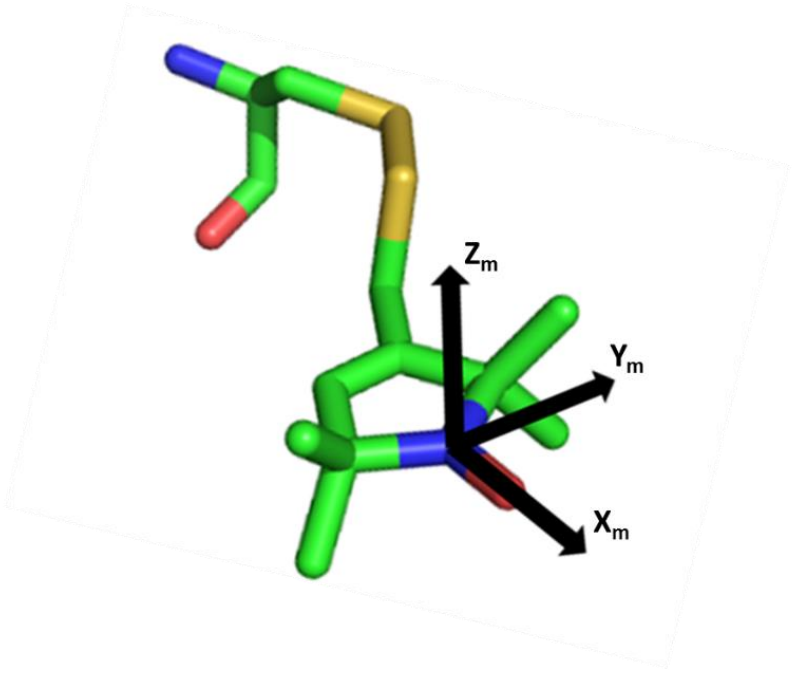

*Figure 2.2 Nitroxide spin magnetic frame***.** The three principle axis of the nitroxide magnetic frame are shown. Z_m is parallel to the nitroxide p_z orbital and the N-0 bond lies along the X_m axis. In this figure carbon is green, oxygen is red, nitrogen is blue and sulfur is yellow. (Figure adapted from Freed. D. Thesis)

2.2 Nitroxide and Site Directed Spin Labeling

Unpaired electrons are normally very reactive and are not normally present in proteins or other macromolecules. In site-directed spin labeling, the molecule most often used is MTSL (Figure 2.3) although other labels based upon nitroxides and other stable free radicals have been used.

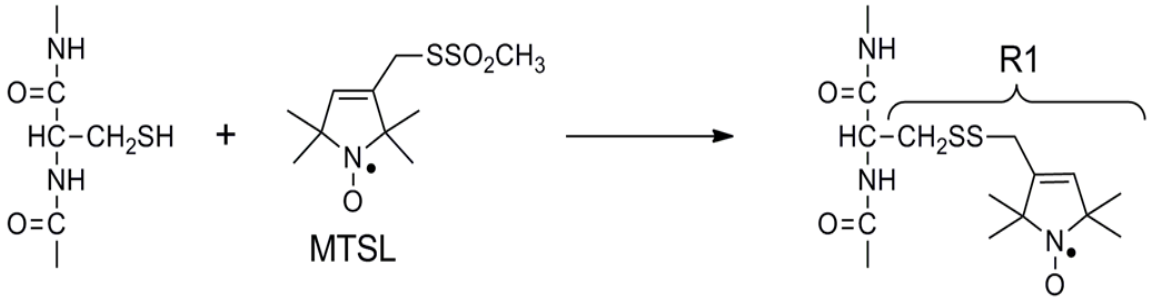

Figure 2.3 Diagram of the spin labeling reaction. The disulfide reaction of the amino acid cysteine with an MTSL molecule to form the EPR probe MTSL. The dot on the N-O bond indicates the free electron.

As seen in figure 2.3 MTSL reacts with cysteines on proteins to form the R1 group. This reaction is specific and spontaneous under normal laboratory conditions.[7] R1 is about the size of a large aromatic amino acid such as tyrosine or tryptophan. The labeled side chain R1 can generally be incorporated into proteins without perturbing their structure, although the stability of the protein can be altered when R1 is placed within the protein interior.[8] In addition to g and A tensor effects described above, lineshape is affected by the polarity of the environment due to the nitroxide resonance forms. The neutral form [N – O·] is favored by nonpolar solvents while the zwitterionic resonance form [$\cdot N^+ - O^-$] is favored when the solvent is polar.[9] Spin labels have also been developed that are rigidly fixed to a protein

backbone, that are sensitive to pH and that can be incorporated into nucleic acids. Amino acid spin labels that can be directly synthesized into a protein have also been developed.[10]

2.3 Lineshapes and spin label dynamics

R1 is most often used because it is small, bonds specifically to free cysteines and is sensitive to motions of the protein, specifically those that occur in the nanosecond time scale: rotational diffusion of the protein, bond rotation of the spin label and protein backbone fluctuations. The rotational diffusion of the protein is not important for any protein larger than 40kDa, and viscous solutes such as sucrose can be used to slow the diffusion of smaller proteins.[11]

2.3.1 Relaxation

Interactions between the nitroxide and its surroundings limit the lifetime of spin states. The Bloch equations describe relaxation of spin states, and a brief overview of the main components of this set of equations is presented. Here a number of spins N is considered in the magnetic field H. The spins separate into two populations where N_α spins are in the state α and N_β are in the state β. Spins populate these energy states according to a Boltzmann distribution equation:

$$\frac{N\alpha}{N\beta} = e^{-\frac{gBH}{kT}} \qquad (2.3.1)$$

Where N_α and N_β are the populations of the m_s = -½ and m_s = +½ Zeeman levels, respectively, T is the temperature and k is the Boltzmann constant. Net absorption of energy in the presence of an external magnetic field occurs because there is a slightly larger

particle population in N_β at thermal equilibrium. The spins have a bulk magnetic moment represented by **M**. **M** is a combination of all the individual magnetic moments **μ**, thus we can represent the z component of the magnetic moment as:

$$\mathbf{M_z} = \Sigma\boldsymbol{\mu} = \gamma_e\hbar(N_\alpha - N_\beta) = \gamma_e\hbar n \tag{2.3.2}$$

Here $n = N_\alpha - N_\beta$. After the external magnetic field is removed the spin population difference n relaxes back to equilibrium exponentially by:

$$\frac{dn}{dt} = \frac{-n}{T_1} \tag{2.3.3}$$

T_1 is the spin-lattice relaxation time and describes relaxation in the z direction. Since M_z is proportional to dn:

$$\frac{dM_z}{dt} = \frac{-M_z}{T_1} \tag{2.3.4}$$

In the presence of a magnetic field M_z decays to an equilibrium value M_0 after the time T_1. M_0 is proportional to the magnetic susceptibility χ:

$$\chi = \frac{(N\gamma_e{}^2\,\hbar^2 S)}{3kT} \tag{2.3.5}$$

Therefore relaxation in the z direction or spin-lattice relaxation can be expressed by equation 2.3.6:

$$\frac{dM_z}{dt} = -\frac{(M_z - M_0)}{T_1} \tag{2.3.6}$$

The transverse relaxation time T_2 is relaxation in the M_x and M_y directions. This can be expressed as:

$$\frac{dM_x}{dt} = \frac{-M_x}{T_2} \tag{2.3.7}$$

And

$$\frac{dM_y}{dt} = \frac{-M_y}{T_2} \tag{2.3.8}$$

Experiment has shown that for a nitroxide on a peptide T_1 is about 3 μs[12] and T_2 is about 30 ns.[13] These data lead to the conclusion that in general T_2 is much smaller and so would dictate the total line width. In fact the line width is on the order of $\frac{1}{\gamma_e T_2}$.

There are several factors that affect line shape. They can most easily be broken down into relaxation and non-relaxation effects. Non-relaxation effects such as proton hyperfine splitting contributes to broadening the intrinsic line shape by about .1 to .4G.[14,15] Relaxation effects can change the T_1 or T_2, however the linewidth is almost exclusively driven by the shorter T_2, the T_1 broadening does not show up in the line shape. T_2 is affected by spin-spin interaction such as spin diffusion. The oxygen dissolved in the sample can also homogenouly broaden a line shape by about 150 mG.[16]

The final and most important aspect of line shape is its response to molecular motion, that is, nitroxide motion with respect to the magnetic field. The speed of this motion or the rotational correlation time, τ_R, is related to the average time in which a molecule moves in any given direction[17]. When working at X-band, rotational, correlation times greater than 50ns give a rigid limit line shape. τ_R smaller than ~1ns produce a completely motionally averaged line shape representing the fast motional limit of this technique. Another important measure of nitroxide motion is the order parameter S. Using the "wobble" model[18], the order parameter measures the amplitude of motion of the spin label moving in a cone with maximum angle θ about the *Z*-axis.

$$S = \tfrac{1}{2}(3\langle\cos^2\theta\rangle - 1) \qquad (2.3.9)$$

The values of S range from 0 to 1, at S = 1, θ = 0° and all motion is completely restricted. When S = 0, θ = 90° and all motions are allowed indicating a completely free motion of the label.

2.3.2 Regimes of nitroxide motion

The three regimes of motion for a nitroxide include rigid limit, isotropic limit and intermediate motion. Fast and isotropic limit motions are defined by rotational correlation times that are faster than 500ps for X-band. In this time regime, relaxation effects are negligible as the magnetic parameters are almost completely averaged, and the speed of nitroxide reorientation is too fast to be broadened by transverse relaxation effects. This type of motion can be simulated by the time dependent effective Hamiltonian. At the rigid limit of motion the nitroxide is frozen on the EPR timescale and the resulting spectra are

indistinguishable from a crystal crushed into powder. All orientations are represented in this very broad spectrum. The final regime of motion encompasses $\tau_R < 50$ns and $\tau_R > 2$ns. This type of motion includes a large variety of motions and can be simulated by the Microscopic Order Macroscopic Disorder Model (MOMD).[19]

2.4 Pulsed EPR to determine intraprotein distances

One of the most powerful and most commonly utilized applications of site directed spin labeling EPR is double electron-electron resonance (DEER) spectroscopy. This technique selectively measures pairwise couplings between electrons spins. The power of this technique comes from its ability to measure spin couplings, allowing distance information to be extracted. The DEER experiment produces a signal that decays over time. This technique was first introduced by Milov et al[20,21] and was later extended to the four pulse sequence used currently in commercial spectrometers by Pannier et al.[22] DEER is widely used to study macromolecular distances between 1.8 and 8 nm.[23,24] DEER is used to study both soluble proteins[25] and membrane proteins[26]. Constraints obtained from this technique have been used to determine changes to protein structure that can't be obtained using crystallography.[27] Unstructured proteins are also good targets for this technique especially because they are normally too flexible to crystallize.[28] DEER is unusually amenable to diverse environments and whole cell DEER experiments have been pioneered, first with a gadolinium spin label[29] and then with a nitroxide spin labels incorporated into the protein.[30]

DEER measures the dipole-dipole interaction between unpaired electrons. A pair of coupled spins, S_1 and S_2, are shown in figure 2.4. Their distance and orientation relative to the magnetic field are given by an inter-spin vector.

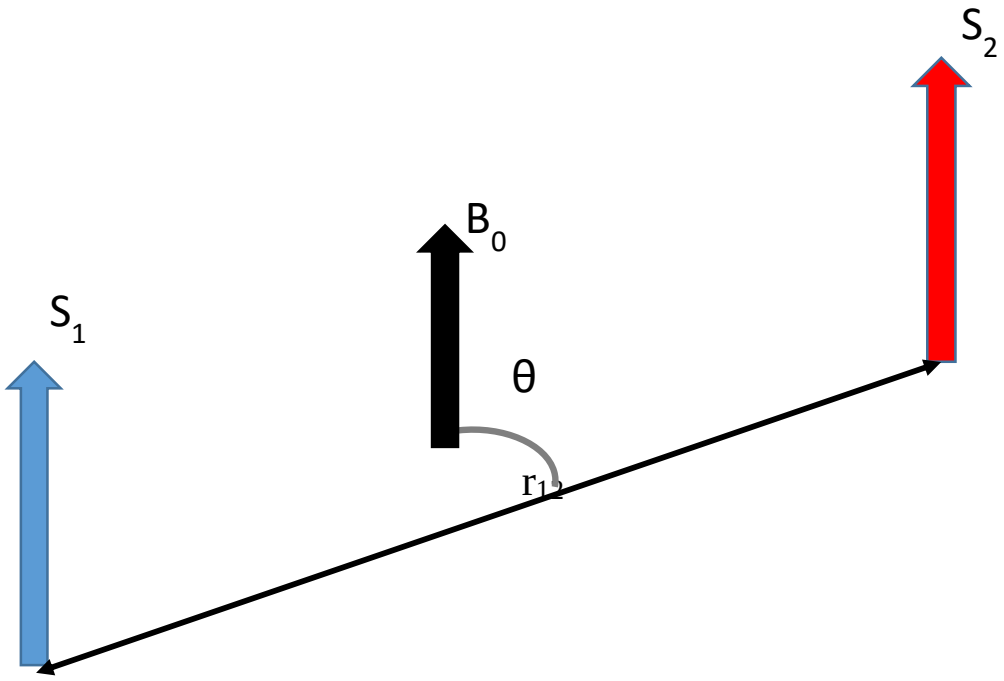

Figure 2.4. Diagram of spins coupled in a DEER experiment. S_1 and S_2 represent a pair of electron spins are separated by a distance r_{12} in the z axis. B_0 represents the direction of the magnetic field.

The dipolar coupling, a, depends on the distance between the spins:

$$a(r, \theta) = \omega_d (1 - 3\cos^2\theta) \quad (2.4.1)$$

Where ω_d is the dipolar frequency and is described by:

$$\omega_d = 2\pi\nu_d = \frac{\gamma_e^2 \hbar}{r^3} \quad (2.4.2)$$

During the DEER experiment the pulse sequence consists of pulses at the observer frequency, ω_1 followed by a time variable inversion pulse at the pump frequency, ω_2. The

second π pulse at the observer frequency refocuses the inhomogeneous broadening allowing the DEER echo to be measured (Figure 2.5).

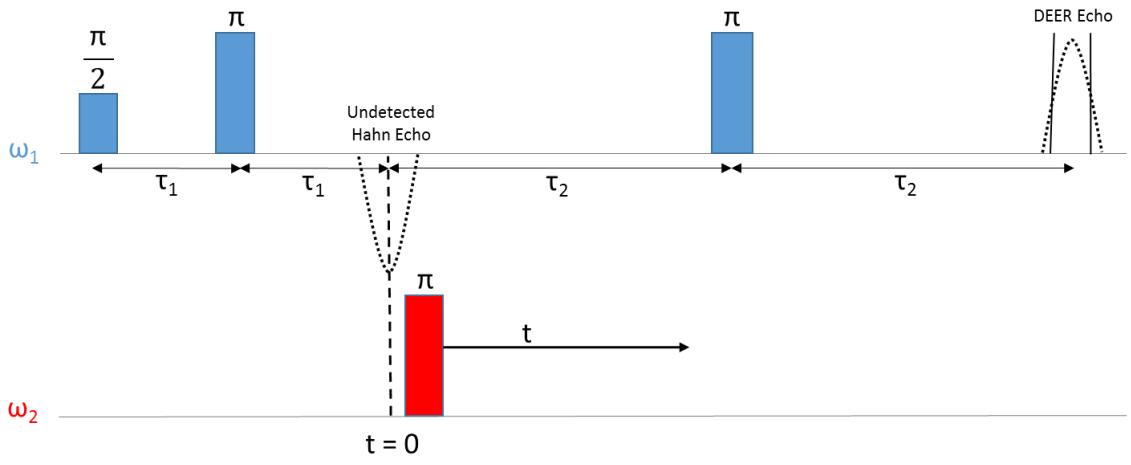

Figure 2.5 The DEER pulse sequence. The DEER pulse sequence is comprised of four pulses. The spins at ω_1 are coupled to those at ω_2 in a dipolar interaction that is dependent on distance. Varying the timing, t, of the π at the pump frequency modulates the DEER echo intensity as a function of this dipolar coupling.

The DEER experiment aims to extract the dipolar frequency ω_d from the other magnetic components of the electron. This is achieved by first applying a π/2 pulse at ω_1, which tips the magnetization into the xy plane. The S_1 spins precess at ω_1 and start to dephase after the pulse ends due to transverse relaxation and inhomogeneous broadening. This dephasing leads to echo attenuation by a factor $e^{-2k(\tau_1+\tau_2)}$. Here the decay constant k= $\frac{1}{T_{2S1}+k_{ID}}$ and depends on S_1 transverse relaxation time and instantaneous diffusion K_{ID} = c_1K_1. The concentration of S_1 spins is given by c_1 and K_1 is related to the length of the observer π pulses.[28] The inversion of S_2 spins increases the frequency of a fraction λ of S_1 spins by w_d. The frequency of the S_1 spins is now $\omega_1 + ½\ \omega_d$. λ is the fraction of S_2 spins

coupled to the S_1 spins that are excited by the π pulse at ω_2, which is always less than 1. During the DEER experiment we adopt certain assumptions. First the exchange coupling between spins is neglected and spins S_1 and S_2, are assumed to be quantized along the magnetic field. This allows us to modify equation 2.4.1 to

$$\omega_d = \frac{C}{r^3}\ (1 - 3cos^2\theta) \tag{2.4.3}$$

where C is proportional to the g values for the two spins in the system. Next a π pulse is applied at the observer frequency. This flips the spins by 180° into the – z axis resurrecting the signal by refocusing the S_1 spins. This results in the undetected Hahn echo. This signal is not detected because the high energy kW pulses would damage the nW detector. As the S1 spins in the –z axis again begin to dephase, an inversion π pulse is applied at the pump frequency. This changes the dipolar contribution experienced by the S_1 spins from + $w_d/2$ to – $w_d/2$. The final π pulse at the observe frequency produces a DEER echo that is a function of the dipolar frequency, ω_d, and the phase lag of the S_1 spins which is dependent on the timing, t, of the π pulse at the pump frequency.

Using equation 2.4.3 we can express the amplitude of the DEER echo as a function of time t as:

$$V(t)\ \{\ 1 - \lambda\ [\ 1 - \int_0^1 \left(\frac{C}{r^3}\ (1 - 3cos^2\theta)t\right) d\cos\theta]\}B(t) \tag{2.4.4}$$

B (t) is the background form factor and is expressed by equation 2.4.5

$$B(t) = e^{-c_2 K_B t^{D/3}} \tag{2.4.5}$$

D is the fractional dimension which contains information on S2 homogenous spatial distribution. For membrane proteins in liposomes $D \approx 2$.[32] This background form factor is not analytically known and so the background must be fitted to the raw signal and subtracted to extract distance information. This distance information is encoded as a cosine function of the DEER signal. Information about the width of the distribution of distances can be extracted from the amplitude of the signal oscillations after the initial decay. This distribution is very valuable because unlike other techniques DEER data allows us to not only get the main distance but also the relative populations of minor distances.

2.5 References

1. Wertz, J.E. & Bolton, J.R. *Electron Spin Resonance: Elementary Theory and Practical Applications*, (McGraw-Hill, 1972).

2. Nordio, P.L. General Magnetic Resonance Theory. in *Spin Labeling: Theory and Applications* (ed. Berliner, L.J.) (Academic Press, New York, 1976).

3. Hubbell, W.L. & Altenbach, C. Investigation of structure and dynamics in membrane proteins using site-directed spin labeling. *Curr Opin Struct Biol* **4**, 566-573 (1994).

4. Stone, T.J., Buckman, T., Nordio, P.L. & McConnell, H.M. Spin-labeled biomolecules. *P. Natl. Acad. Sci. USA.***54**, 1010-7 (1965).

5. Columbus, L. Ph. D. Thesis. University of California Los Angeles, California (2001).

6. Mobius, K., Savitsky, A., Schnegg, A., Plato, M. & Fuchs, M. High-field EPR spectroscopy applied to biological systems: characterization of molecular switches for electron and ion transfers. *PCCP*. **7**, 29-42 (2005).

7. Owenius, R., Engstrom, M., Lindgren, M. & Huber, M. Influence of solvent polarity and hydrogen bonding on the EPR parameters of a nitroxide spin label

studied by 9-GHz and 95-GHz EPR spectroscopy and DFT calculations. *J. Phys. Chem. A*. **105**, 10967-10977 (2001).

8. Fanucci, G. E. and Cafiso, D. S. Recent advances and applications of site-directed spin labeling. *Curr Opin Struct Biol* **16**, 644-653 (2006).

9. Columbus, L., Kalai, T., Jeko, J., Hideg, K. & Hubbell, W.L. Molecular motion of spin labeled side chains in alpha-helices: analysis by variation of side chain structure. *Biochemistry* **40**, 3828-46 (2001).

10. Fielding, A. J., Concilio, M. G., Heaven, G., Hollas, M. A. New developments in spin labels for pulsed dipolar EPR. *Molecules* **19**, 16998-17025 (2014).

11. Altenbach, C. A., Foncisz, W., Hyde, J.S., Hubbell, W.L. Conformation of Spin-Labeled Melitin at Membrane Surfaces Investigated by Pulse Saturation Recovery and Continuous Wave Power Saturation Electron Paramagnetic Resonance. *Biophys J.* **56,** 1183-1191 (1989).

12. Poole, C. P. (1983) Electron Spin Resonance a Comprehensive Treatise on Experimental Techniques. (Dover Publications, Inc., Mineola, New York 1983).

13. Bales, B. L. (1989) Inhomogenously Broadened Spin-Label Spectra. In Biological Magnetic Resonance: Spin Labeling Theory and Applications, Vol. 8, (ed. L. J. Berliner, Reuben, J.), pp. 77-126, Plenum Press, New York.

14. Robinson, B. H., Mailer, C., Reese, A.W. Linewidth Analysis of Spin Labels in Liquids I. Theory and Data Analysis. *J. Magn. Reson.* **138,** 199-209 (1999).

15. Wilhelm, E., Battino, R., Wilcock, R.J. Low Pressure Solubility of Gases in Liquid Water. *Chem. Rev*. **77,** 219-262 (1977).

16. Budil, D.E., Lee, S., Saxena, S. & Freed, J.H. Nonlinear-least-squares analysis of slow-motion EPR spectra in one and two dimensions using a modified Levenberg-Marquardt algorithm. *Journal of Magnetic Resonance Series A* **120**, 155-189 (1996).

17. Knowles, P. F., Marsh, D. & Rattle, H. E. Magnetic resonance of biomelecules. (Wiley, New York, 1976).

18. Griffith, O. H., & Jost, P.C. Lipid Spin Labels in Biological Membranes. *In Spin Labeling Theory and Applications*, (ed. L. J. Berliner), (Academic Press, New York. 1976)

19. Milov, A. D., Salikhov, K. M. & Schirov, M. D. Use of the double resonance in electron spin echo method for the study of paramagnetic center spatial distribution in solids. *Fiz. Tverd. Tela.* **23**, 975-82 (1981).

20. Milov, A. D., Ponomarev, A. B. & Tevetkov, Y. D. Electron-electron double resonance in electron spin echo: model biradical systems and the sensitized photolysis of decalin. *Chem. Phys. Let.* **110**, 67-72 (1984).

21. Pannier, M., Viet, S., Godt, A., Jeschke, G. & Spiess, H. W. Dead-time free measurement of dipole-dipole interactions between electron spins. *J. Magn. Reson.* **142**, 331-40 (2000).

22. Jeschke G, Polyhach Y. Distance measurements on spin-labelled biomacromolecules by pulsed electron paramagnetic resonance. *Phys. Chem. Chem. Phys.* **9**, 1895–910 (2007).

23. Schiemann O, Prisner TF. Long-range distance determinations in biomacromolecules by EPR spectroscopy. *Q. Rev. Biophys.* **40**, 1–53 (2007).

24. Bennati M, Weber A, Antonic J, Perlstein DL, Robblee J, Stubbe J. Pulsed ELDOR spectroscopy measures the distance between the two tyrosyl radicals in the R2 subunit of the *E. coli* ribonucleotide reductase. *J. Am. Chem. Soc.* **125**, 14988–89 (2003).

25. Jeschke G, Wegener C, Nietschke M, Jung H, Steinhoff H. Interresidual distance determination by four-pulse double electron-electron resonance in an integral membrane protein: the Na+/proline transporter PutP of *Escherichia coli*. *Biophys. J.* **86**, 2551–57 (2004).

26. Borbat PP, Mchaourab HS, Freed JH. Protein structure determination using long-distance constraints from double-quantum coherence ESR: study of T4 lysozyme. *J. Am. Chem. Soc.* **124**, 5304–14 (2007).

27. Rao JN, Jao CC, Hegde BG, Langen R, Ulmer TS. A combinatorial NMR and EPR approach for evaluating the structural ensemble of partially folded proteins. *J. Am. Chem. Soc.* **132**, 8657–68 (2010).

28. Martorana, A., Bellapadrona, G., Feintuch, A., DiGregorio, E., Aime, S. & Goldfarb, D. Probing protein conformation in cells by EPR distance measurements using Gd3+ spin labeling. *J. Am. Chem. Soc.* **136**, 13458-65 (2014).

29. Jospeh, B., Sikora, A., Bordington, E., Jeschke, G., Cafiso, D., Prisner, T. Distance Measurement on an Endogenous Membrane Transporter in *E. coli* Cells and Native Membranes Using EPR Spectroscopy. *Angew. Chem. Int. Ed.*, **10**, 1002 (2015).

30. Borbat, P. P. & Freed. J H. Pulse Diploar Electron Spin Resonace: Distance Measurements. *Struc Bond.* **430**, 1-82 (2013).

31. Jeschke, G. DEER distance measurements on proteins. *Annu. Rev. Phys. Chem.* **63**, 419-46 (2012).

32. Milov A. D. & Tsvetkov, Y. D. Double electron-electron resonance in electron spin echo: conformations of spin-labeled poly-4-vinilpryridine in glassy solutions. *Appl. Magn. Reson.* **12**, 495-504 (1997).

Chapter 3: Distance Measurement on an Endogenous Membrane Transporter in *E. coli* Cells and Native Membranes Using EPR Spectroscopy[1*]

3.1 Abstract

Membrane proteins may be influenced by environment, and they may be unstable in detergents or fail to crystallize. As a result, approaches to characterize structure in a native environment are highly desirable. Here, we report a novel general strategy for precise distance measurements on outer membrane proteins in whole Escherichia coli cells and isolated outer membranes. In this work, the cobalamin transporter BtuB was overexpressed and spin labelled in whole cells and outer membranes and interspin distances were measured to a spin labelled cobalamin using pulse EPR. A comparative analysis of the data reveals a similar interspin distance distribution between whole cells, outer membranes and synthetic vesicles. This approach provides an elegant way to study conformational changes or protein-protein/ligand interactions for large outer membrane protein complexes in whole cells and native membranes, and provides a method to validate high-resolution structures of membrane proteins in their native environment.

***** This chapter is based on the publication Distance Measurement on an Endogenous Membrane Transporter in *E. coli* Cells and Native Membranes Using EPR Spectroscopy. Jospeh, B., Sikora, A., Bordington, E., Jeschke, G., Cafiso, D., Prisner, T. *Angew. Chem. Int. Ed. Engl.* **54**, 6196-99 (2015), and has been reformatted to departmental guidelines.

3.2 Introduction

Membrane protein function often depends upon local and global motions that occur over a wide range of time scales (from ps to ms). These motions may be modulated by the surrounding environment and tools to study membrane proteins under native conditions are of great value.[2] However, determining membrane protein structure or dynamics with high resolution in whole cells is challenging and yet to be demonstrated. DEER is a tool with the potential to examine conformational changes in biomolecules in the cellular environment.[3] DEER enables distance measurements in the 1.5-8 nm range between two paramagnetic centers with high precision and reliability.[4,5] It is more sensitive than NMR and there is no size limit to the protein of interest, both important features for in-cell spectroscopy.

Most biomolecules are not paramagnetic, and for EPR they must be modified with an appropriate spin label. Generally, labels are attached by covalently linking a MTSL to cysteines generated by site-directed mutagenesis.[6] Alternatively, spin probes may be incorporated using genetic encoding in response to a nonsense codon.[7,8] Both whole cell labeling of endogenously expressed proteins using MTSL and genetic encoding have been demonstrated in *E. coli*.[8,9] Distance measurements using DEER have also been performed by microinjection of spin labeled RNA, DNA, peptide and ubiquitin into eukaryotic cells.[10-14] However, the application of DEER on an endogenously expressed biomolecule (RNA, DNA or protein) has not been performed, primarily due to difficulties in obtaining high expression levels and the difficulties of specific and efficient labeling in a complex environment.

Here we introduce a general strategy to make accurate distance measurements on an arbitrary outer membrane protein in intact *E. coli* using DEER. Gram-negative bacteria are surrounded by a cell envelope (CE) composed of an OM and a CM separated by a periplasmic space containing a thin peptidoglycan layer. The OM is intrinsically asymmetric and is composed of phospholipids (PL), LPS and numerous β-barrel proteins that function in transport, signaling, motility, resistance to toxic compounds and membrane biogenesis.[15] The function of many of these proteins requires the presence of a PMF and an interaction with proteins in the periplasm or the CM. For cysteine labeling with MTSL, the target protein should lack reactive cysteines or have all the natural reactive cysteines replaced. Proteins in the OM of bacteria are generally free of reactive cysteines, thereby minimizing potential sources of non-specific signals.[9,16]

Here, we chose the high affinity (K_D < 1 nM)[17] CNCbl outer membrane transporter BtuB from *E. coli* as a model system to determine whether in-cell DEER can be performed on a membrane protein. BtuB belongs to the TBDT protein family that all require the inner membrane ExbB-ExbD-TonB complex and the PMF for function. A conserved segment near the N-terminus of BtuB termed the Ton box acts as an energy-coupling segment and is believed to interact with the C-terminal region of TonB to release substrate into the periplasm.[18] BtuB has been crystalized in apo-, vitamin B_{12}-bound[19] and TonB-bound[20] states. In these crystal structures the barrel is occluded with a central plug domain and the mechanism by which substrate is released is presently not known.

3.3 Results and Discussion

Typically, 200-300 copies of BtuB are expressed per *E. coli* cell when CNCbl is omitted from the medium[21], which is far below the level required for a DEER experiment (10-50 µM). Therefore we over expressed WT BtuB and the cysteine mutants 188C and 404C located on extracellular loops 2 and 7, as seen in Figure 1A and spin labeled the *E. coli* cells (termed whole cells) with MTSL. Reaction of the MTSL with cysteine forms the spin-labeled side chain R1 to produce 188R1 and 404R1 derivatives of BtuB.

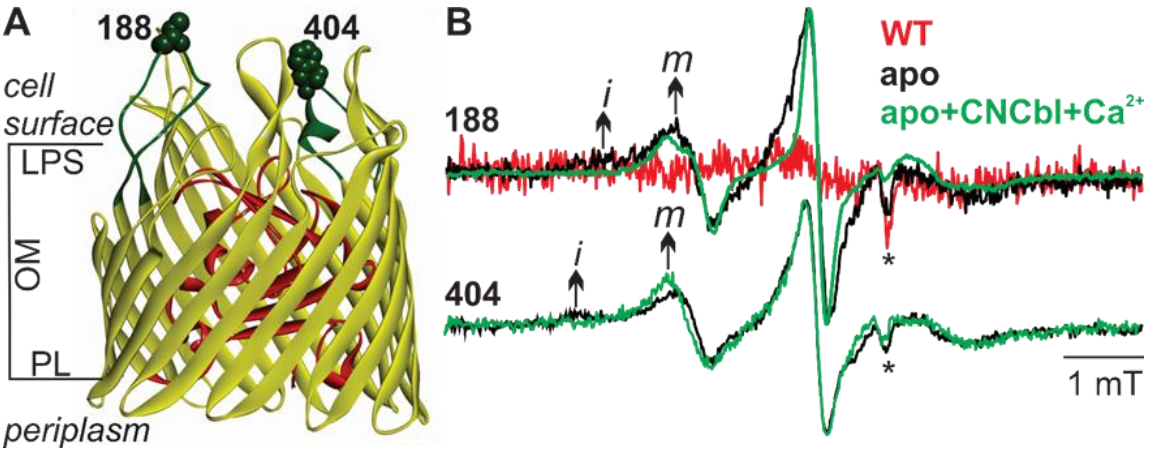

Figure 3.1: MTSL labeling of BtuB in live E. coli cells. A) Spin labeled positions (shown in space filling model) and the loops carrying them highlighted in green using PDB 1NQH. The core domain inside the barrel is in shown in red. B) X-band RT CW EPR spectra for MTSL-labeled *E. coli* expressing WT, 188C or 404C BtuB using a 20 µL suspension containing $2x10^9$ cells. For 188R1, the WT control and the apo- samples were measured under identical conditions for a quantitative comparison. The spectra of 188 apo+CNCbl+Ca^{2+} (100 µM CNCbl + 1 mM $CaCl_2$) is scaled to the intensity of 188-apo sample. Calcium increases the affinity of substrate binding. For position 404, the spectra are scaled to the same intensity. The arrow indicates the mobile (*m*) and the immobile (*i*) components in the spectra and the asterisk indicates artifacts from sample tubes.

The X-band, 9.4 Gigahertz (GHz), CW-EPR of whole cells is shown in Figure 3.1B and yielded a two-component spectrum composed of a mobile and an immobile component (marked '*m'* and '*i'*) for both 188R1 and 404R1. These two components are resolved due

to their different correlation times and suggests the existence of two distinct modes of R1 motion at these positions in whole cells. When calcium (Ca^{2+}) or CNCbl and Ca^{2+} were added to the *E. coli*, the immobile components vanish, and for 188R1 the spectra narrowed as a result of greater averaging of the magnetic anisotropy of R1 reflecting an increased motion of the loop. This observation indicates that overexpression does not affect the ability of BtuB to bind the ligand and undergo conformational changes. An earlier study with 188R1 reconstituted in 1-palmitoyl-2-oleoylphosphatidylcholine (POPC) vesicles revealed a different line shape and the presence of the ligands reduced loop mobility (Figure 3.2), showing that the dynamics and conformational changes are modulated by the surrounding environment [22]. Unlike the poor stability of nitroxide spin labels against reduction observed inside the cells[8,10,23] the signal intensity for both 188R1 and 404R1 was stable for at least 7 hours when the cells were kept on ice. When WT BtuB was expressed at levels comparable to the mutants (Table 3.1), the EPR signal was very weak indicating that most of the signal from the cysteine mutants originated from specific reaction with the MTSL. In contrast to residues 188 and 404 that face the cell surface, residue 10 in the Ton box that faces the periplasm could not be labeled in whole cells, likely due to spin label reduction upon entry into the periplasm. Thus in whole cells, labeling is limited to those surface-exposed residues with direct access to MTSL from outside.

Table 3.1: Calculated labelling efficiency for BtuB cysteine mutants in intact E. coli cells and isolated outer membranes. Spin concentrations were estimated from the double integral of the room temperature CW EPR spectrum of MTSL labelled BtuB and the amount of BtuB was quantified using the TEMPO-CNCbl bound. A 15-20% error is estimated for the given values of BtuB labelling.

Position	[spin, µM] [A]	[BtuB, µM] [B]	% spin labelling[C]
WT whole-cell	below detection	25	Cys-less control
188 whole-cell	30	29	97%
WT - OM	77	21.5	Cys-less control
188 - OM	100	23	23
404 - OM	100	20	20

[A] MTSL labelled BtuB. [B] Obtained using TEMPO-CNCbl binding. [C] Calculated as ([B] / [A]) x 100.

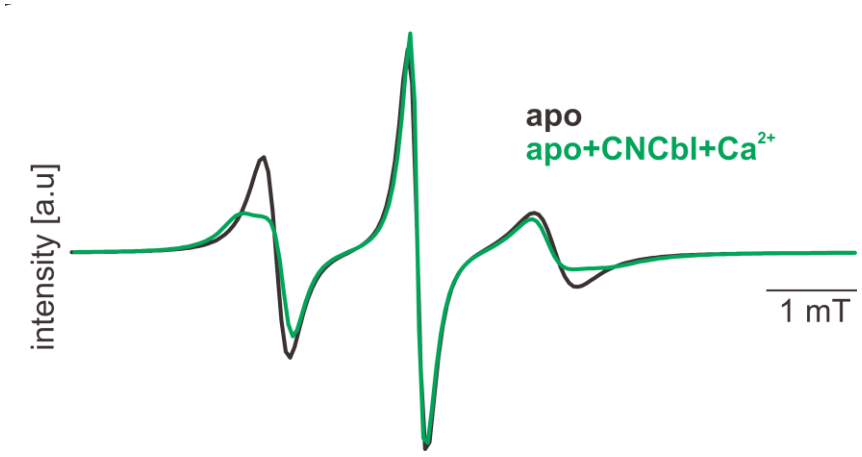

Figure 3.2: Cyanocobalamin mediated changes to BtuB loop position 188. 188R1 spectra in apo-state (black line) and in presence of 300 µM CNCbl and 1.4 mM Ca^{2+} (green) obtained in POPC vesicles. The data has been published previously.[21]

In addition to whole cells we also isolated CE membranes (OM+CM) following over expression of the protein. Our attempts to spin label BtuB in these CE membranes was not successful due to a high level of non-specific labeling. Positions 188 and 404 were tested and found to have identical spectra to the WT control samples (Figure 3.3A). Previously, it was shown that sites in the Ton box of BtuB (residues 6-12) could be labeled with the MTSL in isolated OM preparations.[16] Therefore, we prepared isolated OM membranes by selective removal of the CM with sarkosyl solubilization (see materials and methods).[16,24] As expected, removal of CM reduced non-specific labeling (Figure 3.3B). However, the spectra for 188R1 and 404R1 still contained significant contributions from non-specific signals, making a direct comparison to the in-cell or POPC spectra difficult. We succeeded in labeling position 399 on loop7 (see Figure 3.13) and position 10 in the Ton box at the periplasmic face (see Figure 3.11) for which labeling failed in whole cells.

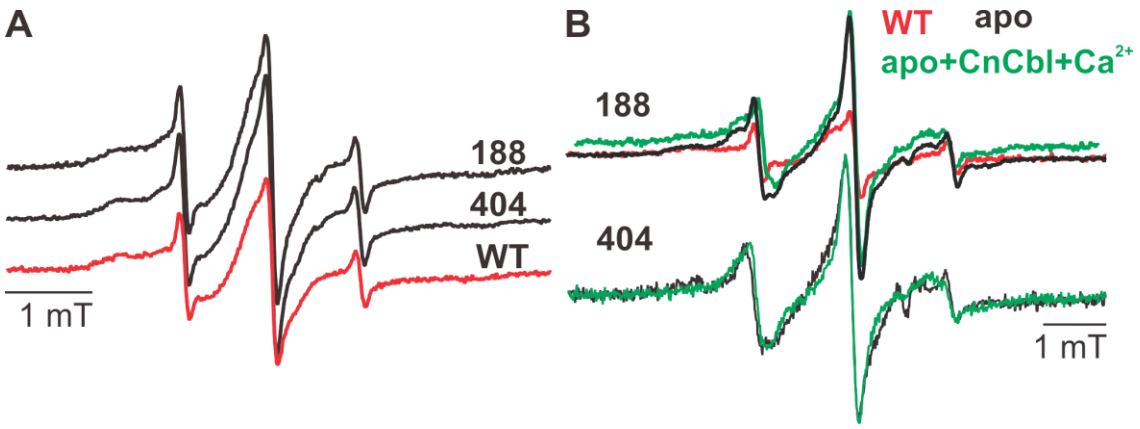

Figure 3.3: Labeling of BtuB in cell envelope (CE, OM+CM) and isolated OM. A) X-band CW-EPR spectra in CE. Membranes were isolated from a 1 L overnight culture of *E. coli* RK5016 cells expressing WT, 188C or 404C BtuB. MTSL labeling was performed as described in the materials and methods. The spectra were acquired under identical conditions for a quantitative comparison. Similar shape and intensity of the spectra for WT, 404R1 and 188R1 samples reveal a large non-specific signal. B) RT CW EPR spectra in OM. The CM was selectively removed by sarkosyl solubilization and MTSL labeling was performed on isolated OM. Even after removal of CM, a significant amount of signal originates from non-specific labeling as evident from the WT control spectrum. Addition of the ligands (100 µM CNCbl + 1 mM $CaCl_2$, the spectra are shifted for clarity) did not induce any visible changes for 188R1 spectra. For 404R1, the presence of these ligands induced changes similar to those observed in whole cells.

Non-specific spin-labeling influences DEER distance distributions if the resulting dipolar interactions are within the measureable range. If the non-specifically attached labels are far apart or the two cysteines on BtuB are only partially spin labeled, the modulation amplitude and the signal to noise (S/N) are reduced. Another complication could arise from overexpression if this promotes protein oligomerization or aggregation. In order to determine the feasibility of measuring DEER signals in native systems with intrinsic background signals, a (2,2,6,6-Tetramethylpiperidin-1-yl)oxyl (TEMPO)-labeled cyanocobalamin (Figure 3.4 A-E and Figure 3.7) was synthesized, which should yield a specific distance to another spin label on BtuB.

Figure 3.4: Synthesis and Characterization of TEMPO-CNCbl.

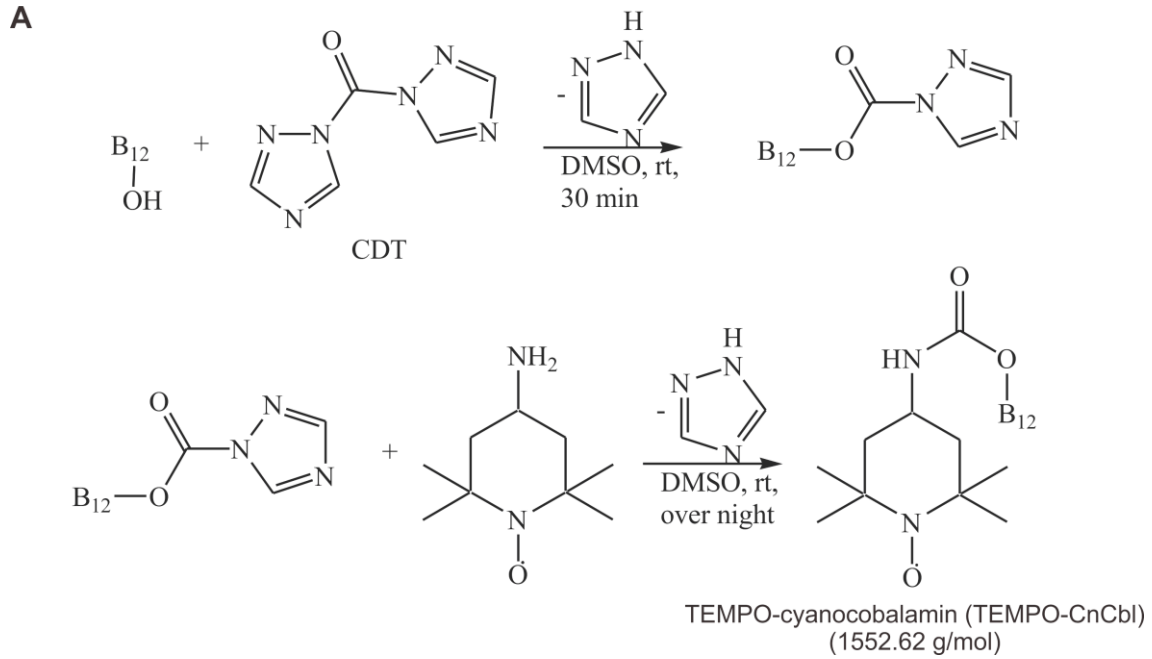

A) Reaction scheme for the attachment of 4-amino TEMPO to CNCbl, (1355.38 g/mol). CNCbl and CDT were incubated in DMSO at room temperature (rt) for 30 minutes. Following incubation, 4-amino TEMPO was added and incubated for overnight at room temperature and TEMPO-CNCbl (1552.62 g/mol) was purified as described in Materials and Methods.

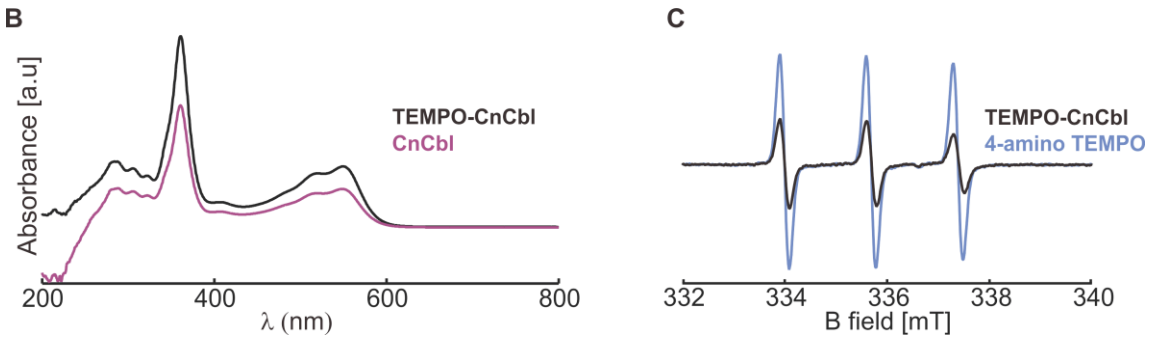

B) The UV-vis absorbance spectra for 50 µM CNCbl and 50 µM TEMPO-CNCbl (after precipitation, calculated with the molecular mass of TEMPO-CNCbl). Modification of CNCbl with TEMPO gives some changes in absorbance particularly at the lower wave lengths. A quantitative analysis by A_{361} (calculated with $\varepsilon = 27108\ cm^{-1}M^{-1}$ for CNCbl) revealed that the crude mixture contained only 31.8 µM cobalamin constituting 63.6% of the total weight. C) CW EPR spectra of the above sample compared to a 50 µM 4-amino-TEMPO standard. Quantitative analysis of the spectra (by double integration) reveals that crude reaction mixture contains 27 µM spins constituting 54% of the total weight, which is lower than the cobalamin content determined by UV. This reduction of cobalamin content from EPR determination is mostly due to a fraction of TEMPO-CNCbl existing in reduced from (see the high performance liquid chromatography (HPLC) data below).

D

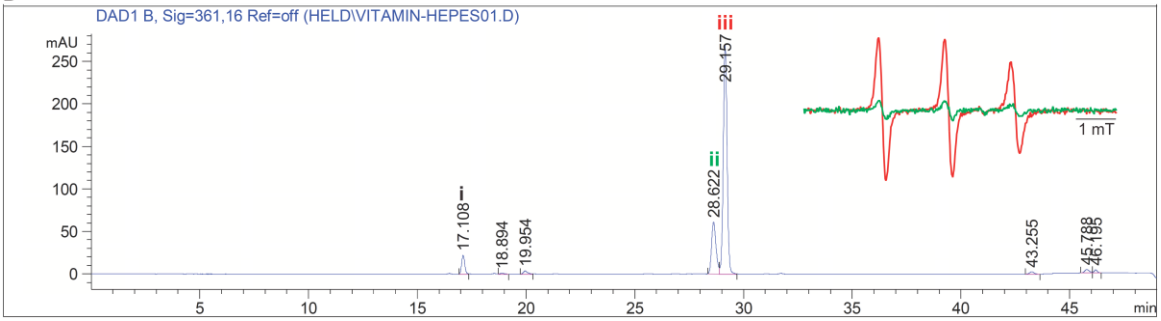

D) Reverse Phase (RP)-HPLC of TEMPO-CNCbl preparation (after precipitation) with detection at 316 nm. Peak at t_R = 17.108 (i) is unreacted CNCbl (1355.38 g/mol) as identified with the standard. Peaks at t_R = 28.622 (ii) and t_R = 29.157 (iii) are TEMPO-CNCbl peaks (1552.62 g/mol). RT CW EPR spectra of the peaks (ii) and (iii) are given as inset. Peak (ii) gave a very weak EPR signal, which most likely comes from small overlap with peak (iii) during fraction collection. Thus, peak (ii) contains TEMPO-CNCbl in a reduced form.

E

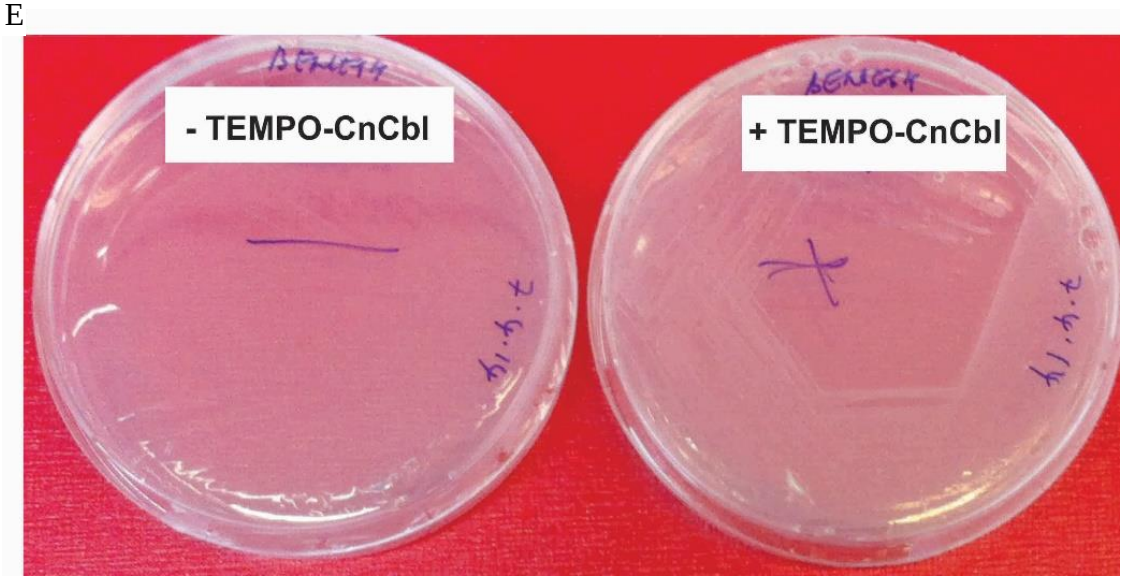

E) Growth assay for TEMPO-CNCbl with *E. coli* cells. *E. coli* strain RK5016 (*argH*, *btuB*, *metE*) cells can grow only in presence of methionine or CNCbl. Cells were grown for overnight on minimal media agar plates containing 0.24% w/v glucose, 150 µ*M* thiamine, 3 m*M* MgSO4, 300 µ*M* $CaCl_2$, 0.01% w/v of Arg and 1 µM TEMPO-CNCbl (peak (iii) separated from RP-HPLC in Figure 3.4D). Media containing TEMPO-CNCbl could support the growth of the cells, revealing that modification of CNCbl does not perturb its function.

TEMPO-CnCbl binds to both BtuB (Figure 3.5) and the periplasmic binding protein BtuF (Figure 3.6). Moreover, TEMPO-CNCbl supported the growth of *E. coli* RK5016 cells on minimal media (Figure 4H) indicating that the modification did not significantly disturb structure and function. Using the binding of TEMPO-CnCbl, we estimated the amount of BtuB in whole cells and OM (see materials and methods). For whole cells, we could achieve up to 30 µM BtuB concentration with 97% specific labeling, whereas for the OM preparations we obtain only 20-25% specific labeling due to a large background signal (Table3.1).

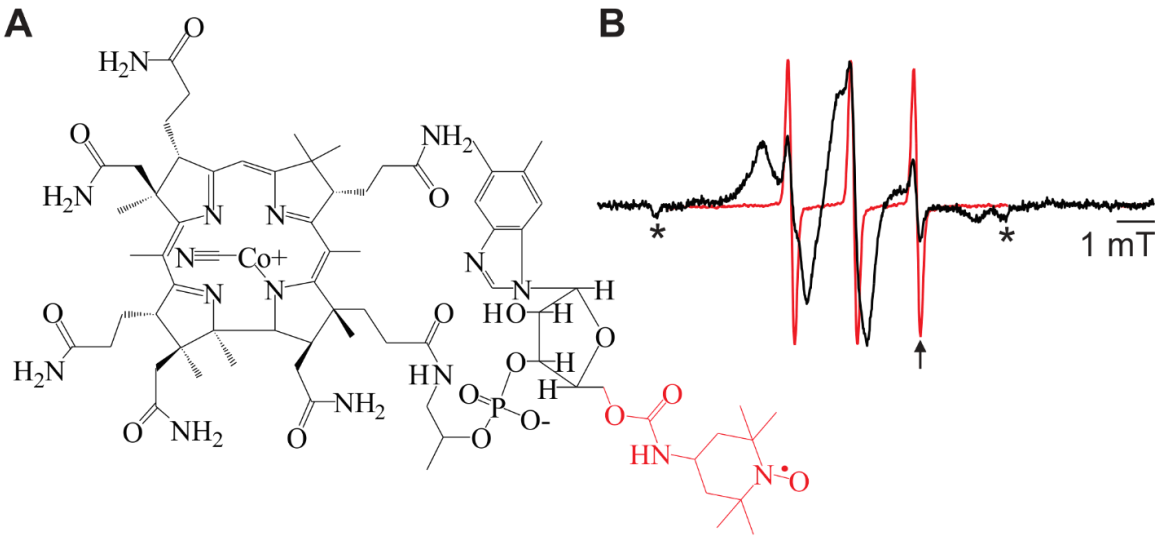

Figure 3.5: TEMPO-CNCbl structure and binding. A) Structure of TEMPO-CNCbl with the TEMPO and the bonds to the 5′ carbon of ribose highlighted in red. B) RT CW EPR spectra of 10 µM TEMO-CNCbl (red) or 10 µM TEMPO-CNCbl + 1 mM $CaCl_2$ + BtuB reconstituted in POPC vesicles (black). The arrow indicates the characteristic resonance position for the third hyperfine line of free TEMPO-CNCbl due to its smaller correlation time and the asterisks indicate artifacts from sample tubes.

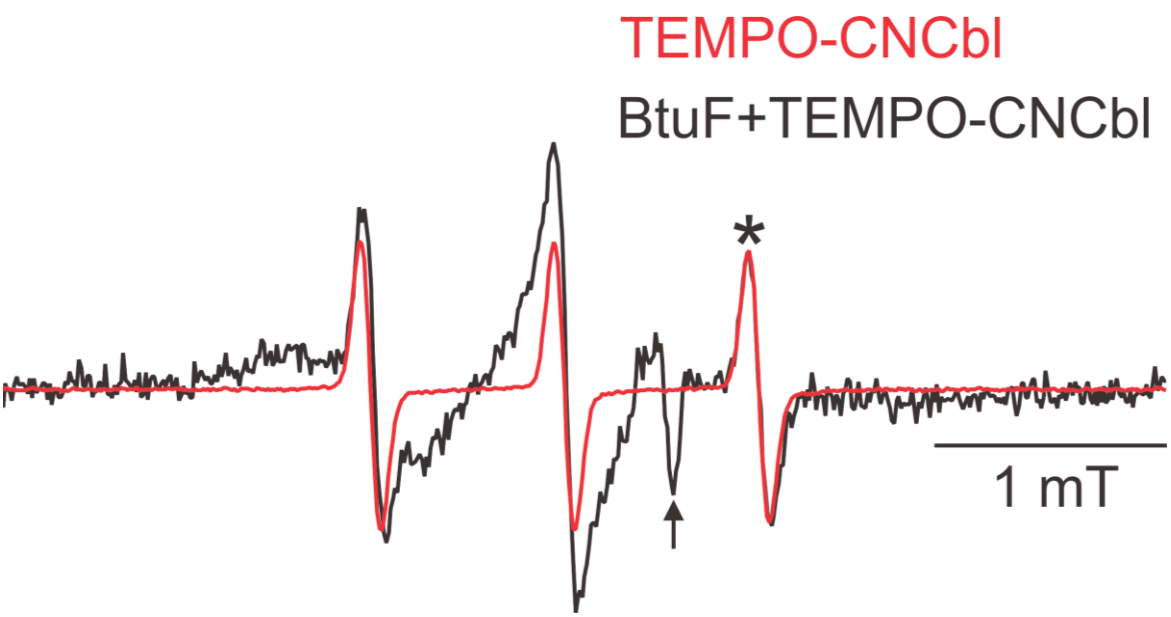

Figure 3.6: Binding of TEMPO-CNCbl with the periplasmic binding protein BtuF. BtuF is the periplasmic cobalamin binding protein, which delivers the substrate to the inner membrane ABC transporter BtuCD-F for transport into cytoplasm. The spectrum was obtained by mixing 40 µM BtuB with 10 µM TEMPO-CNCbl (black). The asterisk indicates the free (unbound) ligand, which is easily distinguished at the high-field hyperfine line. The spectrum of free TEMPO-CNCbl normalized to the high-field hyperfine line is shown for comparison (red). The arrow indicates an artifact from paramagnetic contaminant in the sample tube.

In a second step, we performed DEER measurements using 188R1 in whole cells, OM and reconstituted DLPC vesicles after addition of TEMPO-CNCbl (in 1:1 molar ratio to BtuB). The presence of 15% [D_8]glycerol significantly improved the spin echo decay both for whole cells and OM samples (Figure 3.8).

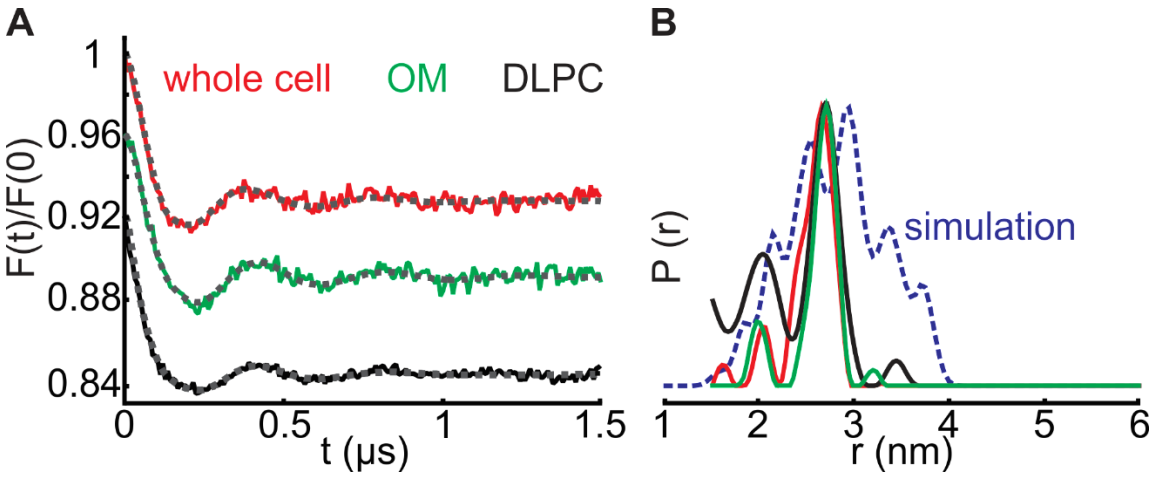

Figure 3.7: DEER between BtuB188R1 and TEMPO-CNCbl spin pairs in whole cells, OM and DLPC vesicles. The whole cells or outer membrane preparations contained 25-30 μM BtuB after MTSL labeling, and DEER was performed after adding an equal amount of TEMPO-CNCbl. A) Normalized form factors obtained after intermolecular background correction of the primary data (Figure 3.9 C-E) with the fittings overlaid (in dotted grey lines). B) Distance distributions calculated with the DeerAnalysis2013[25] software using Tikhonov regularization of the form factors. The Tikhonov regularization parameter α was set to 10 with a 3D spin distribution. In DLPC, the modulation amplitude obtained is not directly comparable to the other samples due to the bidirectional orientation and unknown concentration of BtuB. Even with a large fraction of non-specific labeling (Table 3.1) the OM sample gave ~8% modulation amplitude. Although devoid of non-specific signals, whole cell samples as well gave similar modulation amplitudes, which might be due to the transport of a fraction of TEMPO-CNCbl into the periplasm. The blue line shows the MMM simulation[26] (www.epr.ethz.ch/software/index) for DEER between 188R1 and TEMPO-CNCbl on PDB 1NQH.

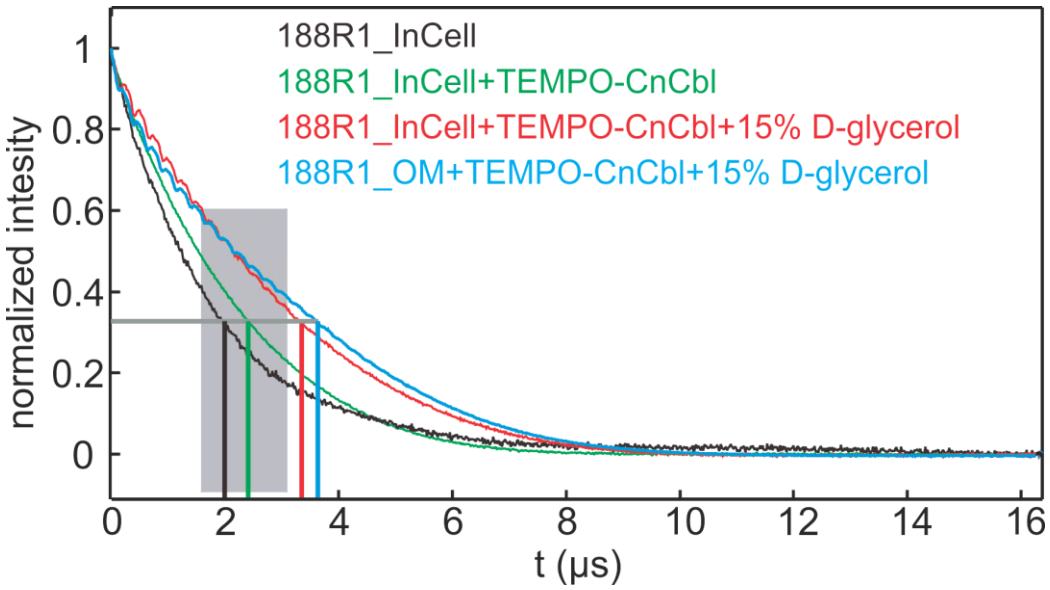

Figure 3.8: Spin echo decay in whole cells and OM. The data were obtained at 50K by observing at the maximum of the field swept echo at Q-band frequency using a π/2 - π pulse sequence with 500 ns inter pulse delay, which was increased by 8 ns for 1024 steps. The grey highlighted area indicates the range of $\boldsymbol{\tau}_2$ values used in the DEER experiments. The vertical lines indicate the 1/e time, which is approximately equal to the transverse relaxation time (T_2). A reduction of the echo decay rate when TEMPO-CNCbl is added to 188R1 in whole cells (green) is probably due to a slow relaxation of the TEMPO-CNCbl in the binding pocket. Addition of deuterated glycerol (D-glycerol) significantly improved the echo decay for both OM and whole cells.

In the absence of TEMPO-CNCbl, both whole cells and OM gave only an exponentially decaying signal (Figure 3.9 A,B), demonstrating that overexpression of BtuB does not cause oligomerization or aggregation and that the non-specific labeling particularly in the OM results in spins spatially separated by distances longer than 7 nm.

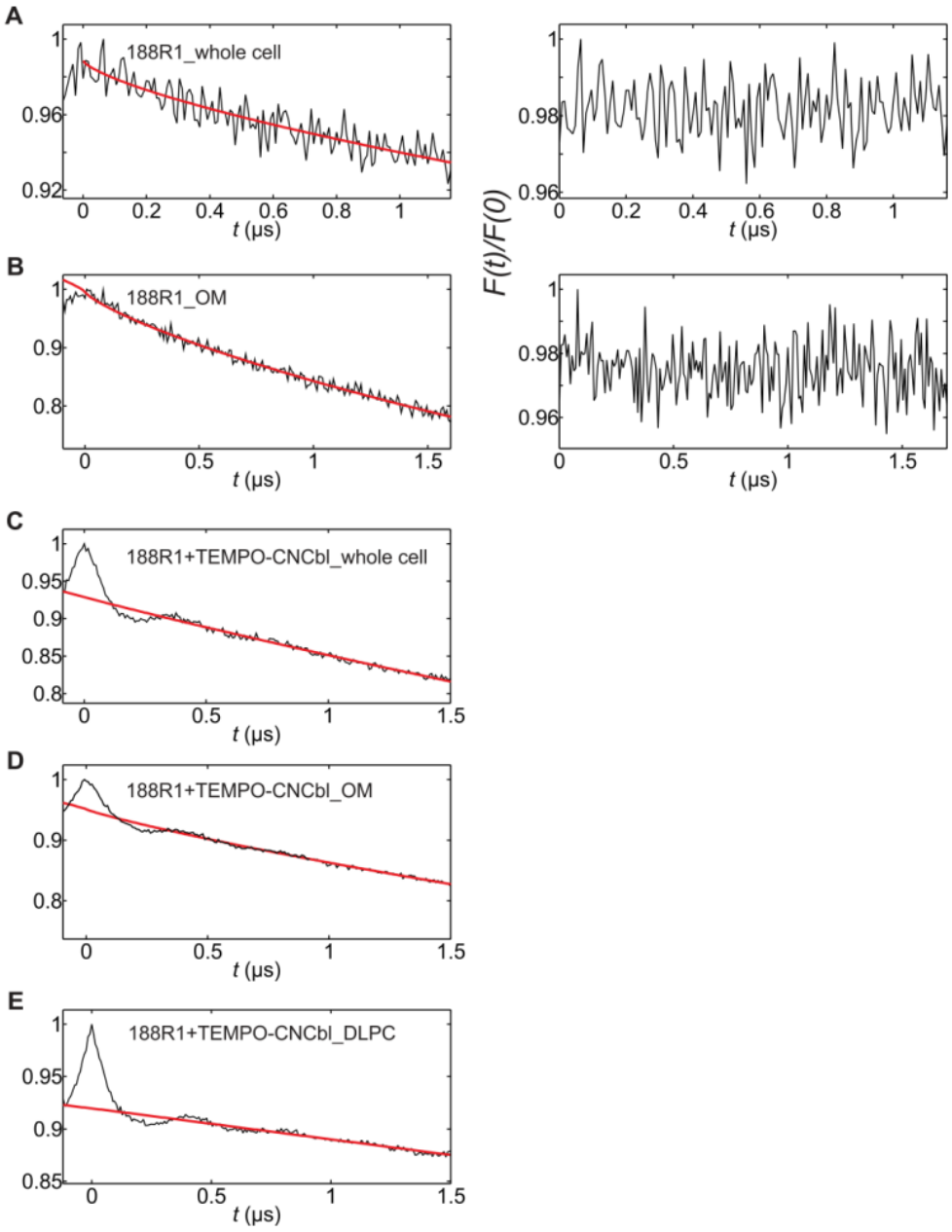

Figure 3.9: Q-band DEER between 188R1 and TEMPO-CNCbl in whole cells and OM. A, B) Normalized primary data *V(t)/V(0)* from DEER with 188R1 in whole cells and OM respectively are given on the left with an exponentially decaying intermolecular background (red lines). Corresponding form factors *F(t)/F(0)* obtained after removal of the background with DeerAnalysis2013 software.[25] C,D,E) Normalized primary data *V(t)/V(0)* from DEER between 188R1 and TEMPO-CNCbl in whole cells, OM and DLPC vesicles respectively with an exponentially decaying intermolecular background (red lines). The corresponding form factors and distance distributions are shown in Figure 3.7.

In presence of TEMPO-CNCbl, whole cells gave a DEER trace yielding a bimodal distance distribution with mean values at 2.02 ± 0.07 and 2.60 ± 0.15 nm respectively (Figure 3.7). Despite the dramatic differences in the surrounding environments, the measured distance distributions in whole cells, OM and 1,2-diauroyl-*sn*-glycero-3-phosphocholine (DLPC) vesicles were similar. Remarkably, even with a large amount of non-modulated signals from nonspecific labeling, OM preparations gave clean DEER traces, confirming that there is specific binding of TEMPO-CNCbl to BtuB. To compare the experimental data with the crystal structure, we computed 188R1 - TEMPO-CNCbl distance distributions in BtuB-CNCbl structure (PDB 1NQH) using rotamer libraries calculated for R1[28] and TEMPO-CNCbl (see materials and methods). In addition to distances seen experimentally, simulations revealed the presence of longer distances (Figure 3.7), which arose primarily from rotamers of TEMPO-CnCbl seen in the crystal-structure based simulation that were not populated in the membrane environment (Figure 3.10).

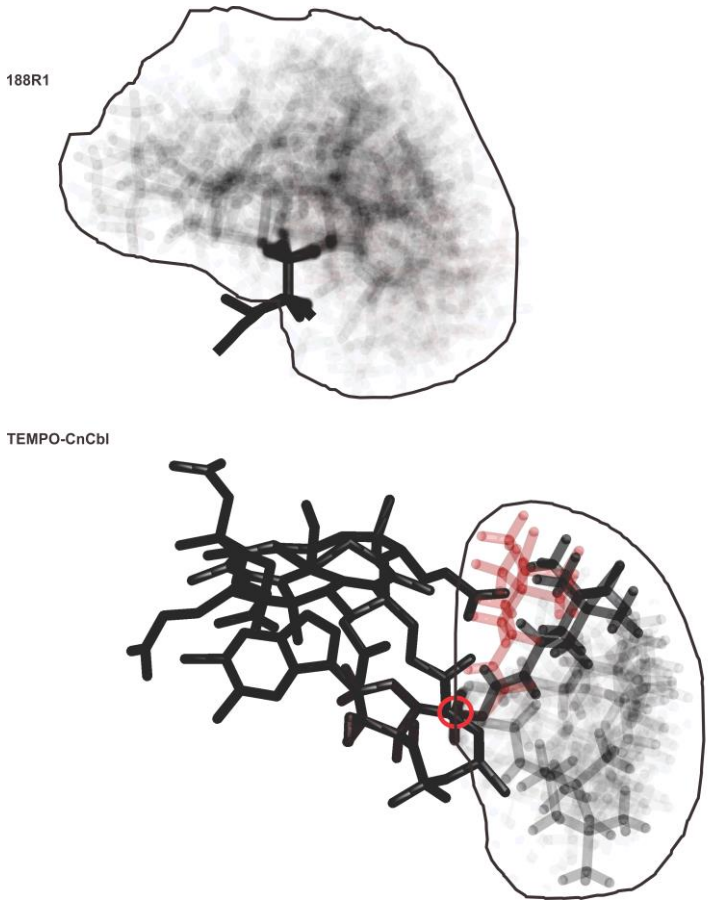

Figure 3.10: Simulation of rotamers for 188R1 and TEMPO-CNbl. The rotamers were calculated on the BtuB-CNCbl crystal structure (PDB 1NQH) as described in Materials and Methods. For clarity all residues except position 188 and CNCbl carrying the spin labels (R1 side chain and TEMPO respectively) are hidden. The predicted rotamers (115 and 24 rotamers respectively for 188 and CNCbl) lie inside the area marked by black curves. The rotamers contributing to the experimentally detected distances (see Figure 3.7) were computed with the "any rotamers" function available in MMM2014 software (http://www.epr.ethz.ch/software/index) and are highlighted in red.[26] For position 188, the identified rotamers are distributed over the entire area (hence lower intensity for the color). For TEMPO-CNCbl, only few of the simulated rotamers contribute to the experimental distance. The red circle inside TEMPO-CNCbl indicate the 5' carbon of the ribose moiety to which TEMPO is attached.

To determine whether distances could be measured to sites that were not labeled in whole cells, we attempted DEER across the OM between 10R1 located in the Ton box and TEMPO-CNCbl (Figure 12A).

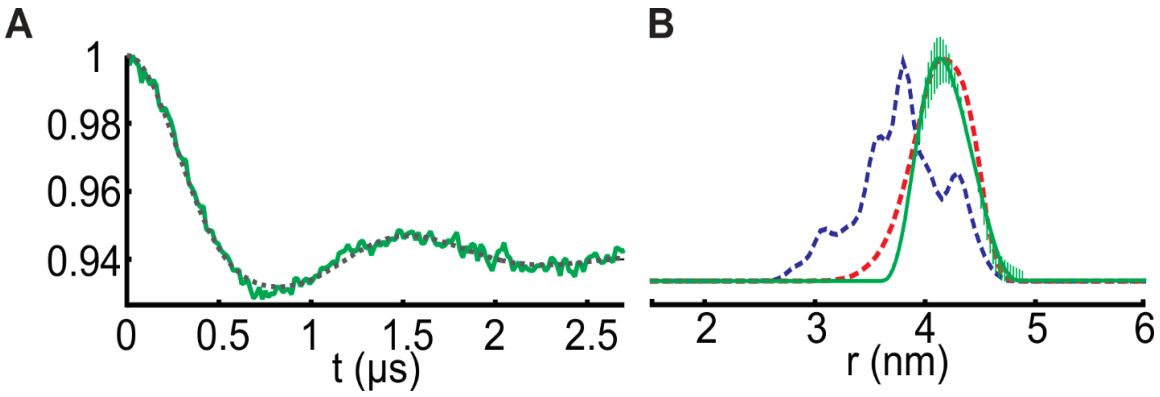

Figure 3.11: DEER between BtuB10R1 and TEMPO-CNCbl spin pairs in OM. A) Normalized form factor obtained after intermolecular background correction of the primary data (Figure 3.12B) with the fitting overlaid (in dotted grey lines). B) Distance distributions calculated with the DeerAnalysis2013 software using Tikhonov regularization of the form factor.[25] The vertical bars shows the full variation of the probability of a given distance when the beginning of the background was varied between 600-1000 ns in 11 steps with a 3D spin distribution and the Tikhonov regularization parameter α set to 10. The blue dotted line is the distance distribution obtained from the simulation for DEER between 10R1 and TEMPO-CNCbl using BtuB-CNCbl structure (PDB 1NQH). The red dotted line is an additional simulation using the "any rotamers" function in MMM software (www.epr.ethz.ch/software/index), in which the side chain packing is disregarded to match the experimental data.

Figure 3.12: DEER data between V10R1 and TEMPO-CNCbl in OM.

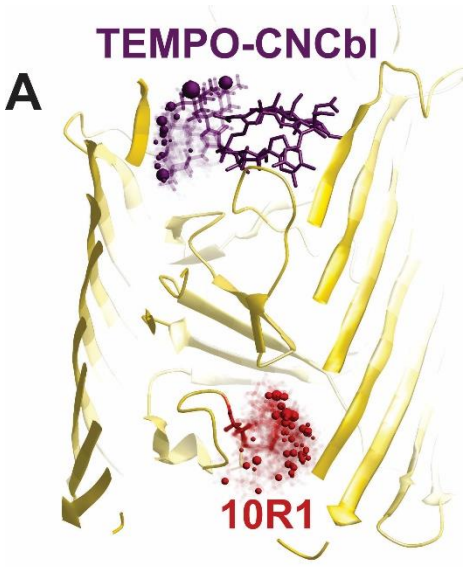

A) Position 10 and TEMPO-CNCbl highlighted with the simulated rotamers on the BtuB-CNCbl crystal structure (PDB 1NQH) using MMM2014 software (http://www.epr.ethz.ch/software/index).[26] The residues of the structure at the front surface was depth cued to visualize the rotamers clearly. The balls indicate the midpoints of N-O bonds and their size corresponds to the probability for each rotamer.

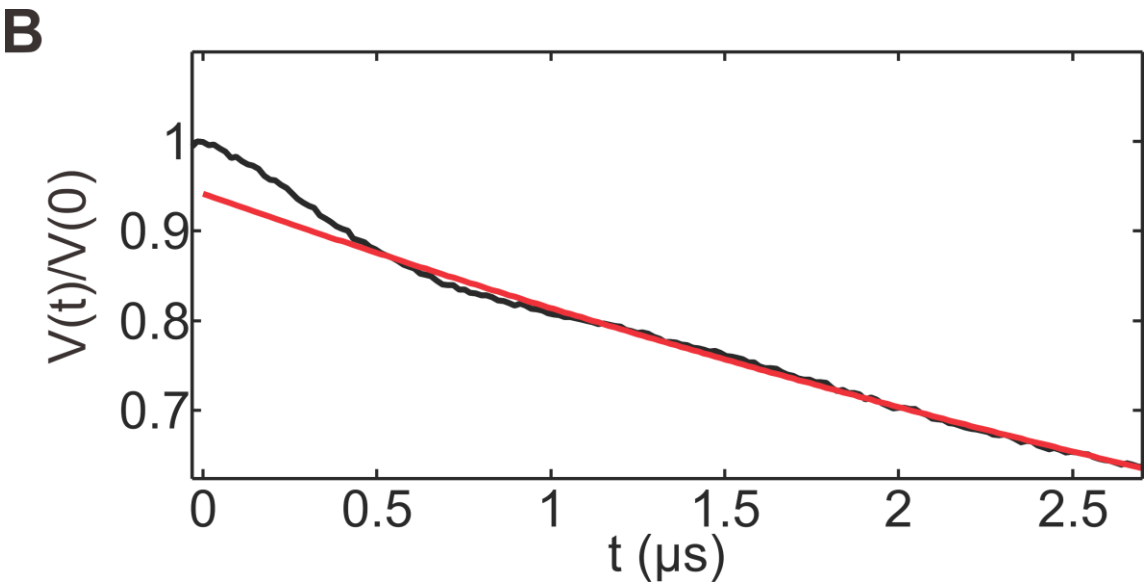

B) Normalized primary data $V(t)/V(0)$ for DEER between V10R1 and TEMPO-CNCbl in OM with an exponentially decaying intermolecular background (red lines) fitted with DeerAnalysis2013 software.[25] The corresponding form factor and the distance distribution is shown in Figure 3.11.

Interestingly, DEER gave a single distance with mean value at 4.17 ± 0.21 nm (Figure 3.11). Simulations on BtuB-CNCbl structure (1NQH) revealed a distance distribution between 2.6-4.75 nm with mean distance at 3.78 ± 0.40 nm (Figure 3.11). This discrepancy with experimental data may be accounted for by the differences in side chain packing predicted in the crystal structure when compared to the OM (red line in Figure 3.4). Additionally, DEER between spin labels attached to loop2 and loop7 (Figure 3.13) in OM indicates that this approach can be used to follow conformational changes of the loops and other flexible regions in native environments.

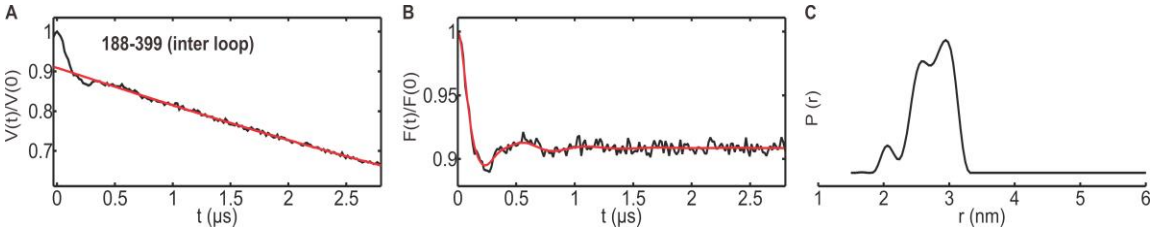

Figure 3.13: DEER between 188R1 and 399R1 in OM. A, B) Normalized Q-band DEER trace $V(t)/V(0)$ for DEER between 188R1 and 399R1 spin pairs in outer membranes with an exponentially decaying intermolecular background (red lines). B) Corresponding form factor $F(t)/F(0)$ obtained after removal of the background. C) Distance distribution obtained using Tikhonov regularization with DeerAnalysis2013 software.[25]

3.4 Conclusions:

In summary, we have demonstrated for the first time the application of DEER in complex whole cell and native membrane environments to extract precise distance constraints for an endogenously expressed membrane protein. In this study, the concentration of BtuB used (30 μM) corresponds to about 10^5 copies per cell, which is comparable to the expression level of some endogenous outer membrane proteins. A comparison of 188R1 and TEMPO-CNCbl DEER data between three different membrane environments indicates that lipid composition does not significantly influence loop conformation. Further measurements with other positions on BtuB will tell us whether this observation holds in general. OM preparations provide a versatile tool to study membrane proteins and unlike the alternate approaches such as nanodiscs,[27] it does not require the tedious processes of solubilization, purification and membrane reconstitution of the target protein. The approach presented here provides an opportunity to validate outer membrane protein structures and to make new structural and functional investigations of several outer membrane macromolecular complexes critical for Gram negative bacterial physiology under native conditions.

Contributions to the work

This work is a product of a great collaboration with many talented scientists. Dr. Jeschke preformed the calculations of the TEMPO-CNCbl rotomer library. Dr. Bordignon was instrumental with the purification and characterization of the TEMPO-CNCbl spin label. All protein purification, label optimization, mutation design and CW-EPR measurements were performed in the lab of Dr. Cafiso by Arthur Sikora. DEER measurements and CNCbl growth assays were performed by Dr. Joseph in the lab of Dr. Prisner

3.5 Materials and Methods

Mutagenesis and expression of BtuB

Plasmids harbouring wild-type or 10C, 188C, 404C and 188C-399C mutations in BtuB on a pUC8 backbone were engineered using the Agilent Technologies (Santa Clara, CA) QuikChange Site Directed Mutagenesis Kit. The mutants were overexpressed in the *E. coli* strain RK5016 (*argH*, *btuB*, *metE*).[28] Cells were grown for overnight in minimal media containing 100 μg/mL ampicillin and supplemented with 0.24% w/v glucose, 150 μ*M* thiamine, 3 m*M* MgSO4, 300 μ*M* $CaCl_2$, and 0.01% w/v of Met and Arg.

Isolation of membranes

Following overnight growth in 1 L minimal Media, the cells were pelleted at 6000 rpm for 10 minutes using Sorval SLA-3000 rotor. The cells were suspended in 30 mL of 10 μM HEPES buffer (pH 6.5) with 10nM 4-(2-Aminoethyl) benzenesulfonyl fluoride hydrochloride (AEBSF) and lysed with a French press 2-3 times. The cell debris were removed by centrifugation at 12,000 rpm for 20 minutes in Sorval SS-34 rotor and the supernatant was collected. To isolate the intact membrane or CE, which is composed of the OM plus the CM, the supernatant was centrifuged at 100,000 x g for 1.5 hours. To isolate outer membranes alone, the inner membrane was removed by adding 0.5% sarkosyl and the outer membranes were pelleted by centrifugation at 200,000 x g for 1.5 hour. Following centrifugation, the pellets were suspended into 10 mL of the same buffer.

Spin Labelling of E. coli cells and membranes

Following overnight growth, cells from 1 L culture were pelleted and suspended in 50 mL of 50 mM Tris buffer (pH 7.5g) containing 60 mM NaCl and 0.5% glucose and spin labelled with 20 µM MTSL (Toronto Research Chemicals, North York, ON, Canada) for 1 hour at room temperature. Following incubation, cells were pelleted and washed 2 times and suspended into 2.5 mL total volume with the same buffer and kept on ice. The membrane fraction was suspended in 10 mL of 50 mM Tris buffer (pH 7.5) with 60 mM NaCl and was spin labelled with 40 µM MTSL at room temperature for 1 hour. Following incubation, the membranes were washed until free spin label was completely removed and suspended into 500 µL of the same buffer.

Synthesis of spin labeled cyanocobalamin (TEMPO-CNCbl)

TEMPO-CNCbl was synthesized using a two-step reaction, in which the ribose-5'-hydroxyl was first activated with CDT and subsequently reacted with 4-amino TEMPO. Previously, this scheme was used for attaching cyanocobalamin to insulin.[29] The synthesis was performed under argon atmosphere using dry solvents. For the synthesis, 0.1 g of cyanocobalamin was dissolved in 50 mL DMSO and 0.036 g of 1,1′-Carbonyl-di-(1,2,4-triazole) (CDT, Sigma) was added and the reaction mixture was stirred for 30 minutes at room temperature. Following incubation, 0.13 g of 4-amino-TEMPO (Sigma) was added and the reaction mixture was stirred at room temperature for overnight. TEMPO-CNCbl was precipitated with 200 mL of 1:1 mixture of acetone and diethylether. The precipitate was centrifuged at 4^{o}C for 15 min at 4000 x g. The supernatant was precipitated again and the precipitate was removed by centrifugation as before. The pooled precipitate was

washed with acetone, centrifuged, dried overnight under air and afterwards freeze-dried. The yield of the crude product was 0.069 g corresponding to 69 % of the theoretical yield.

Purification and characterization of TEMPO-CNCbl

The crude reaction product was purified by HPLC (Agilent 1200 series) on a BDS-C18 column (5 µM, 2x250 mm from Hewlett-Packard) with detection at 254 and 316 nm. An 8 µL volume of a 1 mM stock of the TEMPO-CNCbl was injected and eluted with 1 mL/min flow rate with 400 bar pressure at room temperature. The following solvent system was used for elution: solvent A: water; solvent B: methanol and elution was performed at a linear gradient of 15-60% B in 40 min. MALDI-ToF –MS measurements were performed on a Voyager STR Workstation DE pro (Applied Biosystems) with 100 kW laser (337 nm) peak power using a matrix made of 2,5 Dihydroxybenzoic acid and 6-Aza-thiothymine. The LC-ESI-MS measurements were performed either with a ThermoFisher Surveyor MSQ or Shimadzu LCMS-2020 system. A 50:50 (v/v) mixture of methanol/water (ThermoFisher) or 0.1% acetonitrile/formic acid (Shimadzu) solvent system was used for column elution. Other conditions: capillary voltage - 3-4 kV, dry gas (N_2) pressure - 5 bar, mass range 80-2000 Da, detection: single quad.

Growth assay with TEMPO-CNCbl

E. coli strain RK5016 (*argH, btuB, metE*) cells,[28] which can grow only in presence of methionine or CNCbl, was grown at 37ºC for overnight on minimal media A agar plates containing 0.24% w/v glucose, 150 µ*M* thiamine, 3 mM MgSO4, 300 µM $CaCl_2$, 0.01% w/v of Arg and 1 µM TEMPO-CNCbl (peak (iii) separated from RP-HPLC shown in

Figure 3.4D). Following incubation, the ability of TEMPO-CNCbl to support growth was confirmed by observing for colony formation on the plates. TEMPO-CNCbl was used to estimate BtuB in OM and whole cells after overexpression. When bound to BtuB, TEMPO-CNCbl produces a broad CW EPR spectrum (Figure 3.5). Any free TEMPO-CNCbl can be easily quantified by measuring the intensity of its high-field hyperfine line, which stands out from the baseline without significant overlap with the signals coming from BtuB-bound TEMPO-CNCbl. This method works only if the K_D of this interaction is much lower than the total concentration of BtuB and TEMPO-CNCbl. Cyanocobalamin binds to BtuB with high affinity (K_D < 1 nM)[17] and it is possible that its modification with TEMPO increases K_D. We did not observe any EPR signal corresponding to free (unbound) form when 10 µM TEMPO-CNCbl was added to whole cells or outer membrane preparations, indicating that the K_D for the interaction is lower than 10 µM. Thus we added increasing amounts of TEMPO-CNCbl to whole cells and OM and quantified free TEMPO-CNCbl if any, by comparing the intensity of the high-field hyperfine line with that for an external standard (100 µM 4-amino TEMPO). The amount of BtuB ([BtuB]) was estimated by subtracting the amount of free-TEMPO-CNCbl from the total amount of TEMPO-CNCbl added. For whole cells, 100 µM CCCP (carbonyl cyanide 3-chlorophenylhydrazone, Sigma) was added to eliminate the proton motive force (pmf) and prevent transport of TEMPO-CNCbl into the periplasm. The spin concentration ([spin]) after MTSL labelling of whole cells or OM was calculated from the double integral of the RT CW EPR spectra using an external standard (100 µM 4-amino TEMPO). The labelling efficiency for whole cells or OM was calculated by multiplying the ratio of [BtuB] (obtained using TEMPO-CNCbl) to [spin] (from the double integral of the MTSL labelled OM or whole cells) with 100. Here it is

assumed that all BtuB present in whole cells or OM are labelled with MTSL. The modulation amplitudes obtained,~ 8 %, in our DEER experiments with OM samples are in agreement with this assumption.

Calculation of rotamer library for TEMPO-CNCbl

A rotamer library for TEMPO-labelled vitamin B_{12} was generated on the basis of a Density Functional Theory (DFT) computation of the geometry of 5'-labelled ribose and a Monte Carlo search of torsion angles space. The DFT computation was performed on spin-restricted Kohn-Sham B3LYP/VDZP level with ORCA 2.8.[30] In Monte-Carlo sampling torsion angles of five rotatable bonds starting with the 4'-5' bond of ribose were varied. Torsion and non-bonding interaction potentials were taken from the universal force field (UFF)[31] and all bond lengths and bond angles were kept fixed. The torsion potentials were considered in random selection of test conformations by assuming a Boltzmann distribution at 298 K. An estimate for the minimum non-bonding energy was obtained from a pre-run with 1'000'000 Monte Carlo trials. In the production run, only conformations were accepted with a non-bonding energy that led to at least 1% of the Boltzmann population of the conformation with minimum non-bonding energy that was encountered during the pre-run. The ensemble of 20'000 of such low-energy conformations was reduced to 144 rotamers by hierarchical clustering in torsion-angle space. The UFF non-bonding energy between rotamer atoms on the one hand and vitamin B_{12} atoms not included in the rotamer construct as well as protein atoms on the other hand is considered during attachment of the rotamers with the MMM software (www.epr.ethz.ch/software/index), omitting the phosphorus atom of vitamin B_{12} that is directly bonded to the construct. Rotamers are attached by

superposition of a right-handed coordinate frame defined by C4' (origin), the ring oxygen (on the *x* axis), and C3' (in the xy plane) of ribose. Quality of the geometry resulting from such attachment was tested on PDB structures 1CCW, 1EGM, 1ET4, 1N2Z, 1N4A, 1NQH, 2GSK, 3M8D, and 4KKI. In most cases the remaining atoms common to the construct and vitamin B_{12} superimpose within a few tenths of an Angstrom or better. We note, however, that quality of the geometry of vitamin B_{12} in x-ray crystal structures of proteins may not be as good as backbone and side group geometry of the protein itself, which could lead to a somewhat larger prediction error for distance distributions compared to the case where both labels are attached to cysteine residues.

CW-EPR and DEER measurements

CW-EPR measurements were performed at X-band frequency (9.4 GHz) using a Bruker E500 spectrometer equipped with a TE102 cavity. Experimental parameters: 100 kHz modulation frequency, 0.15 milli Tesla (mT) modulation amplitude, 0.2 mW microwave power, 20.48 ms time constant, 81.92 ms conversion time, 1024 points, 15 mT sweep width. The EPR signal was recorded as the first derivative of the absorption signal.

For DEER measurements, 15-20 µL of whole cells or OM samples with TEMPO-CNCbl at 1:1 molar ratio (when present) containing 15% deuterated glycerol was transferred into 1.6 mm outer diameter quartz EPR tubes (*Suprasil*, Wilmad LabGlass). Pulsed EPR data were recorded on an ELEXSYS E580 EPR spectrometer (Bruker) equipped with a DEER unit (E580-400U, Bruker), a continuous-flow helium cryostat (CF935, Oxford Instruments), and a temperature control system (ITC 502, Oxford Instruments). Experiments were performed at Q-band frequencies (33.7 GHz) using an ELEXSYS SuperQ-FT accessory unit and a Bruker AmpQ 10 W amplifier with a Bruker EN5107D2

cavity at 50 K. For DEER experiments, the dead-time free four-pulse sequence with phase-cycled π/2-pulse was used.[32] Typical pulse lengths were 32 ns (π/2 and π) for the observer pulses and 20 ns (π) for the pump pulse. The pump pulse was set to the maximum of the echo-detected field swept spectrum and the observer pulses were set 60 MHz lower. The deuterium modulations were averaged by increasing the first interpulse delay by 16 ns for 8 steps. To obtain distance distributions, the normalized primary DEER data $V(t)/V(0)$ were processed to remove the background function from intermolecular interactions and the resulting form factors $F(t)/F(0)$ were fitted with a model-free Tikhonov regularization to distance distributions with DeerAnalysis2013 software package.[25] The MMM 2014 software package was used for *in silico* spin labeling and simulation of distance distributions based on the crystal structures using a rotamer library approach.[26]

3.6 References

1. Jospeh, B., Sikora, A., Bordington, E., Jeschke, G., Cafiso, D., Prisner, T. Distance Measurement on an Endogenous Membrane Transporter in *E. coli* Cells and Native Membranes Using EPR Spectroscopy. *Angew. Chem. Int. Ed. Engl.* **54**, 6196-99 (2015).

2. McHaourab, H. S., Steed, H. S. & Kazmier, K. Toward the foourth dimesnsion of membrane protein structure: insight into dynamics from spin-labeling EPR spectroscopy. *Structure.* **19**, 1549-61 (2011).

3. Hansel, R., Luh, L. M., Corbeski, I., Trantirek, L. & Dotsch, V. In-cell NMR and EPR spectroscopy of biomacromolecules. *Angew. Chem. Int. Ed. Engl.* **53**, 10300-14 (2014).

4. Jeschke, G. DEER distance measurements on proteins. *Annu. Rev. Phys. Chem.* **63**, 419-46 (2012).

5. Schiemann, O. & Prisner, T. F. Long-range disatnce determinations in biomacromoleccules by EPR spectroscopy. *Q. Rev. Phys. Chem.* **63**, 1-53 (2012).

6. Hubbell, W. L. & Altenbach, C. Investigation of structure and dynamics in membrane proteins using site-directed spin labeling. *Current Opinion in Structural Biology* **4**, 566-573 (1994).

7. Fleissner, M. R., Brustad, E. M., Kalai, T., Altenbach, C., Cascio, D., Peters, F. B., Hideg, K., Peuker, S., Schultz, P. G. & Hubbell, W. L. Site-directed spin labeling of a genetically encoded unnatural amino acid. *Proc. Nat.l Acad. Sci. U.S.A.* **106**, 21637-42 (2009).

8. Schmidt, M. J., Borbas, J., Drescher, M. & Summerer, D. A genetically encoded spin label for electron paramagnetic resonance distance measurements. *J. Am. Chem. Soc.* **136**, 1238-41 (2014).

9. Jiang, X., Payne, M. A., Cao, Z., Foster, S. B., Feix, J. B., Newton, S. M. & Klebba, P. E. Ligand-specific opening of a gated-porin channel in the outer membrane of living bacteria. *Science.* **276**, 1261-4 (1997).

10. Krstic, I., Hansel, R., Romainczyk, O., Engels, J. W., Dotsch, V. & Prisner, T. F. Long-range distance measurements on nucleic acids in cells by pulsed EPR spectroscopy. *Angew. Chem. Int. Ed. Engl.* **50**, 5070-4 (2010).

11. Azarkh, M., Singh, V., Okle, O., Seemann, I. T., Dietrich, D. R., Hartig, J. S. & Drescher, M. Site-directed spin-labeling of nuleotides and the use of in-cell EPR to determine long-range distances in a biologially relevant enviroment. *Nat. Protoc.* **8**, 131-147 (2013).

12. Qi, M., Gross, A., Jeschke, G., Godt, A. & Drescher, M. Gd(III)-PyMTA label is suitable for in-cell EPR. *J. Am. Chem. Soc.* **136**, 15366-78 (2014).

13. Igarashi, R., Sakai, T., Hara, H., Tenno, T., Tanaka, T., Tochio, H. & Shirakawa, M. Distance determination in proteins inside *Xenopus laevis* oocytes by double electron-electron resonance experiements. J. *Am. Chem. Soc.* **132**, 8228-9 (2010).

14. Martorana, A., Bellapadrona, G., Feintuch, A., Di Gregorio, E., Aime, S. & Goldfarb, D. Probing protein conformation in cells by EPR distance measurements using Gd^{3+} spin labeling. *J. Am. Chem. Soc.* **136**, 13458-65 (2014).

15. Fairman, J. W., Noinaj, N. & Buchanan, S. K. The structural biology of β-barrel membrane proteins: a summary of recent reports. *Curr. Opin. Struct. Biol.* **21**, 523-31 (2011).

16. Merianos, H. J.,Cadieux, H., Lin, C. H., Kadner, R. J. & Cafiso, D. S. Sunstrate-induced exposure of an energy-coupled motif of a membrane transporter. *Nat. Struct. Biol.* **7**, 205-9 (2000).

17. Bradbeer, C., Reynolds, P. R., Bauler, G. M. & Fernandez, M. T. A requirement for calcium in the transport of cobalamin across the outer membrane of *Escherichia coli*. *JBC.* **261**, 2520-3 (1986).

18. Heller, K. J., Kadner, R. J. & Gunther, K. Suppression of the btuB451 mutation by mutations in the tonB gene suggests a direct interaction betweeb TonB and TonB-dependent receptor proteins in the outer membrane of *Escherichia coli*. *Gene*. **64**, 147-53 (1988).

19. Chimento, D. P., Mohanty, A. K., Kadner, R. J. & Wiener, M. C. Substrate-induced transmembrane sgnaling in the cobalamin transporter, BtuB. *Nat. Struct. Biol.* **10**, 394-401 (2003).

20. Shultis, D. D., Purdy, M. D., Banchs, C. N & Wiener, M. C. Outer membrane active transport: structure of the BtuB:TonB complex. *Science.* **312,** 1396-9 (2006).

21. Di Masi, D. R., White, J. C., Schnaitman, C. A. & Bradbeer, C. Transport of vitamin B12 in Escherichia coli: common receptor sites for vitamin B12 and the E colicins on the outer membrane of the cell envelope. *J. Bacteriol.* **115**, 506-13 (1973).

22. Kim, M., Xu, Q., Murray, D. & Cafiso, D. S. Solutes alter the onformation of the ligand binding loops in outer membrane transporters. *Biochemistry*. **47**, 670-9 (2008).

23. Japtap, A. P., Krstic, I., Kunjir, N. C., Hansel, R., Prisner, T. F. & Sigurdsson, S. T. Sterically shielded spin labels for in-cell EPR spectroscopy: analysis of stability in reducing enviroment. *Free. Radical. Res.* **49**, 78-85 (2015).

24. Filip, C., Fletcher, G., Wulff, J. L. & Earhart, C. F. Solubilization of the cytoplasmic membrane of *Escherichia coli* by the ionic detergent sodium-lauryl sarcosinate. *J. Bacteriol.* **115**, 717-22 (1973).

25. Jeschke, G., Chechik, V., Ionita, P., Godt, A., Zimmermann, H., Banham, J., Timmel, C. R., Hilger, D. & Jung, H. DeerAnalysis2006 – a comprehensive software package for analyzing pulsed ELDOR data. *Appl. Magn. Reson.* **Vol. 30**, 473-498 (2006).

26. Polyhach, Y., Bordignon, E. & Jeschke, G. Rotamer libraries of spin labelled cysteines for protein studies. *Phys. Chem. Chem. Phys.* **13**, 2356-66 (2011).

27. Bayburt, T. H. & Sligar, S. G. Membrane protein assembly into nanodiscs. *FEBS. Lett.* **584**, 1721-7 (2010).

28. Gudmundsdottir, A., Bell, P. E., Lundrigan, M. D., Bradbeer, C. & Kadner, R. J. Point mutations in a conserved region (TonB box) of *Escherichia coli* outer membrane protein BtuB affect vitamin B12 transport. *J. Bacteriol.* **171**, 6526-33 (1989).

29. Fazen, C. H., Valentin, D., Fairchild, T. J. & Doyle, R. P. Oral delivery of the appetite suppressing peptide hPYY(3-36) trough the vitamin B12 uptake pathway. *J. Med. Chem.* **54**, 8707-11 (2011).

30. Neese, F. The ORCA program system. *Wiley Interdisciplinary Reviews-Computational Molecular Science* **2**, 73-8 (2012).

31. Rappe, A. K., Casewit, C. J., Colwell, K. S., Goddard, W. A. & Skiff, W. M. UFF, a full periodic table force field for moleccular mechanics and molecular dynamics simulations. *JACS.* **114**, 10024-36 (1992).

32. Pannier, M., Veit, S., Godt, A., Jeschke, G. & Spiess, H. W. Dead-time free meadurement of dipole-dipole interactions between electron spins. *J. Magn. Reson.* **142**, 331-40 (2000).

Chapter 4: Ligand Induced Conformational Changes of a Membrane Transporter in *E. coli* Cells Observed with DEER[1*]

4.1 Abstract

An unrealized goal in structural biology is the determination of structure and conformational change at high resolution for membrane proteins within the cellular environment. DEER is a well-established technique to follow conformational changes in purified membrane protein complexes. Here we demonstrate the first proof of concept for the use of DEER to observe conformational changes in a membrane protein in intact cells. We exploit the fact that outer membrane proteins usually lack reactive cysteines and the fact that paramagnetic spin labels entering the periplasm are selectively reduced to achieve specific labeling of the cobalamin transporter BtuB in *Escherichia coli*. We characterize conformational changes in the second extracellular loop of BtuB upon ligand binding and compare the DEER data with high-resolution crystal structures. Our approach avoids detergent extraction, purification and reconstitution usually required for these systems. With this approach structure, function, conformational changes and molecular interactions of outer membrane proteins can be studied at high resolution in the cellular environment.

***** This chapter is based on the publication Ligand induced conformational changes of a membrane transporter in *E. coli* cells with PELDOR/DEER. Joseph B., Sikora A. & Cafiso D.S. *JACS*. **6**, 1844-47 (2016), and has been reformatted to departmental guidelines.

4.2 Introduction

Determining biomolecular structures and their conformational changes at high resolution has primarily been achieved with X-ray crystallography, NMR spectroscopy and more recently with cryo-electron microscopy (EM). In many cases these studies have provided detailed models for conformational transitions that drive function in many macromolecules including several membrane proteins. In almost all these cases, the structures have been obtained after isolating the target molecule from its native environment. This approach masks the effect of the cellular conditions such as molecular crowding, specific localization, interaction with other molecules/ions, pH or ionic gradients, the lipid environment and physiological responses. All these factors may critically influence the structure, function and dynamics of a biomolecule. For membrane proteins, there is increasing evidence on the vital role of the native lipid environment on protein folding, structure and activity.[2,3] Thus, the next challenge for membrane protein structural biology is to obtain structural and dynamic information in the cellular environment.

Membrane proteins are often extracted and purified in detergent and are typically returned to a lipid environment by reconstituting the protein into a lipid bilayer consisting of native or non-native lipids. In this manner, conformational changes in several membrane proteins have been studied with EPR,[4,5] Fluorescence resonance energy transfer (FRET)[6] and ssNMR.[7] *In-cell* FRET usually employs fluorescent proteins as tags, and due to their large size these tags can provide only low resolution information.[6] *In-cell* NMR experiments are limited due to low sensitivity and the requirement that the macromolecule be small and rapidly tumbling.[8] The requirement for a well-ordered 2D crystal severely limits the use

of diffraction techniques to study membrane proteins in native environments. Thus obtaining high resolution *in-cell* information for membrane proteins remains a challenge that necessitates new approaches.

DEER[9,10] has received a great deal of attention in structural biology, particularly for membrane proteins. The technique can resolve distance distributions between spin pairs with high precision in the range of 1.5 to 10.0 nm.[5,11,12] Combined with simulations and modeling, these distance distributions can validate existing structures and provide information on alternate structural states that have not been observed.[13,14] DEER experiments are typically performed at low temperature, although under proper conditions it can be carried out in liquid solutions using spin labels having long phase memory time (T_m).[15-17] Since proteins are usually diamagnetic, paramagnetic spin labels, most commonly MTSL, are introduced into a protein by covalent attachment to an engineered cysteine residue.[18] Spin-labeling of a cysteine with MTSL generates the side chain named R1. Recently, Gd(III) spin labels are attracting attention for *in-cell* DEER because they are resistant to the reducing environment inside the cell.[19,20] The *in-cell* DEER proof of principle with spin-labeled ubiquitin was demonstrated previously.[20,21] In these experiments a spin-labeled ubiquitin was introduced into the oocytes or the HeLa cells. Distance measurements have been reported on spin labeled colicin A added to *E. coli*.[22] However, the signal-to-noise ratio was poor and such exogenous introduction of a protein does not work for most of the membrane proteins. Recently, we used DEER to measure distances between the endogenous cobalamin transporter (BtuB) and its spin-labeled substrate in intact *E. coli*.[23]

4.3 Results and Discussion

Here we report ligand-induced conformational changes in the extracellular loops of the outer membrane cobalamin transporter BtuB in intact *E. coli*. To our knowledge, this is the first report of conformational changes in a membrane transporter in the cellular environment. We show the potential of this approach to verify conformational changes observed in crystal structures and to obtain additional information in the cellular environment. Beta-barrel proteins are ubiquitous in Gram-negative bacteria, chloroplasts and mitochondria and they perform vital physiological functions such as membrane biogenesis, substrate and protein translocation, motility, drug resistance, and signaling. BtuB is a 22-stranded β-barrel protein with a 130 residuce N-terminal plug or hatch domain in the center. It is a member of the TBDT family, requiring a PMF and the inner membrane ExbB-ExbD-TonB complex for CNCbl transport. We expressed BtuB in *E. coli* having two cysteines at the desired positions that were spin-labeled by adding MTSL to the cell suspension. OM proteins in *E. coli* are often cysteine-free (cys-less) or have cysteines that are not reactive. Thus labeling of the solvent-accessible target sites could be achieved by adding MTSL to the cell exterior.[23,24]

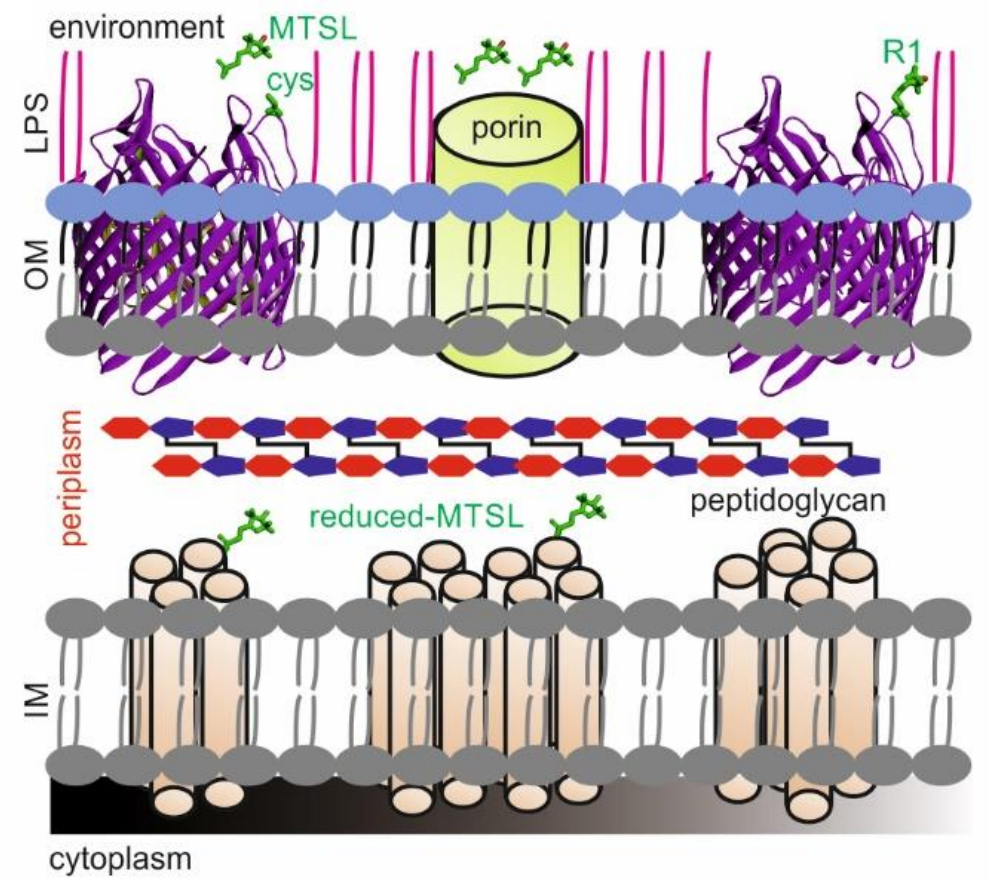

Figure 4.1 MTSL is reduced in the periplasm. A) Structure of the the Gram-negative bacterial cell wall. The OM is assymetric consisting of an inner phospholopid layer and an outer LPS layer. The CM consists of a phosopholipid bilayer containing numerouns α-helical proteins. Exposed cysteines on β-barrel proteins can be labeled by additon of MTSL from outiside. Those MTSL molecules which enter periplasm through the porins are reduced.

The outer membrane is permeable to molecules below 600 Da, and the MTSL could easily reach periplasm and react with exposed cysteines of inner membrane proteins (Figure 4.1A). However, we have never observed an EPR signal following labeling of *E. coli* cells expressing 'cys-less' BtuB or other cysteine mutations located in periplasm. Attempts to label cysteines at the periplasmic interface with maleimido-proxyl also did not give a signal, indicating that there is no interference from the disulfide bond formation (Dsb) system. These observations suggest that the MTSL is reduced following entry into the periplasm. We demonstrated previously that a spin-labeled CNCbl, which binds tightly to

BtuB, is not reduced by cells[23] confirming that the reduction must happen only after entry into the periplasm.

To further understand the reduction process, we added 150 µM MTSL to a 30 mL suspension containing cells collected from a 2 L overnight culture. Samples were collected at periodic intervals and MTSL concentration in the supernatants was monitored using CW-EPR. As shown in Figure 4.2 and 4.3A, the spin concentration in the supernatant quickly decreased reaching less than 10 µM in 45 minutes. Similar results have been observed for the reduction of Tempone (4-oxy-Tempo) and spin-labeled gentamycin by *Psuedomonas aeruginosa* and *E. coli* cells[25] and for the TPOA spin label (2,2,5,5-tetramethyl-pyrroline-1-oxyl-3-carboxylic acid amide) in *Xenopus laevis* oocytes.[26] Greater stability has been reported for another modified five-membered nitroxide spin-label in *E. coli*.[27] It is possible that the rather high concentration of the spin-label (10-20 fold) compared to what we used and other experimental conditions might have contributed to the apparent greater stability. The apparent MTSL reduction was much faster for 188C-399C mutant. At present we do not understand the reasons for this observation and it needs to be further investigated whether the presence of unfolded precursors with reactive cysteines in periplasm somehow accelerates MTSL reduction.

As we reported earlier, no signal could be detected for the WT cell pellet[23] or for cysteine mutations located in periplasm (8C, 9C, Figure 4.4), whereas single or double cysteine mutants located on the extracellular loops or the exposed surface of the hatch domain yielded signal from bound MTSL (Figure 4.3C-E). We conclude that upon entry into periplasm, MTSL may stay free, react with accessible cysteines or even cross the inner

membranes. In any case it is quickly reduced. As suggested previously,[25] interaction with the electron transport chain in the inner membrane might be a reason for the rapid reduction. Whatever the exact mechanism of MTSL reduction is, this process eliminated signals from unwanted sites, which is very critical for the DEER experiment.

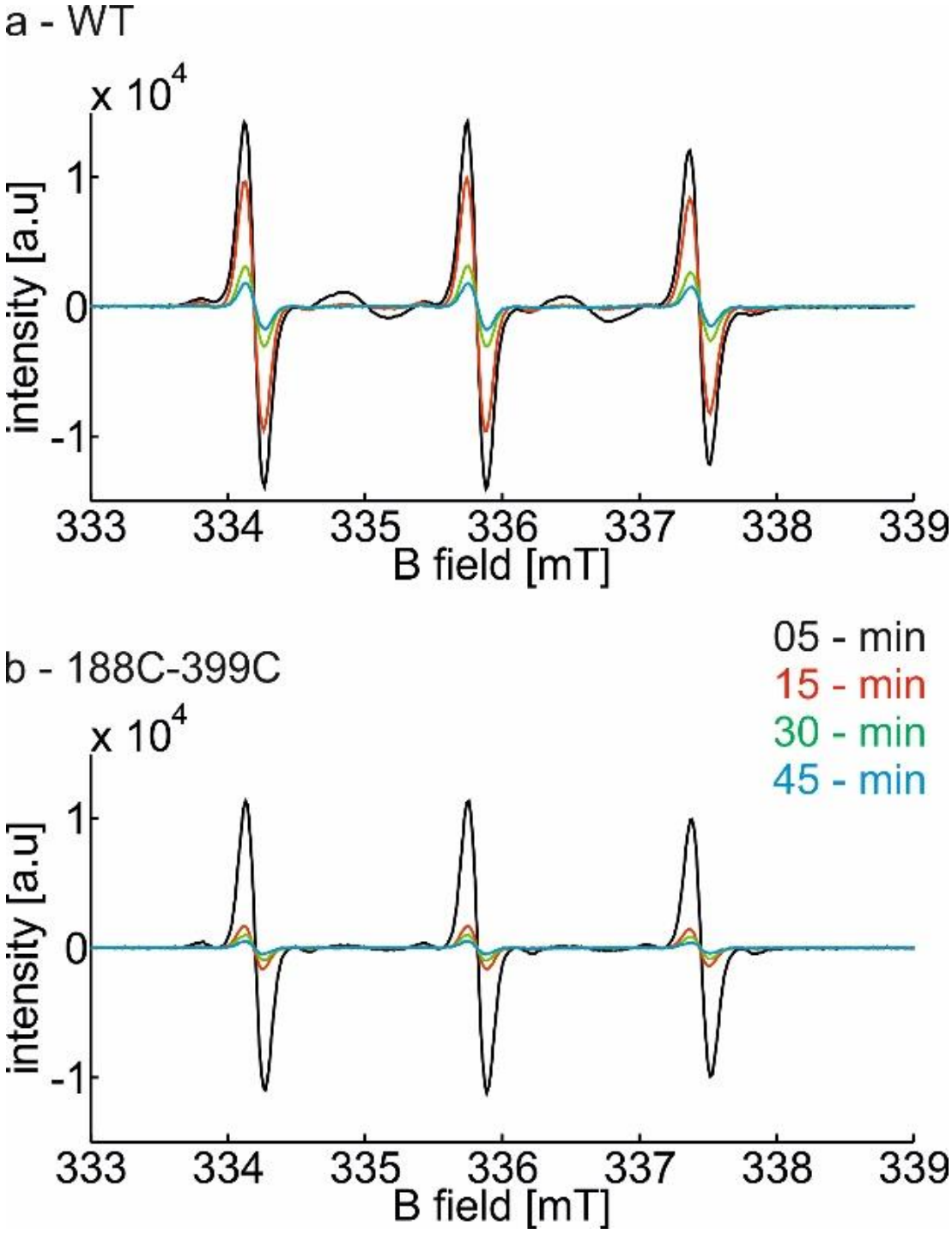

Figure 4.2: Raw EPR data for the reduction of MTSL by E. coli cells. Original RT CW-EPR spectra (analysis shown in Figure 4.3A) for the reduction of MTSL by *E. coli* cells expressing WT or 188C-399C BtuB obtained at different time intervals after addition of 150 μM MTSL (see material and methods). The broad spectral feature between the hyperfine lines is likely arising from biradical formation.

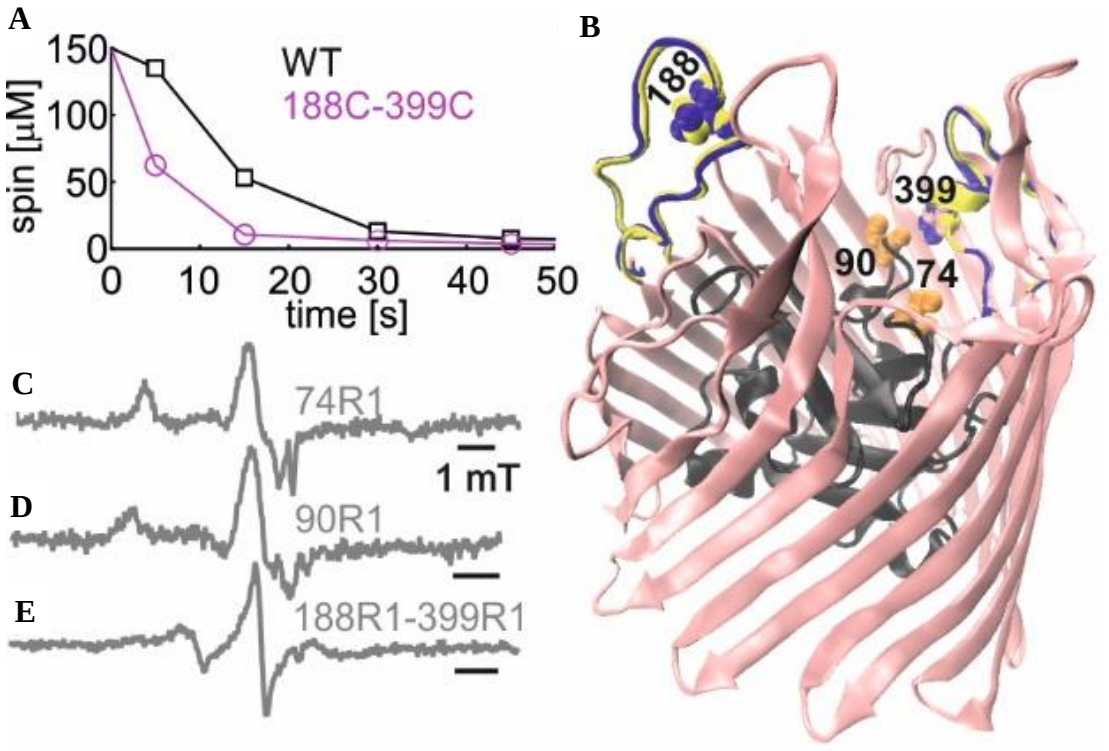

Figure 4.3: Labeling of the BtuB plug domain in whole cells. A) Reduction of MTSL by *E. coli* cells expressing WT or 188C-399C BtuB. A 10-15% error is estimated for the spin concentration calculated using RT CW-EPR. B) apo-BtuB structure (1NQE) with the plug domain in black. Spin-labeled positions are highlighted in CPK representation. The 3/4 loop conformation as observed in the BtuB-Ca^{2+} (blue, 1NQG) and BtuB-Ca^{2+}-CNCbl (yellow, 1NQH) is overlaid. (C, D, E) RT CW-EPR spectra measured in live *E. coli* cells as indicated.

Despite the availability of several crystal structures, the mechanism for substrate transport remains unclear for TBDTs.[28] In all the structures, the N-terminal hatch domain occludes the barrel leaving no space for substrate movement. It has been suggested that the N-terminal domain may remain within the barrel and rearrange,[29] exit the barrel partially[30] or completely[31] during translocation. It is possible that a native cellular environment is necessary for the N-terminal domain to achieve a translocation-competent conformation. We attempted to spin label positions 66C, 74C and 90C located on the N-terminal domain in BtuB (Figure 4.3B). We could label 74C and 90C whereas labeling failed for 66C probably because it is sterically restricted as observed in the crystal structures (Figure

4.4C). Interestingly, both 74R1 and 90R1 revealed spectra in the rigid limit (correlation time (τ_c) > 100 ns, Figure 4.5) suggesting a static conformation for the N-terminal domain in the cellular environment. In future, it will be interesting to explore how this rigid conformation is modulated by the presence of ligands, PMF or TonB in the cellular environment.

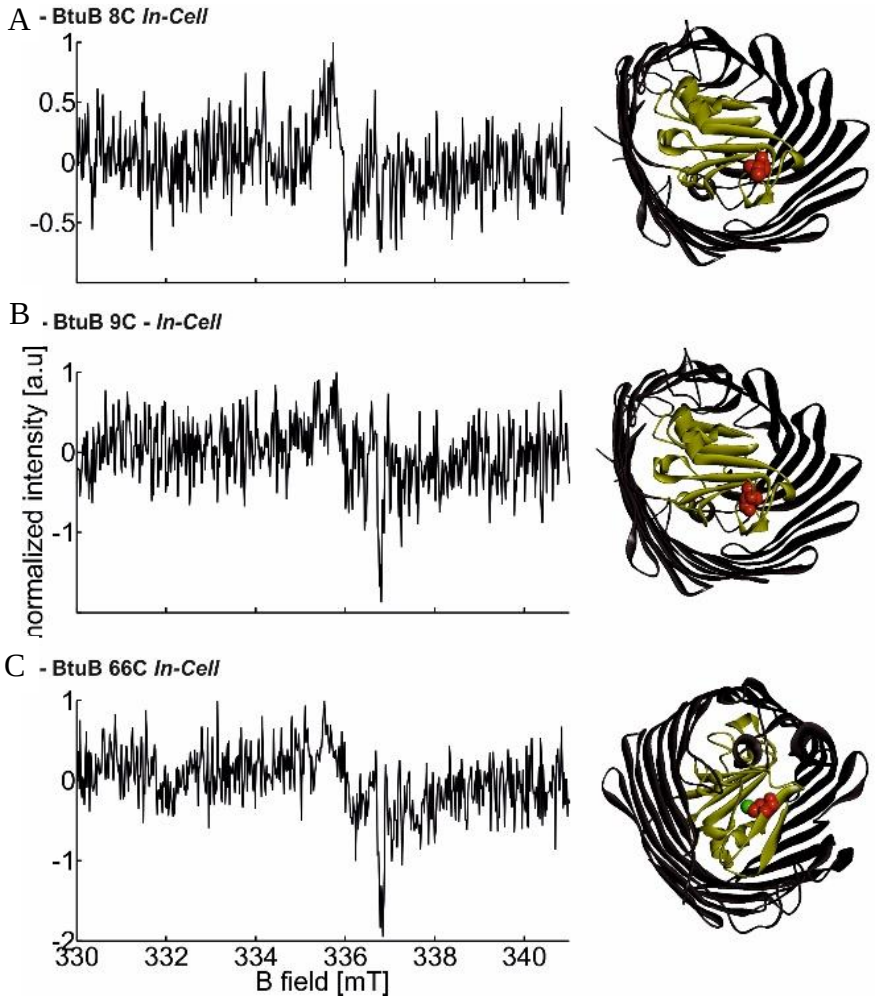

Figure 4.4: In-cell spin labeling of cysteines located in periplasm or on the plug domain in BtuB. RT CW-EPR spectra for spin-labeling of 8C, 9C (located on the Ton box in periplasm) and 66C (located on the plug/hatch domain) obtained in live *E. coli* cells. Spin-labeling failed for all the three positions. For 8C and 9C, a view of the corresponding residues L8 and V9 as observed from periplasm in the BtuB-Ca^{2+} (1NQG) crystal structure is shown. MMM simulation predicted 73 rotamers for position 8R1 (partition function, 0.35) whereas only one rotamer for position 9R1 (partition function, 0.33). Thus, labeling for 9C might have failed due to limited accessibility as well, whereas 8C could not be labeled most likely due to the reduction of the MTSL in periplasm (Figure 4.3A). For 66C, a view from top of the corresponding residue I66 in the structure (1NQG) is shown with the terminal carbon atom highlighted in green showing its location into the core of the plug. MMM simulation predicted three rotamers (partition function, 0.00) for 66R1 revealing that the site is too tight for labeling.

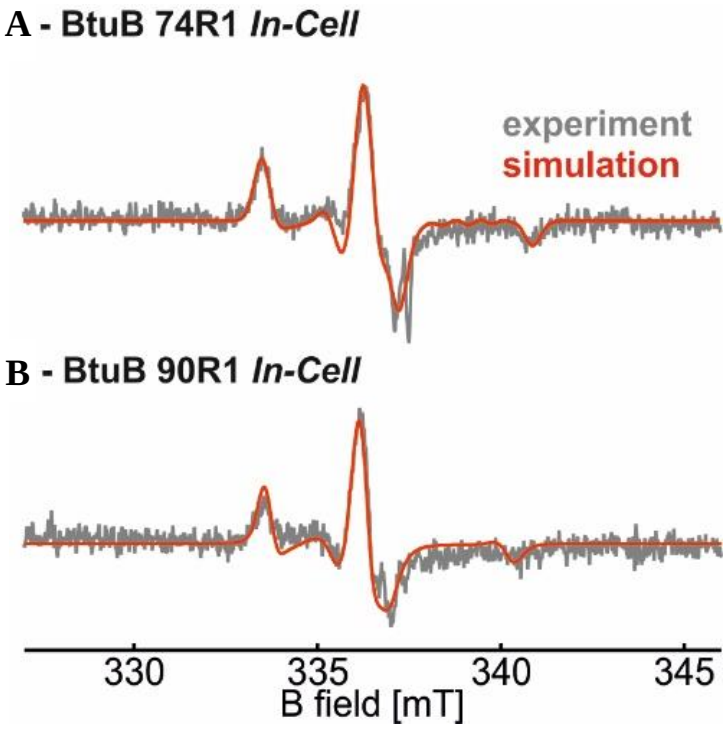

Figure 4.5: Simulation of the in-cell RT CW-EPR spectra.[32] EasySpin simulated RT CW-EPR spectra for 74R1 A) and 90R1 B) overlaid on the experimental data obtained in live *E. coli* cells. For 74R1 simulation, g_{xx} = 2.00800, g_{yy} = 2.00600, g_{zz} = 2.00200; A_{xx} = 19.169, A_{yy} = 17.276, A_{zz} = 102.2 (in MHz) and an anisotropic diffusion tensor with an average correlation time of $2.64*10^{-7}$ s was used. For 90R1 simulation, g_{xx} = 2.00800, g_{yy} = 2.00614, g_{zz} = 2.00186; A_{xx} = 16.217, A_{yy} = 15.426, A_{zz} = 99.800 (in MHz) and an average correlation time of $1.03*10^{-7}$ s was used.

To investigate the possibility of observing conformational changes in intact *E. coli* cells, we spin labeled 188C–399C located on the 2nd extra cellular loop (connecting β-strands 3 and 4) and 7th loop (connecting β-strands 13 and14), respectively. The 2nd loop shows very large conformational changes in the crystal structures in response to ligand binding.[33] It is not resolved in the BtuB-apo crystal structure, whereas it is completely ordered in both BtuB-Ca^{2+} and BtuB-Ca^{2+}-CNCbl structures (Figure 4.3B). BtuB binds two Ca^{2+} ions with high affinity through an aspartate cage consisting of several residues from the loop 2 and 3. Loop 7 carrying position 399 is well ordered even in the absence of the ligands and has

a very similar conformation to all three crystal structures (Figure 4.3B). Thus changes in the 188R1-399R1 distance are expected to result from motion of the 2nd loop.

Unlike the positions located on the hatch domain, RT CW-EPR spectroscopy revealed a rather mobile spectra for 188R1-399R1 in agreement with their location on the loops (Figure 4.3E). For the 188R1 single mutant, we could achieve up to 30 μM spin concentration using a $2x10^{11}$ cells/mL suspension.[23] However, for the 188R1-399R1 double mutant we could obtain only 30 μM spin (instead of the expected 60 μM) at the same cell density. The modulation depth (λ) of the DEER traces for the in-cell samples presented below is in the 6-8 % range (Figure 4.8). This is about 25% of the maximum λ achievable with our Q-band instrument for a sample with 100 % spin-labeling efficiency. Thus we obtained only 50-60% spin-labeling efficiency for the 188C-399C double mutant in *E. coli* cells. There could be several reasons for this low labeling efficiency in whole cells. The surrounding LPS molecules may interfere with MTSL accessibility (Figure 4.1A). As the reduction appears to be very fast (Figure 4.3), some of the reduced MTSL might have diffused back from periplasm and reacted with 188C and 399C. In spite of the low spin concentration and λ, we could achieve high quality DEER data in intact *E. coli* cells with 36-48 hrs of accumulation. The DEER data were analyzed using DeerAnalysis software[40] employing Tikhonov regularization with L-curve criterion and the error of the distance distribution was estimated by systematically varying the intermolecular background function (Figures 4.6 & 4.7).

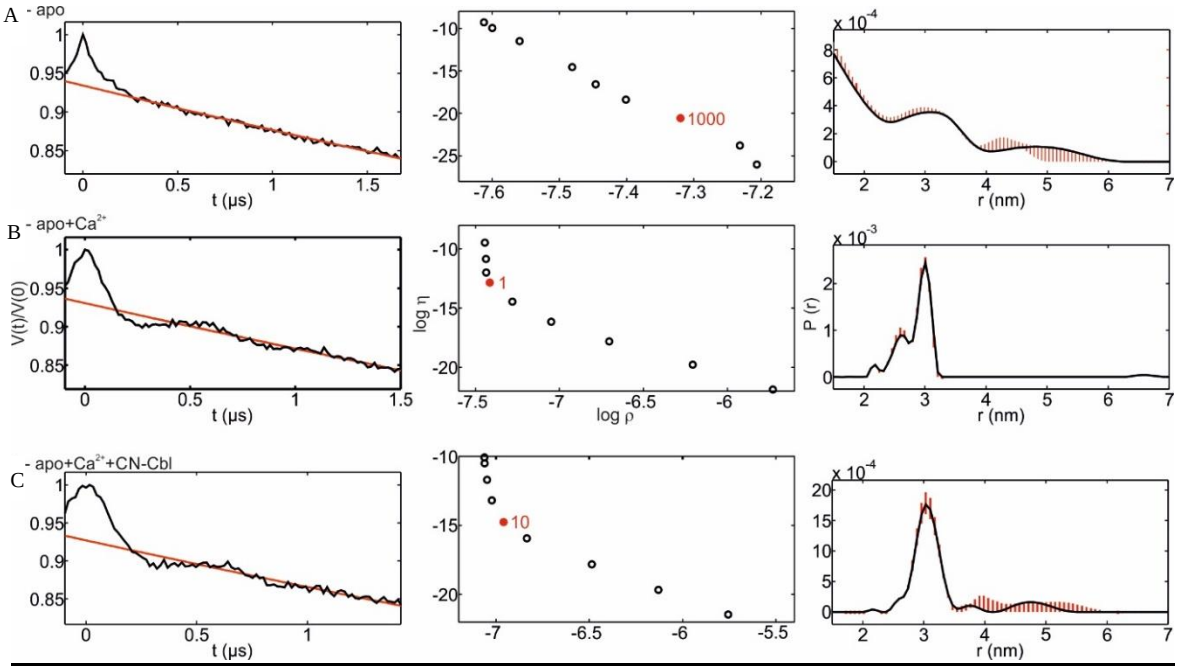

Figure 4.6: DEER data analysis for whole cell samples. Data analysis was performed with DeerAnalysis[34] software. (A, B, C) Left panels; original DEER data for BtuB in different functional states obtained in whole cells (black) with an exponential background function overlaid (red). Middle panels; the corresponding L-curves with the used regularization parameter (α) highlighted in red. The symbol ρ is the mean squared deviation between the experimental and simulated dipolar evolution functions and η is a measure of the roughness of P(r) given by the square norm of the second derivative of P(r) weighted by α. Right panel; error validation for the obtained distance distributions. The beginning of the background function was varied from 200ns to 1000 ns in discrete steps using the validation tool in DeerAnalysis software.

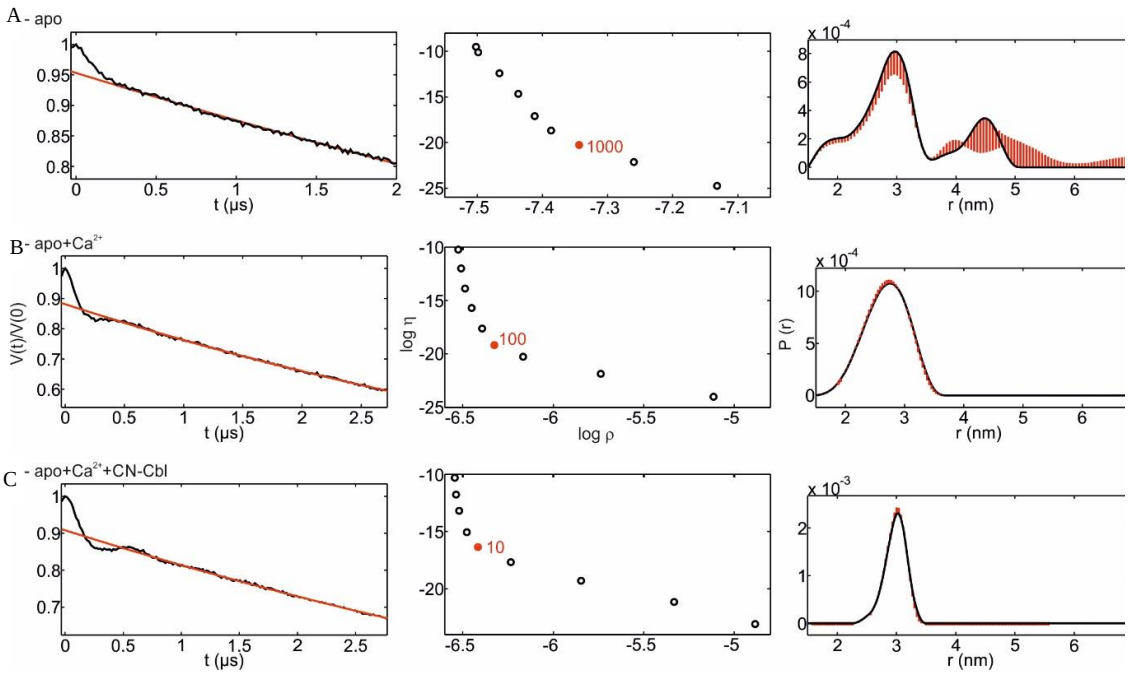

Figure 4.7: DEER data analysis for the OM samples. Data analysis was performed with DeerAnalysis software. (A, B, C) Left panels; original DEER data for BtuB in different functional states obtained in native outer membranes (black) with an exponential background function overlaid (red). Middle panels; the corresponding L-curves with the used regularization parameter (α) highlighted in red. The symbols ρ and η are explained in Figure 4.6. Right panels; error validation for the obtained distance distributions. The beginning of the background function was varied from 200 ns to 1500 ns (A) or from 320 ns to 2000 ns for the Ca^{2+} and Ca^{2+}+CNCbl samples using the validation tool in DeerAnalysis software.

In the apo-state (no Ca^{2+} or CNCbl) in *E. coli* cells, 188R1-399R1 cells showed a broad interspin distance distribution with a mean distance at 2.66±0.9 nm (Figure 4.8D, red). It is likely that the dynamic nature of the 2nd loop contributes to the broad conformational distribution and explains why this loop is not resolved in the BtuB-apo crystal structure (Figure 4.4B). Thus in the absence of Ca^{2+}, the 2nd loop occupies a large conformational landscape in *E. coli* cells and might completely occlude the binding pocket in some states. Interestingly, addition of Ca^{2+} ions to the cells populated a distinct conformation with a mean distance at 2.82±0.30 nm (Figure 4.8E, red), in agreement with the appearance of the 2nd loop in BtuB-Ca^{2+} structure.[33] Simulation of this spin pair in the context of this crystal

structure (1NQG) using MMM[35] gave a predicted distribution that was broader with a mean distance at 2.61±0.39 nm (Figure 4.8E, cyan). Further addition of CNCbl to form the ternary complex shifted the main peak giving a mean distance at 3.12±0.33 nm. Simulation on the corresponding crystal structure (1NQH) predicted a broader distribution with a mean distance at 2.73±0.37 nm (Figure 4.8F, cyan). Despite the differences between the experimental results and the simulations, the DEER data validated the Ca^{2+}-induced ordering of the 2nd loop observed in the crystal structures in the cellular environment.

To further investigate the role of the cellular environment, we isolated OM containing BtuB using an established protocol.[36] DEER with the OM revealed (Figure 4.8D-E, black) some differences compared to the whole cell samples in the apo- and Ca^{2+}-bound states. In the apo-sate, the overall distance distributions are similar, however in whole cells there is a higher population of shorter distances (mean distance of 2.6±0.89 nm as compared to 3.16±0.84 nm in OM). In the Ca^{2+}-bound state, the 2nd loop again becomes ordered (mean distances at 2.72±0.31 nm) as observed in whole cells and in the crystal structure. The shape of the distance distribution in OM appears different when compared to whole cells. In presence of both Ca^{2+} and CNCbl, the distances obtained in OM (2.98±0.18 nm) were virtually identical to the whole cell samples (Figure 4.8F). Notably in OM, the presence of both Ca^{2+} and CNCbl induced a narrower distance distribution as compared to Ca^{2+} alone. In summary, there exists small differences in the distance distribution between whole cell and OM environments, however the overall responses of the loops to ligand(s) binding are very similar. The differences observed between the simulations and the experiment could be explained by the exclusion of some of the rotamers (populated in the crystals) in the native membrane environment (Figure 4.8E-F, cyan vs. red and black). Such selective

rotamer exclusion might result from additional steric interference around the spin labels perhaps due to interactions with LPS, proteins or due to other components present in the cellular environment.

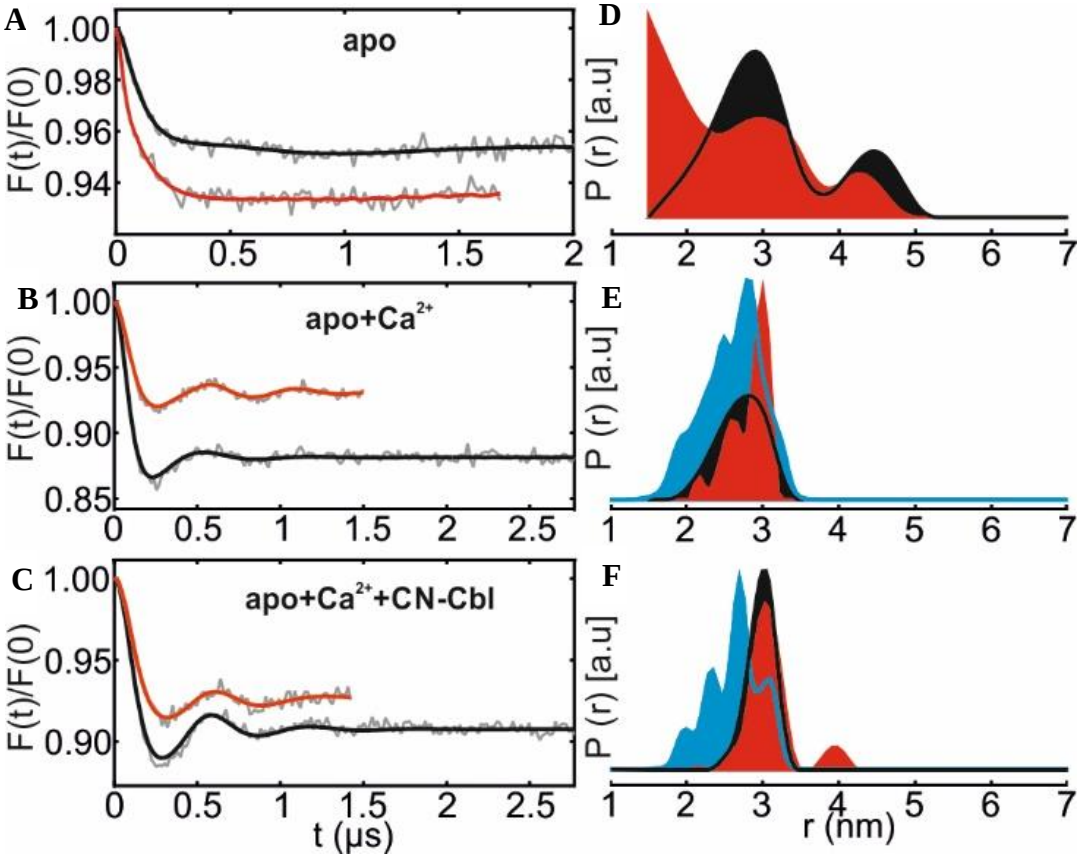

Figure 4.8: Calcium and substrate effects on the 3-4 loop in whole cells. (A-C) Background corrected Q-band DEER data for 188R1-399R1 mutant in *E. coli* cells (red) or OM (black) in different functional states. (D-F) Area normalized distance distributions and the corresponding simulations (cyan) normalized to the maximum of the experimental data.

The data presented here demonstrate that conformational changes in a membrane protein can be observed using DEER in an isolated native membrane. The OM DEER data suggest that isolation of the outer membrane using the standard procedure does not severely alter the behavior of OM proteins such as BtuB. Moreover when compared to whole cells, the

OM samples are very stable and may be concentrated allowing higher quality DEER data and shorter acquisition times (Figure 4.8). In addition, these OM preparations are leaky and provide access to both membrane surfaces, a feature that will be useful for studying interactions between OM proteins and other molecular partners located in the periplasm or inner membrane (with BtuF or TonB for example) or to investigate interaction and folding of proteins into native outer membranes. In summary, we demonstrated the measurement of conformational changes in a membrane protein within the native cellular environment of intact *E. coli* cells for the first time. Our results reveal a very dynamic conformation of the 2nd loop in the apo-state that is not resolved in the crystal structure. Further, we validated the conformational changes of this loop upon ligand binding observed in BtuB crystal structures in the cellular environment. Two important features of the *E. coli* cells make this observation possible; the lack of native reactive cysteines in OM proteins and the selective reduction MTSL that enters the periplasm.

With its higher sensitivity and ability to examine structures of any molecular weight, DEER is ideally suited to obtain distance constraints in the cellular environment. In principle any of the solvent exposed sites other than those located in the periplasm can be spin-labeled. Thus, residues on the extra-cellular loops or the N-terminal domain which are involved in substrate recognition and translocation in numerous β-barrel proteins can spin-labeled and studied in intact cells. The general applicability of the method would be extended with further improvement in sensitivity. The signal can be increased with optimization of the labeling efficiency and by using stronger and tunable promoters to increase expression levels. Addition of d_8-glycerol can improve T_m in both OM and whole cell samples,[23] and it might be possible to increase the sensitivity by growing cells

in a deuterated media. Normally, BtuB is expressed at less than 10^3 copies/cell and the overexpression used here increases the expression up to 10^5 copies/cell.[23] Several OM proteins are expressed at more than 10^5 copies per cell, thus it should be possible to study these proteins at physiological concentrations in the cellular environment. Combined with the recent developments in pulsed EPR instrumentation,[37-39] it will be possible to perform DEER at even lower expression levels.

Contributions to the work

This work is a direct continuation of previous published work on whole cell DEER method development.[23] Here all work on mutant production, membrane isolation and OM DEER data was obtained by A. Sikora in the lab of Dr. Cafiso. The in-cell data was obtained by Dr. Joseph.

4.4 Material and Methods

Cell growth

Mutations, culturing and spin labeling were performed as described before.[23] Briefly, the BtuB mutants 8C, 9C, 66C, 74C, 90C and 188C-399C in a pUC8 backbone were generated using Agilent Technologies (Santa Clara, CA) QuikChange Site Directed Mutagenesis Kit. The mutants were overexpressed in the *E. coli* strain RK5016 (*argH*, *btuB*, *metE*).[40] To avoid CNCbl repression of BtuB, cells were grown in minimal media for overnight. Media was supplemented with 3 m*M* MgSO4, 300 μ*M* $CaCl_2$, 0.24% w/v glucose, 150 μ*M* thiamine, and 0.01% w/v of Met and Arg and 100 μg/mL ampicillin.

Membrane isolation

The native outer membranes containing BtuB were isolated after selective removal of the inner membranes with sarkosyl detergent. Briefly, cells from 1 L culture were pelleted following overnight growth and suspended in 30 mL of 10 mM tris buffer (pH 7.5) containing 60 mM NaCl. The cells were lysed by French press for 2-3 times and the cell debris were removed by centrifugation for 20 minutes at 12,000 rpm using Sorvall SS-34 rotor. The supernatant was collected and the cell envelop consisting of both the inner membrane and the outer membrane was pelleted by centrifugation at 100,000 x g for 1.5 hours. The pellet was suspended in the same buffer and the inner membrane was solubilized by adding 0.5% sarkosyl detergent. The outer membranes (OM) were pelleted with centrifugation at 200,000 x g for 1.5 hours. Following centrifugation, the pellet was suspended into 10 mL of the same buffer for spin-labeling.

Spin labeling

For spin-labeling, cells collected from 1 L culture was suspended in 30 mL of 50 mM Tris buffer (pH 7.5) containing 60 mM NaCl and 0.5% glucose. For spin labeling, MTSL (Toronto Research Chemicals, North York, ON, Canada) was added to 100 µM final concentration and incubated with shaking for 1 hour at room temperature. Following incubation cells were washed two times with the same buffer and suspended to $1x10^{11}$ cells/mL. The viability of the cells was checked by plating the serial dilutions on LB-agar plates. DEER samples were immediately prepared with addition of 15% d_8-glycerol and kept at -80^0C until measurements.

The outer membrane fraction as prepared above was spin-labelled by adding 40 µM MTSL and incubating at room temperature for 1 hour. Following incubation, the membranes were pelleted and washed several times until the free spins were completely removed and suspended into 500 µL final volume. As we reported previously, spin-labeling of outer membranes produces signals arising from non-specific labeling as well. However, those spins are far separated and do not give any distances in the measurable range.[1] Thus other than reducing the modulation depth and the absolute sensitivity, the non-specific labeling does not cause any problems for the DEER experiments.

MTSL reduction by E. coli cells

Cells collected from a 2 L overnight culture was suspended into 30 mL of 50 mM Tris buffer (pH 7.5) containing 60 mM NaCl and 0.5% glucose. MTSL was added to 150 µM final concentration and cells were incubated with shaking at room temperature. 1 mL samples were collected at periodic intervals, pelleted immediately and the supernatant was collected in a fresh tube. The spin concentration in the supernatant was determined from

the double integral of the RT CW-EPR spectra using a calibration standard prepared from 4-amino TEMPO.

RT-continuous-wave EPR measurements

An X-band (9.4 GHz) Bruker E500 spectrometer equipped with a TE102 or a SHQE cavity was used for continuous-wave EPR measurements. For whole cell samples the viability of the cells after the measurement was checked by plating on LB agar plates. Measurements were performed in 2 mm quartz tubes at 100 kHz modulation frequency, 0.15 mT modulation amplitude, 0.6 mW microwave power, 20.48 ms time constant, 81.92 ms conversion time, 1024 points and 15 mT sweep width.

DEER measurements

In-cell DEER measurements were performed on a Bruker ELEXSYS E580 EPR spectrometer equipped with a DEER unit (E580-400U, Bruker), a continuous-flow helium cryostat (CF935, Oxford Instruments), and a temperature control system (ITC 502, Oxford Instruments). For measurements, 15-20 µL of whole cells containing 15% d_8-glycerol was transferred into 1.6 mm outer diameter quartz EPR tubes (*Suprasil*, Wilmad LabGlass). DEER measurements were performed at Q-band frequency (33.7 GHz) using an ELEXSYS SuperQ-FT accessory unit and a Bruker AmpQ 10 W amplifier with a Bruker EN5107D2 dielectric resonator at 50 K. A dead-time free four-pulse sequence with phase-cycled $\pi/2$ pulse was used[10] for DEER. For the observer pulses, typical pulse length was 32 ns ($\pi/2$ and π) and for the pump pulse a 20 ns (π) pulse was used. The observer pulses were set 60 MHz lower than the pump pulse, which was set to the maximum of the echo-detected field swept spectrum. For the outer membrane samples, the measurements were

performed on another Elexsys E580 EPR spectrometer fitted with a standalone Q-band bridge with the EN5107D2 resonator. DEER data were acquired with the four-pulse sequence with 16 and 32 ns π/2 and π observation pulses, respectively, and a 32 ns π pump pulse was used. The observation frequency was set 60 MHz lower than the pump frequency, which was positioned to the maximum of the nitroxide spectrum. The deuterium modulations were averaged by increasing the first interpulse delay by 16 ns for 8 steps. The background function arising from intermolecular interactions were removed from the primary data $V(t)/V(0)$ and the resulting form factors $F(t)/F(0)$ were fitted with a model-free Tikhonov regularization to distance distributions with DeerAnalysis2013 software package.[34] The errors in distance distributions arising from uncertainties in background correction was evaluated by systematically varying the background function. *In silico* spin labeling and simulations on the crystal structures were performed using a rotamer library approach with using the MMM 2015[35] software package.

4.5 References

1. Joseph B., Sikora A. & Cafiso D.S. Ligand induced conformational changes of a membrane transporter in *E. coli* cells with PELDOR/DEER. *JACS*. **6**, 1844-47 (2016).

2. Laganowsky, A., Reading, E., Allison, T. M., Ulmschneider, M. B., Degiacomi, M. T., Baldwin, A. J. & Robinson, C. V. Membrane proteins bind lipids selectively to modulate their structure and funtion. *Nature*. **510**, 172-5 (2014).

3. Dowhan, W. & Bogdanov, M. Lipid-protein interactions as determinants of membrane protein structure and funtion. *Biochem. Soc.Trans.* **39**, 767-74 (2011).

4. Klare, J. P. & Steinhoff, H. J. Spin labeling studies of transmembrane signaling and transport: Applications to photoaxis, ABC transporters and symporters. In *Methods in Enzymology*; Peter, Z. Q., Kurt, W., Eds. **Vol. 564**, p 315-47 (2015).

5. Jeschke, G. DEER distance measurements on proteins. *Annu. Rev. Phys. Chem.* **63**, 419-46 (2012).

6. Piehler, J. Spectroscopic techniques for monitoring protein interactions in living cells. *Cur. Opin. Struct. Biol.* **24**, 54-62 (2014).

7. Opella, S. J. Structure determination of membrane proteins by neuclear magnetic resonance spectroscopy. *Annu. Rev. Anal. Chem.* **6**, 305-28 (2013).

8. Hansel, R., Luh, L. M., Corbeski, I., Trantirek, L. & Dotsch, V. In-cell NMR and EPR spectroscopy of biomacromolecules. *Angew. Chem. Int. Ed. Engl.* **53**, 10300-14 (2014).

9. Milov, A. D., Ponomarev, A. B. & Tsvetkov, Y. D. Electron-electron double resonance in electron spin eho: model biradical systems and the sensitized photolysis of decalin. *Chem. Phys. Lett.* **110**, 67-72 (1984).

10. Pannier, M., Veit, S., Godt, A., Jeschke, G. & Spiess, H. W. Dead-time free meadurement of dipole-dipole interactions between electron spins. *J. Magn. Reson.* **142**, 331-40 (2000).

11. Schiemann, O. & Prisner, T. F. Long-range distance determination in biomaromolecules by EPR spectroscopy. *Quart.Rev. Biophys.* **40**, 1-53 (2007).

12. Ward, R., Bowman, A., Sozudogru, E., El-Mkami, H., Owen-Hughes, T. & Norman, D. G. EPR distance measurements in deuterated proteins. *J. Magn. Reson.* **207**, 164-7 (2010).

13. Claxton, D. P., Kazmier, K., Mishra, S. & McHaourab, H. S. Navigating membrane protein structure, dynamics, and energy landscapes using spin labeling and EPR spectroscopy. In *Methods in Enzymology*; Peter, Z. Q., Kurt, W., Eds. **Vol. 564**, p 349-387 (2015).

14. Joseph, B., Korkhov, V. M., Yulikov, M., Jeschke, G. & Bordignon, E. Conformational cycle of the vitamin B12 ABC importer in liposomes detected by double electron-elecctron resonance (DEER). *J.* B*iol. Chem.* **289**, 3176-85 (2014).

15. Yang, Z., Liu, Y., Borbat, P., Zweier, J. L., Freed, J. H. & Hubbell, W. L. Pulsed ESR dipolar spectroscopy for distance measuremnts in immobilized spin labeled proteins in liquid solution. *J. Am. Chem. Soc.* **134**, 9950-2 (2012).

16. Meyer, V., Swanson, M. A., Clouston, L. J., Boratynski, P. J., Stein, R. A., McHaourab, H. S., Rajca, A., Eaton, S. S. & Eaton, G. R. Room-temprature distance measurements of immoblized spin-labeled protein by DEER/DEER. *Biophys. J.* **108**, 1213-9 (2015).

17. Shevelev, G. Y., Krumkacheva, O. A., Lomzov, A. A., Kuzhelev, A. A., Rogozhnikova, O. Y., Trukhin, D. V., Troitskaya, T. I., Tormyshev, V. M., Fedin, M. V., Pyshnyi, D. V. & Bagryanskaya, E. G. Physiological-temprature distance measurement in nucleic acid using triarylmethyl-based spin labels and pulsed dipolar EPR spectroscopy. *J. Am. Chem. Soc.* **136**, 9874-7 (2014).

18. Hubbell, W. L. & Altenbach, C. Investigation of structure and dynamics in membrane proteins using site-directed spin labeling. *Current Opinion in Structural Biology* **4**, 566-573 (1994).

19. Qi, M., Gross, A., Jeschke, G., Godt, A. & Drescher, M. Gd(III)-PyMTA label is suitable for in-cell EPR. *J. Am. Chem. Soc.* **136**, 15366-78 (2014).

20. Martorana, A., Bellapadrona, G., Feintuch, A., Di Gregorio, E., Aime, S. & Goldfarb, D. Probing protein conformation in cells by EPR distance measurements using Gd^{3+} spin labeling. *J. Am. Chem. Soc.* **136**, 13458-65 (2014).

21. Igarashi, R., Sakai, T., Hara, H., Tenno, T., Tanaka, T., Tochio, H. & Shirakawa, M. Distance determination in proteins inside *Xenopus laevis* oocytes by double electron-electron resonance experiements. J. *Am. Chem. Soc.* **132**, 8228-9 (2010).

22. Dunkel, S., Pulagam, L. P., Steinhoff, H. J. & Klare, J. P. In vivo EPR on spin labeled colicin A reveals an oligomeric assembly of the pore-forming domain in E. Coli membranes. *PCCP.* **17**, 4875-8 (2015).

23. Joseph, B., Sikora, A., Bordington, E., Jeschke, G., Cafiso, D., Prisner, T. Distance Measurement on an Endogenous Membrane Transporter in *E. coli* Cells and Native Membranes Using EPR Spectroscopy. *Angew. Chem. Int. Ed. Engl.* **54**, 6196-99 (2015).

24. Jiang, X., Payne, M. A., Cao, Z., Foster, S. B., Feix, J. B., Newton, S. M. & Klebba, P. E. Ligand-specific opening of a gated-porin channel in the outer membrane of living bacteria. *Science.* **276**, 1261-4 (1997).

25. Rapoport, N., Smirnov, A. I., Pitt, W. G. & Timoshin, A. A. Bioreduction of spin-labeled gentamicin and tempone by gram-nagative bacteria: kinetics and effects of ultrasound. *Arch. Biochem. Biophys.* **362**, 233-41 (1999).

26. Krstic, I., Hansel, R., Romainczyk, O., Engels, J. W., Dotsch, V. & Prisner, T. F. Long-range distance measurements on nucleic acids in cells by pulsed EPR spectroscopy. *Angew. Chem. Int. Ed. Engl.* **50**, 5070-4 (2010).

27. Schmidt, M. J., Borbas, J., Drescher, M. & Summerer, D. A genetically encoded spin label for electron paramagnetic resonance distance measurements. *J. Am. Chem. Soc.* **136**, 1238-41 (2014).

28. Cafiso, D. S. Indentifying and quantitating conformational exchange in membrane proteins using site-directed spin labeling. *Acc.Chem.Res.* **47**, 3102-9 (2014).

29. Chakraborty, R., Storey, E. & van der Helm, D. Molecular mechanism of ferricsiderophore passage through the outer membrane receptor proteins of Escherichia coli. *Biometals.* **20**, 263-74 (2007).

30. Devanathan, S. & Postle, K. Studies on colicin B translocation: FepA is gated by TonB. *Mol. Microbiol.* **65**, 441-53 (2007).

31. Ma, L., Kaserer, W., Annamalai, R., Scott, D. C., Jin, B., Jiang, X., Xiao, Q., Maymani, H., Massis, L. M., Ferreira, L. C., Newton, S. M. & Klebba, P. E. Evidence of ball-and-chain transport of ferric enteroactin through FepA. *J. Biol. Chem* **282**, 397-406 (2007).

32. Stoll, S. & Schweiger, A. EasySpin, a comprehensive software package for special simulation and analysis in EPR. *J. Magn. Reson.* **178**, 42-55 (2006).

33. Chimento, D. P., Mohanty, A. K., Kadner, R. J. & Wiener, M. C. Substrate-induced transmembrane sgnaling in the cobalamin transporter, BtuB. *Nat. Struct. Biol.* **10**, 394-401 (2003).

34. Jeschke, G., Chechik, V., Ionita, P., Godt, A., Zimmermann, H., Banham, J., Timmel, C. R., Hilger, D. & Jung, H. DeerAnalysis2006 – a comprehensive software package for analyzing pulsed ELDOR data. *Appl. Magn. Reson.* **Vol. 30**, 473-498 (2006).

35. Polyhach, Y., Bordignon, E. & Jeschke, G. Rotamer libraries of spin labelled cysteines for protein studies. *PCCP*. **13**, 2356-66 (2011).

36. Filip, C., Fletcher, G., Wulff, J. L. & Earhart, C. F. Solubilization of the cytoplasmic membrane of *Escherichia coli* by the ionic detergent sodium-lauryl sarcosinate. *J. Bacteriol.* **115**, 717-22 (1973).

37. Polyhach, Y., Bordignon, E., Tschaggelar, R., Gandra, S., Godt, A. & Jeschke, G. High sensitivity and versatility of the DEER experiment on nitroxide radical pairs at Q-band frequencies. *PCCP*. **14**, 10762-73 (2012).

38. Spindler, P. E., Waclawska, I., Endeward, B., Plackmeyer, J., Ziegler, C. & Prisner, T. F. Carr-Purcell pulsed electron double resonance with shaped inversion pulses. *J. Phys. Chem. Lett.* **6**, 4331-5 (2015).

39. Borbat, P. P., Georgieva, E. R. & Freed, J. H. Improved sensitivity for long-distance measurements in biomolecules: five-pulse double electron-electron resonance. *J. Phys. Chem. Lett.* **4**, 170-5 (2013).

40. Gudmundsdottir, A., Bell, P. E., Lundrigan, M. D., Bradbeer, C. & Kadner, R. J. Point mutations in a conserved region (TonB box) of *Escherichia coli* outer membrane protein BtuB affect vitamin B12 transport. *J. Bacteriol.* **171**, 6526-33 (1989).

Chapter 5: Allosteric Signaling is Bidirectional in an Outer-Membrane Transport Protein

5.1 Abstract

In BtuB, the *Escherichia coli* TonB-dependent transporter for vitamin B_{12}, substrate binding to the extracellular surface unfolds a conserved N-terminal segment termed the Ton box into the periplasm. This transmembrane signaling event increases the affinity of BtuB for the inner membrane protein TonB. In the present work, continuous wave and pulse EPR in a native membrane preparation demonstrate that signaling also occurs from the periplasmic to the extracellular surface in BtuB. The binding of a TonB fragment to the periplasmic interface alters the second extracellular loop to create a more open loop configuration, and it diminishes the affinity of BtuB for substrate. Moreover, mutants in the periplasmic Ton box that are transport-defective alter the binding site for vitamin B_{12} in BtuB. This work demonstrates that the Ton box and the extracellular substrate binding site are allosterically coupled in BtuB, a feature that appears to be critical to the TonB-dependent transport mechanism.

5.2 Introduction

The outer-membrane of Gram negative bacteria contain a family of specific, high-affinity active transport proteins that derive energy from the inner membrane electrochemical proton potential by coupling to the trans-periplasmic membrane protein TonB[1-4]. These TonB-dependent transporters actively transport various forms of iron, vitamin B_{12}, nickel and carbohydrate and are essential for the survival of many pathogens. At the present time, over 40 high-resolution structures of TonB-dependent transporters have been determined[2]; however, the molecular mechanisms by which these proteins facilitate transport remain uncharacterized.

BtuB is the outer-membrane *Escherichia coli* transport protein for vitamin B_{12} (cyanocobalamin or CNCbl). The structure of BtuB is homologous to other TonB-dependent transporters, consisting of a 22-stranded β-barrel where the N-terminal 136 residues are folded within the barrel interior to form a domain that is sometimes referred to as a hatch or core. The crystal structure of the substrate-bound form of BtuB is shown in Figure 5.1, where two Ca^{2+} ions act as co-ligands for vitamin B_{12}. Near the N-terminus, residues 6 through 12 in BtuB encompass a highly conserved energy-coupling segment termed the Ton box, which is responsible for coupling BtuB to the inner-membrane protein TonB. Although not observed in this structure due to the environment imposed by crystallography[5], substrate binding is known to shift a conformational equilibrium in the Ton box to favor an unfolded state, so that the Ton box projects 20 or 30 Angstroms into the periplasm[6]. This transmembrane signaling event enhances the affinity of BtuB for

TonB, and appears to facilitate transperiplasmic coupling between these inner and outer membrane proteins[7].

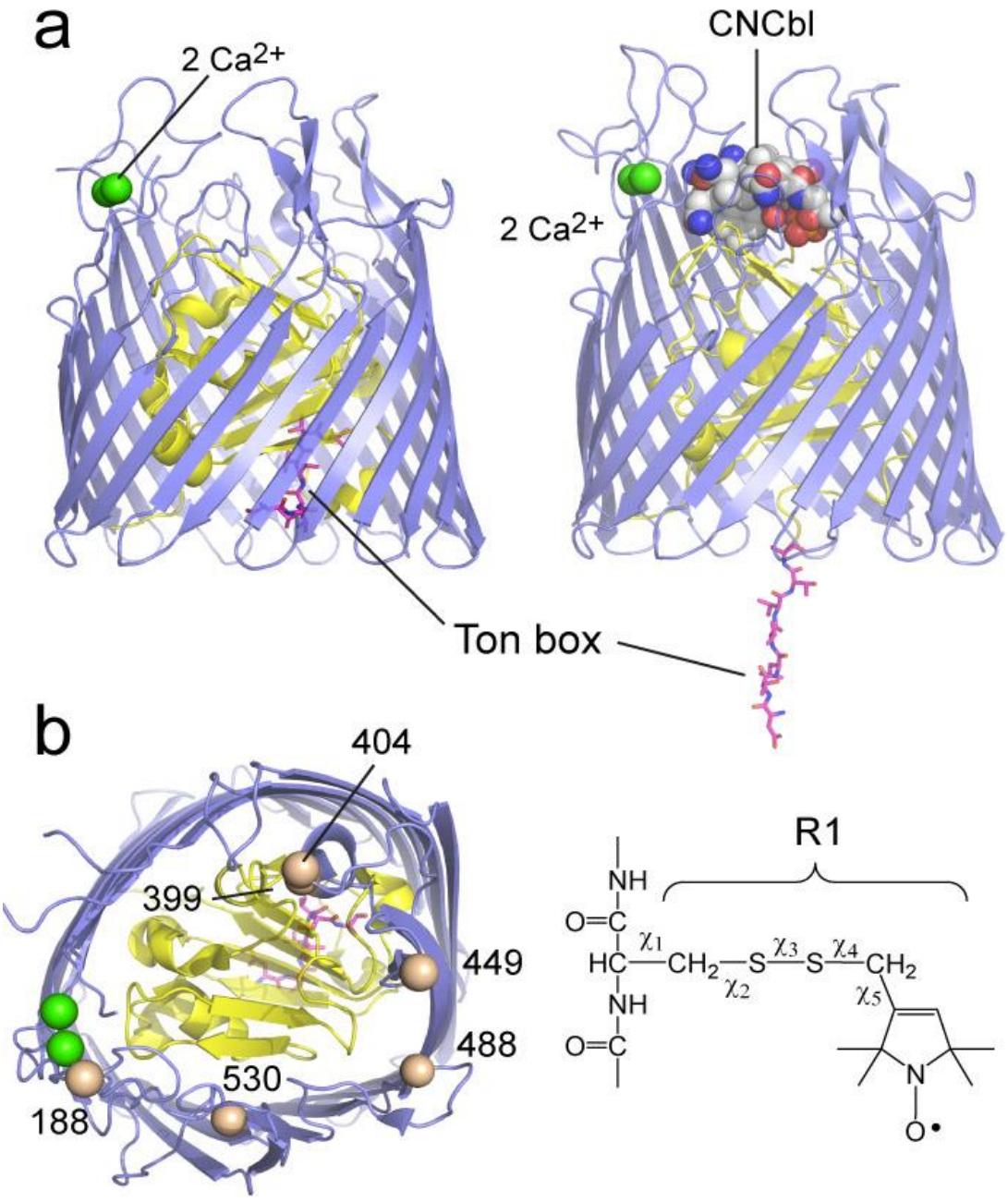

Figure 5.1. Crystal structures of BtuB showing loop positions used in this study. (**a**) High-resolution crystal structure of BtuB in the Ca^{2+}-bound form (PDB: 1NQG) (left) and a modified form of the Vitamin B12 bound form of BtuB (PDB: 1NQH) placing the Ton box in an extended configuration consistent with EPR data (right). Two Ca^{2+}-ions (green spheres) are coordinated by a cage of 4 aspartic acid side chains from the second and third extracellular loops. The structure of BtuB is based upon a 22 stranded antiparallel β-barrel (blue) where the N-terminal region (yellow) is folded within the interior of the barrel. (**b**) Sites that have been labeled with the spin-labeled side chain R1 on the exterior loops of the BtuB barrel.

Important questions remain unanswered regarding TonB-dependent transport and it is not known how TonB-binding to the transporter drives substrate movement across the outer-membrane. It has been suggested that TonB, which is in complex with ExbB and ExbD in the inner membrane, may act by pulling on the N-terminus of BtuB thereby unfolding the N-terminal core[8], or TonB may act by rotating to drive rearrangements in the core domain[9]. Crystal structures have been obtained for a fragment of TonB in complex with BtuB and FhuA (the *Escherichia coli* ferrichrome transporter)[10,11]. In these structures, the Ton box interacts with a three-stranded β-sheet domain in TonB in an edge-to-edge manner. In the case of BtuB, the Ton box must unfold for this interaction to take place, but there do not appear to be significant changes occurring within BtuB upon TonB binding and there are no obvious conformational changes in the core domain that would provide a pathway for vitamin B_{12} movement through the protein interior.

In the present work, the spin labeled side chain R1 (Figure 5.1b) was engineered into several extracellular loops of BtuB, and pulse EPR spectroscopy was used to examine the configuration of the loops in a native outer-membrane preparation. In the apo state, the extracellular loops sample a broad conformational space. Calcium binding to BtuB enhances vitamin B_{12} affinity by altering the configuration of the second extracellular loop and limiting the conformations that are sampled by this loop. Remarkably, the configuration of the second extracellular loop in BtuB is modulated by the binding of a C-terminal fragment of TonB to the periplasmic surface of BtuB, producing a more open extracellular loop configuration. Using a novel spin-labeled substrate (TEMPO-CNCbl)[12], we find that TonB binding to the periplasmic surface diminishes the affinity of the substrate, while transport-defective mutants in the Ton box lock the vitamin B_{12} into the

ligand binding site. The data demonstrate that the Ton box and the substrate binding site are allosterically linked in BtuB, and that interactions on either surface alter conformational equilibria on the opposite surface of the protein. We discuss this two-way transmembrane coupling, which is likely a key feature in the mechanism of TonB-dependent transport.

5.3 Results

In the present work, we carried out distance measurements using DEER on BtuB in intact outer membrane preparations. Previously, it was shown that outer-membrane preparations from *Escherichia coli* may be used to obtain high-quality data from pairs of spin labels on BtuB[12,13]. In these preparations, DEER signals are not obtained from wild-type BtuB or single cysteine labeled sites in BtuB. And although there is typically a significant level of background labeling in these preparations, this background labeling does not interfere with the DEER signal from selectively labeled spin pairs. Moreover, the relaxation characteristics of these samples are often better suited to DEER than those of purified reconstituted membrane preparations.

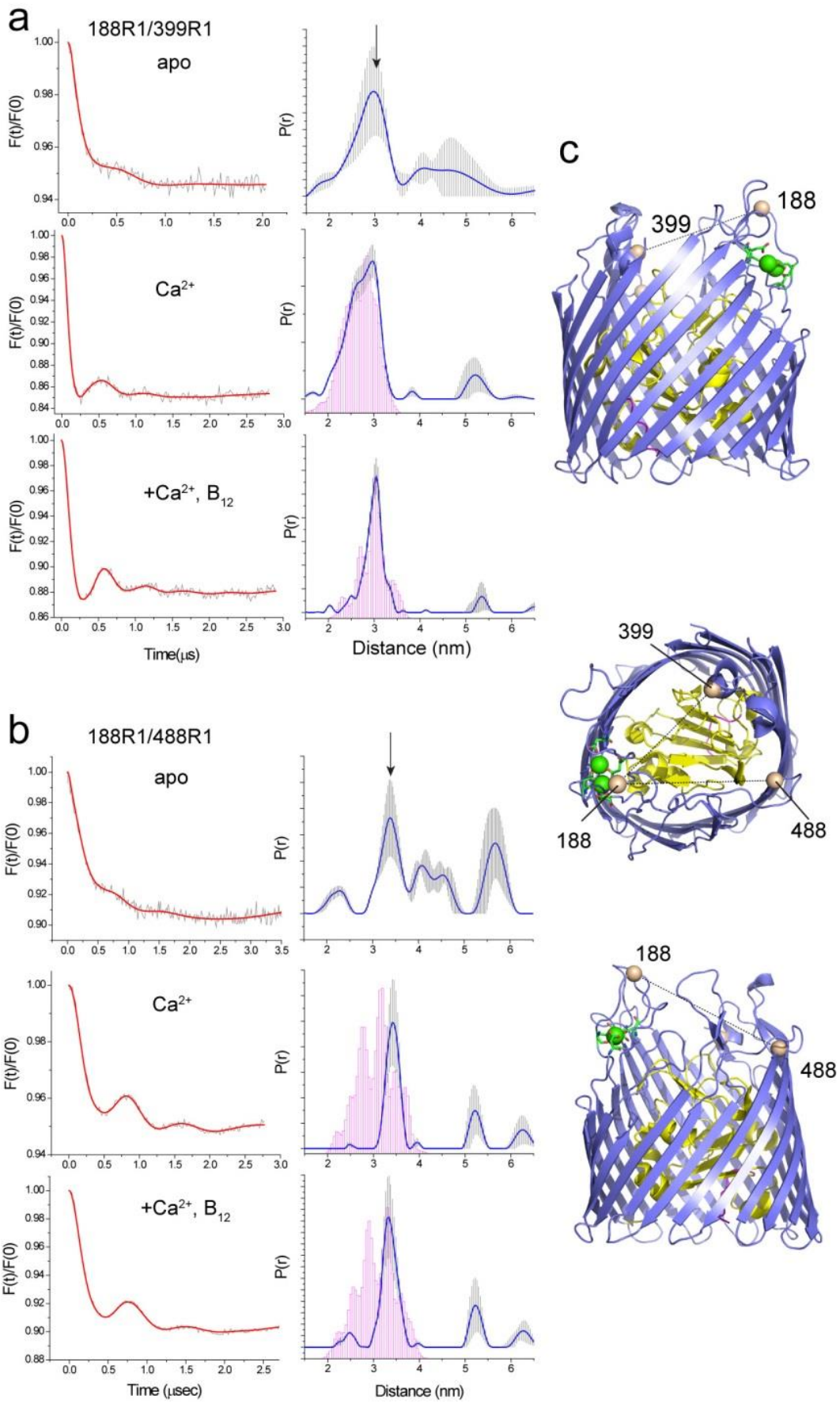
a
188R1/399R1
apo
Ca2+
+Ca2+, B12
F(t)/F(0)
P(r)
Time(μs)
Distance (nm)
b
188R1/488R1
apo
Ca2+
+Ca2+, B12
F(t)/F(0)
P(r)
Time (μsec)
Distance (nm)
c
188
399
399
188
488
188
488

Figure 5.2. Ligand binding narrows the distance distributions sampled by the second extracellular loop. On the left panels are background corrected DEER data for BtuB in outer-membrane preparations and the panels on the right show the corresponding distance distributions obtained from these data. The best fits to the DEER data are shown as red traces and blue traces represent the best fit distribution. The grey error bars in the distribution represent fits obtained by variation of the background form factor producing fits that are within 15% RMSD of the best fit. Data are shown for measurements between (**a**) the apex of extracellular loop 2 and site 399 in loop 7, and (**b**) between the apex of extracellular loop 2 and site 488 in loop 9. Molecular models (PDB: 1NQH) are shown indicating the positions of these spin labels. The histograms (magenta) for the Ca2+ and Ca2+-vitamin B12 distributions represent predicted distance distributions based upon the crystal structures for these states (either PDB: 1NQG or 1NQH) (see Methods). The data in (a) from 188R1:399R1 were presented previously[13]. Data at X-band for the 188R1:399R1 spin pair were also obtained in a purified and reconstituted membrane system[14].

Shown in Figure 5.2 are DEER data obtained under three sets of conditions for two pairs of spin labels where one label is placed near the apex of loop 2 (188R1) and a second label is placed closer to edge of the barrel at either site 399, in loop 7, or at site 488, in loop 9. For both pairs of labels, broad distance distributions are obtained in the apo state, although in both cases defined distances appear in the distribution (30 Å for 188R1:399R1 and 34 Å for 188R1:488R1). Upon Ca^{2+} addition, clear oscillations appear in the background corrected DEER data (F(t)/F(0)), indicating that Ca^{2+} is placing loop 2 in a better defined configuration. The subsequent addition of vitamin B_{12} further narrows the distribution from the 188R1:399R1 pair, but does not significantly change the distribution obtained from the 188R1/488R1 spin pair. Addition of vitamin B_{12} alone in the absence of Ca^{2+} does not significantly alter the distributions measured for loop 2.

In the presence of Ca^{2+}, vitamin B_{12} has an affinity (K_d) for BtuB of approximately 5 nM, which is diminished 1000 fold in the absence of Ca^{2+} to 5 μM[15]. A comparison of the apo and Ca^{2+}-bound states indicates that Ca^{2+} is acting to narrow the conformational space

available to this loop, and the data from Figure 5.2 indicate that Ca^{2+} is acting to pre-configure loop 2 to enable high-affinity vitamin B_{12} binding.

A comparison may be made between the predictions from high-resolution crystal structures and the distance distributions measured by DEER (see Methods). In these crystal structures, the second extracellular loop is not resolved in the apo state, indicating the presence of some disorder in the protein crystal in this region. However, this loop is resolved in the presence of Ca^{2+} or Ca^{2+}-vitamin B_{12}. Shown in Figure 5.2 are the predictions generated by MMM[16] (see Methods) using the crystal structures for the Ca^{2+} and Ca^{2+}-vitamin B_{12} states of BtuB (magenta histograms). For the 188R1:399R1 pair, the distributions from the model match well with the experimental data. The agreement is close, but not quite as good for the 188R1:488R1 spin pair, where the predicted distributions are slightly broader than the experimental distributions. Since sites 399 and 488 are close to the edge of the barrel and are likely fixed relative to the barrel structure, this comparison indicates that the configuration of loop 2 observed in intact outer-membranes is similar to that seen in the high-resolution structures.

In addition to loop 2, we made measurements between pairs of spin labels on loops 7, 8, 9 and 10 on the extracellular surface of BtuB, and the distributions obtained for several sites in the apo state are shown in Figure 5.3. In almost all cases very broad distributions are obtained that span the limits of the accessible distance range in these experiments. For most of these loop sites (Fig. 5.3b), the addition of Ca^{2+} or Ca^{2+}-vitamin B_{12} produces no significant change in the inter-spin distance distribution, suggesting that much of the extracellular region remains unchanged upon the binding of substrate. One exception is

the measurement between loops 8 and 10 shown in Figure 5.3c, where vitamin B_{12} addition acts to shorten the major distance in the distribution by approximately 5 Å. In this case, Ca^{2+} alone produces no change in interspin distance. As seen in Figure 5.3b, the corresponding measurement from loop 8 to loop 9 (449 to 488), yields a much broader distance distribution, with only minor changes seen upon B_{12} addition. This suggests that upon substrate binding loop 8 undergoes a movement towards the opposite side of the protein rather than a movement towards the membrane interface (Figure 5.3).

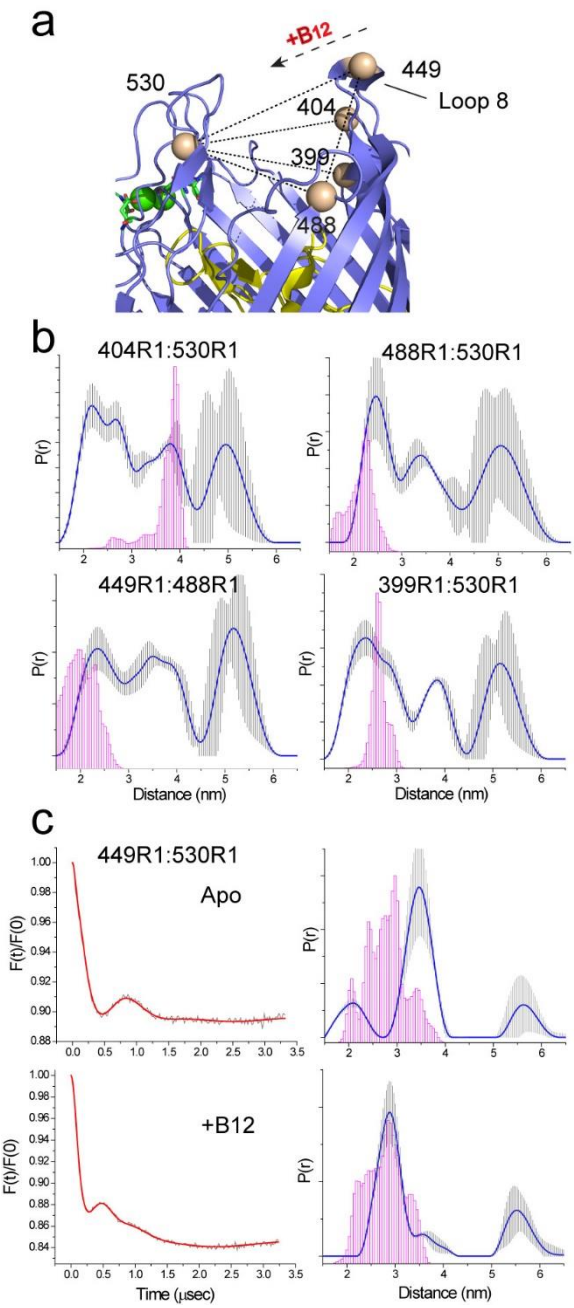

Figure 5.3. Vitamin B12 effects on loop 8. (**a**) Positions of spin-labeled sites in the extracellular loops. (**b**) Distributions measured between extracellular loops 7 and 10 (404R1:530R1 and 399R1:530R1), loop 8 to 9 (449R1:488R1), loop 8 to 10 (449R1:530R1) and loop 9 to 10 (488R1:530R1). The blue traces represent the best fit distribution, and the grey error bars represent fits obtained by variation of the background form factor that produce fits within 15% RMSD of the best fit. (**c**) For measurements to loop 8 from loop 10, vitamin B_{12} acts to shorten the inter-spin distance by approximately 5 Å. Fits to the DEER data are shown in red, and the distributions are as described in (b). Histograms in magenta represent the predicted distance distributions based either on the apo or substrate-bound structures (PDB: 1NQE or 1NQH).

Many of the distributions seen in Figure 5.3 for the BtuB apo state cover distances from 20 out past 50 Å; nonetheless, these loops are resolved in high-resolution crystal structures of the apo state and it is possible to examine the predicted distribution from these structures. The predicted distances from these structures for the *in-sulfo* structure[17] are shown as histograms in Figures 5.3b,c. In most cases, the predictions are far from the actual experimental distributions, suggesting that these loops are conformationally trapped in the crystal and that the loops sample a much broader range of conformations in the outer membrane than is revealed by these structures. Measurements between the periplasmic end of the barrel at site 488 to the ends of loops 8 (449) and 10 (530) yield much longer distances than predicted by the crystal structures (Fig. 5.3b), suggesting that loops 8 and 10 are extended much further into the extracellular space than is indicated in these structures. A meso phase structure has been obtained for BtuB in the apo state[18]. When a comparison is made between the resolved sites in this structure and the DEER data, the crystal structures are generally represented in the shorter ends of the distribution (Figure 5.4), suggesting that this crystal structure represents one of the more compact structures among those sampled in the outer membrane.

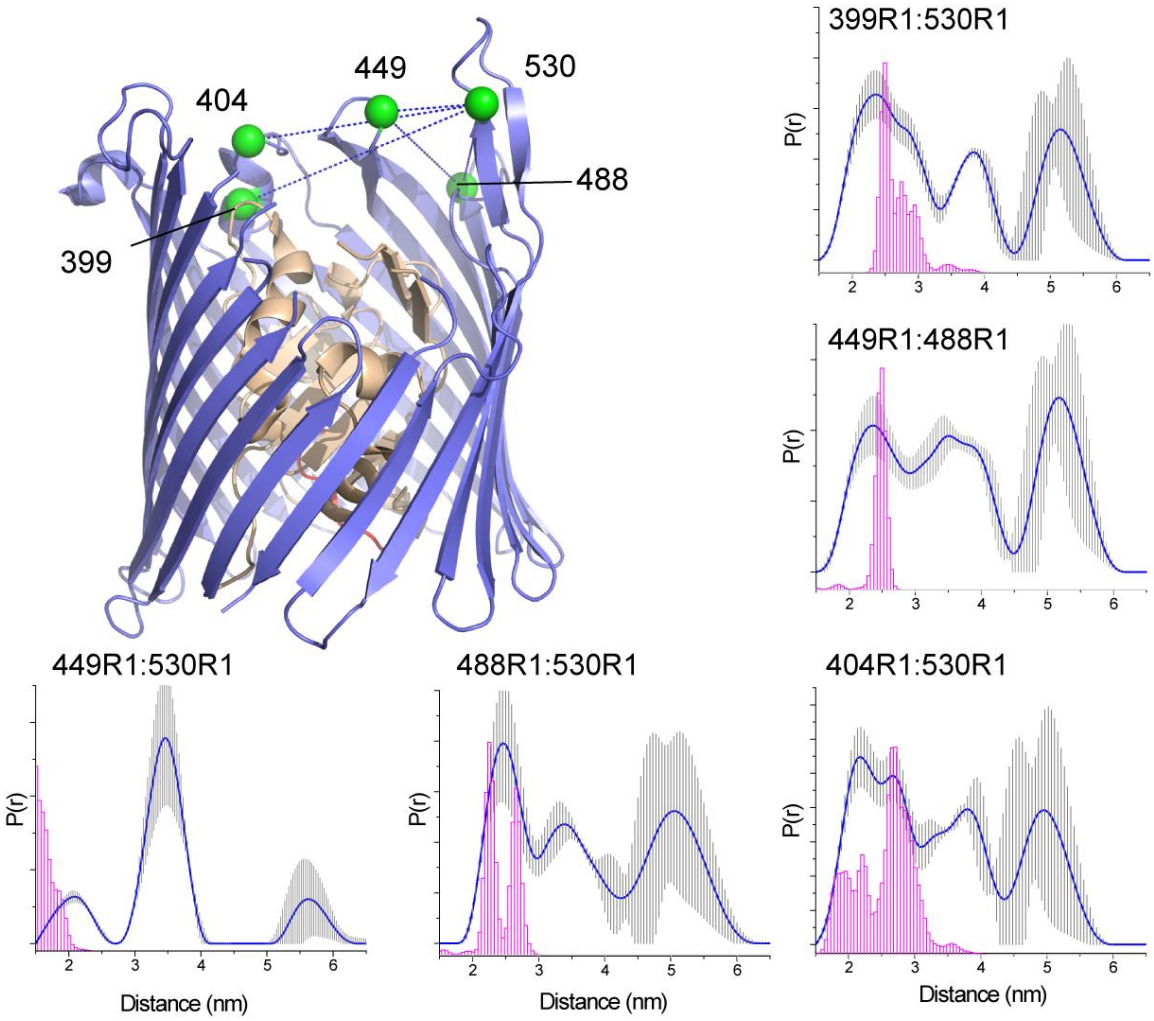

Figure 5.4. The extracellular loops in BtuB span a broad conformational space. Comparison of the DEER-derived distance distributions obtained for measurements between loops 7, 8, 9 and 10 with the lipidic phase crystal structure of BtuB in the apo state (PDB: 2GUF). The solid blue lines represent the best fits to the DEER data and the grey shaded regions represent fits that fall within 15 % RMSD of the best fit at a specific distance. The predictions based upon the structures are shown as histograms in magenta and were obtained using MMM[16] as described in Methods. In many cases, the distances predicted based upon the crystal structures match with the shorter end of the experimental distributions. However, many of the distributions are much broader and exhibit longer inter-spin distances than are expected based upon the structures.

As indicated above, substrate binding is known to unfold the Ton box in BtuB; however, it is not known whether an interaction or modification of the Ton box will alter the vitamin B_{12} binding site or the protein exterior. In the ferrichrome transporter FhuA, antibody binding kinetics and fluorescence quenching suggest that TonB binding alters the configuration of the extracellular loops[19]; however, significant structural changes in FhuA are not revealed in the crystal structure for the FhuA-TonB complex[10]. In the high-resolution structure for the BtuB-TonB complex, there is also little evidence for significant conformational changes in BtuB upon TonB binding[11]. This structure does show a change in the position of loop 8 when TonB is bound, however, this loop is in a region of protein-protein contact within the unit cell.

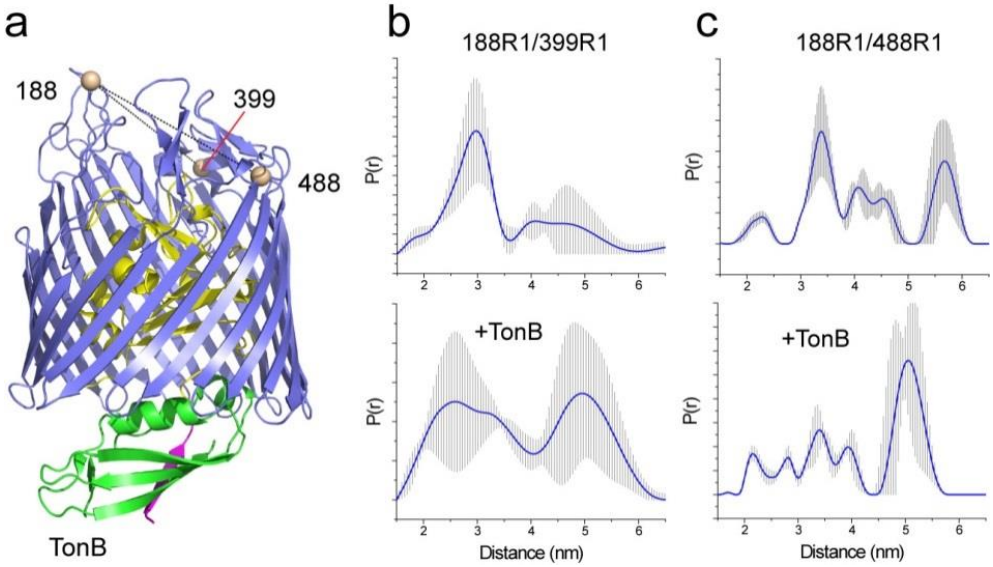

Figure 5.5. TonB binding widens the distance distribution sampled by the second extracellular loop. The configuration of loop 2 is modulated by the binding of TonB. (**a**) High-resolution crystal structure of BtuB bound to ΔN-TonB (PDB: 2GSL). The Ton box is in magenta and ΔN-TonB is in green. (**b**) Distance distribution obtained for 188R1:399R1 in the apo state (top) and TonB bound state (bottom). (**c**) Distance distribution obtained for 188R1:399R1 in the apo state (top) and TonB bound state (bottom).

Pulse EPR measurements allow us to directly probe loop conformations in BtuB in native membrane preparations, and we used DEER to determine whether the binding of a TonB fragment to BtuB might alter the configuration of the extracellular loops. In the substrate bound state, an examination of 8 interspin distances among the labeled loops showed little change in the configuration of the extracellular loops upon the binding of a TonB fragment (TonB(150-239 or ΔN-TonB) ; however, in the apo state, the binding of ΔN-TonB produced clear changes in the distributions for the spin pairs located between loop 2 and either site 399 or site 488. As seen in Figure 5.5, the distributions are broad in the apo state, but there is a significant distance for the 188R1:399R1 pair at 30 Å and a significant distance for 188R1:488R1 pair at 34 Å. Addition of TonB broadens the distribution at both sites, and in the case of the 188R1:488R1 pair, a 50 Å distance rather than the 33 Å appears to be the major feature in the distribution. The broadening and lengthening of these distances suggests that loop 2 is on average displaced further from the central axis of the barrel upon TonB binding and that it samples a broader range of conformations. Thus, TonB binding to the periplasmic surface modulates the structure of the protein at the opposite extracellular interface.

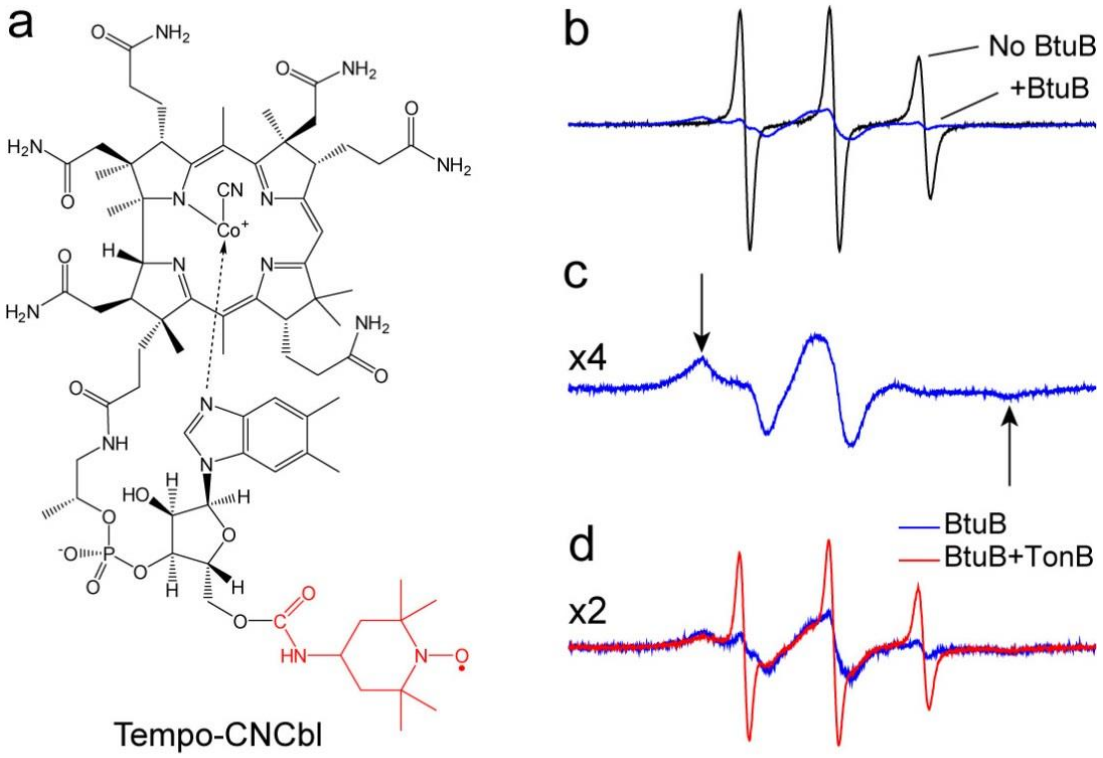

Figure 5.6. TonB binding alters the affinity of a spin-labeled vitamin B_{12} analog and promotes dissociation of the substrate. **a**) Structure of 2,2,6,6- tetramethylpiperidine 1-oxyl-CNCbl (TEMPO-CNCbl). (**b**) Spectra of 100 µM TEMPO-CNCbl in the presence of outer membranes from Escherichia coli in the absence (black trace) or presence (blue trace) or BtuB expression. The unbound lineshape is slightly broader than that obtained in buffer due to the viscosity of the outer-membrane preparation. (**c**) The lineshape of the TEMPO-CNCbl bound to wild-type BtuB. A small fraction of free label has been subtracted from this spectrum and the arrows indicate the position of the incompletely averaged hyperfine resonances. In this case, A_{zz}' = 58 Gauss. (d) Spectra of 50 µM TEMPO-CNCbl in the presence of outer membranes expressing BtuB at approximately 50 µM concentration in the absence (blue trace) and presence (red-trace) of excess TonB (150-239). These spectra are normalized and their amplitudes scaled as indicated.

We recently described a novel spin-labeled vitamin B_{12} analog, TEMPO-CNCbl (see Figure 5.6a), which binds and appears to be transported though BtuB[12]. When this labeled substrate is added to outer membrane preparations in the absence of BtuB expression, the EPR spectrum indicates that the ligand is freely diffusing and shows no evidence for

binding; however, the spectrum is dramatically broadened and reduced in amplitude if added to outer membrane preparations where BtuB has been expressed (Figure 5.6b). The EPR spectrum for bound TEMPO-CNCbl is expanded in Figure 5.6c, and it exhibits hyperfine extrema that are not completely averaged, indicating that the spin label is relatively restricted in its motion on the ns time-scale. The addition of TonB to these samples produces a dramatic change in the EPR spectrum of the spin labeled substrate. As seen in Figure 5.6d, ΔN-TonB addition increases the unbound component in the TEMPO-CNCbl spectrum, indicating that some of the TEMPO-CNCbl has dissociated from BtuB upon TonB binding.

The spectra in Figure 5.6d suggest that TonB binding has diminished the affinity of the substrate for BtuB, and we carried out titrations of TEMPO-CNCbl with outer membrane preparations to estimate the changes in labeled substrate affinity using EPR. Shown in Figure 5.7 are titrations carried out using outer membrane preparations expressing BtuB in the presence and absence of a soluble TonB fragment. For BtuB alone, the titration (Figure 5.7b) yields a dissociation constant of approximately 60 nM. However, because the free ligand concentration is difficult to accurately determine in this measurement, the error in this estimate is quite large. The standard error in this fit covers K_d values from 20 to 100 nM; as a result, the reported affinity for vitamin B_{12} to BtuB, which is 5 nM[14], may or may not be dramatically different than that for the TEMPO-CNCbl analog. In the presence of ΔN-TonB, the affinity is approximately 10 fold weaker, or approximately 700 nM, and standard error in this K_d value is approximately 20%. The bound TEMPO-CNCbl is readily displaced by non-labeled substrate, indicating that the substrate is in equilibrium with the binding site in BtuB (Figure 5.8).

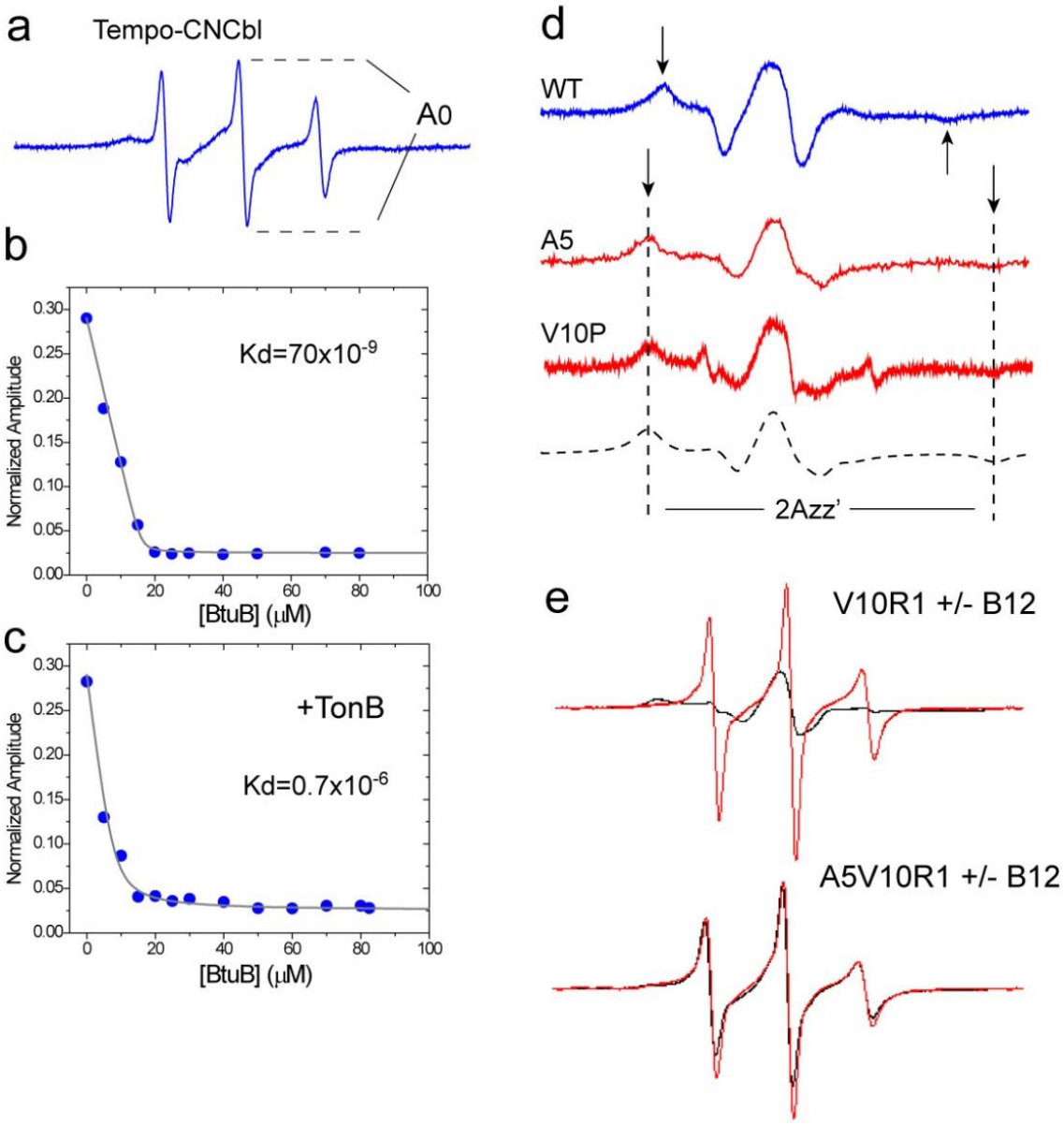

Figure 5.7. Substrate affinity changes in the presence of TonB and binding is altered in transport deficient mutants. (**a**) Titrations were carried out by measuring the amplitude of the central (m_I=0 transition) of the TEMPO-CNCbl spectrum as outer membranes containing BtuB were titrated into the substrate. Titrations in the absence (**b**) and presence (**c**) of TonB that were fit to a 1:1 binding isotherm (see Methods). Substrate concentrations were 20 µM for the BtuB alone and µ10 M for BtuB+TonB. (**d**) A comparison of the bound EPR lineshapes for TEMPO-CNCbl bound to wild-type BtuB, and bound to two transport-defective Ton box mutants (a 5-alanine mutation and V10P – red traces). The dashed spectrum in black represents a rigid limit fit to the mutant spectra, where A_{zz} is approximately 35 Gauss. The arrows and lines indicate the position of the hyperfine extrema. (**e**) EPR spectra obtained for R1 at position 10 within the Ton in the presence (red trace) and absence (black trace) of substrate for protein only with V10R1 mutation (top spectra) or the transport-defective A5 mutant (bottom spectra).

These data suggest that the binding of TonB alters the affinity of the substrate for its binding site and promotes dissociation of the substrate. From the titrations in Figures 5.7b,c and the change in the free substrate population seen in Figure 5.6d, we estimate that TonB binding shifts the free energy of substrate binding by approximately 1.5 kcal/mole; however, the affinity of TEMPO-CNCbl to apo BtuB may be an underestimate, and this shift in energy may be larger or smaller.

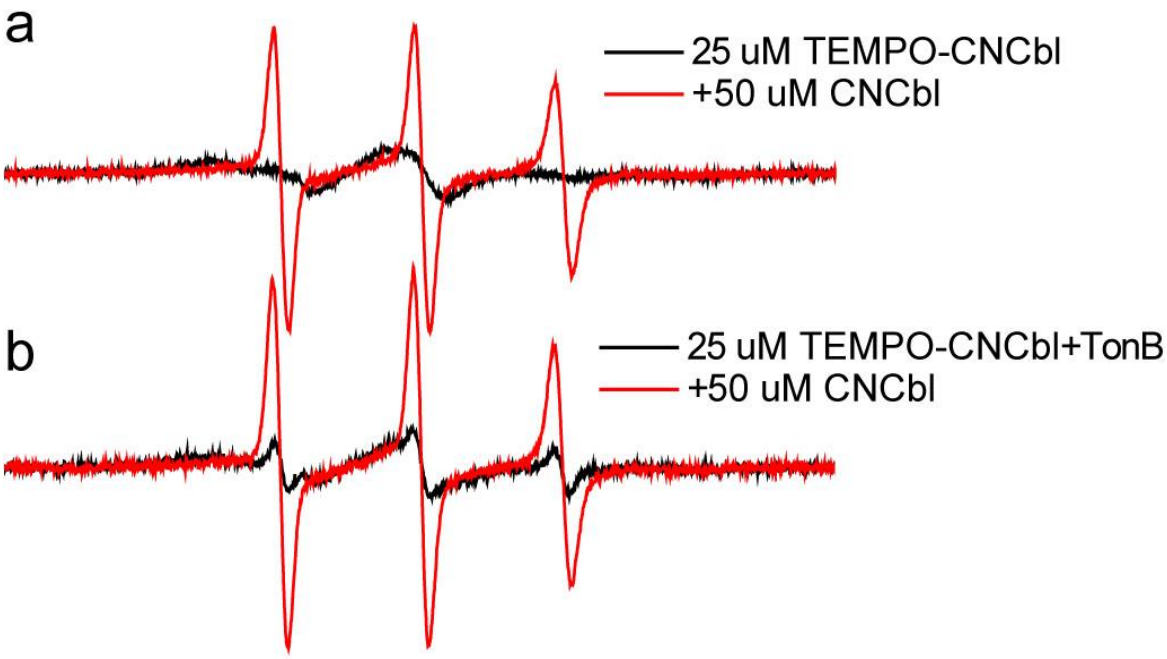

Figure 5.8. Unlabeled vitamin B12 will displace TEMPO-CNCbl. EPR spectra of TEMPO-CNCbl bound to excess BtuB in outer membranes with the addition of 2-fold excess vitamin B12.

The changes in affinity that are seen for TEMPO-CNCbl upon addition of TonB are likely mediated by the binding of TonB to the BtuB Ton box. To ensure that this is the case, we tested to see whether mutants in the Ton box that show diminished TonB affinity[7], and are transport defective[20,21], would suppress or eliminate the substrate-induced changes. When we examined the mutant V10P or a 5 alanine mutant (5AV10C: D6A, T7A, L8A, V9A, V10C, T11A) the reversal of TEMPO-CNCbl binding was either diminished or completely blocked. This indicates that the changes in substrate affinity that are produced by TonB binding are being mediated through the BtuB Ton box. In this experiment, interesting differences appeared in the bound lineshapes for TEMPO-CNCbl. Shown in Figure 5.7d is a comparison of the TEMPO-CNCbl spectrum when bound to wild-type BtuB (blue trace) to the spectra obtained when bound to either the A510C and V10P mutants (red traces). These spectra indicate that the label motion is dramatically altered in the transport-defective mutants. In these spectra, the field difference between the hyperfine extrema has increased, so that value of A_{zz}' has increased from 58 Gauss in the wild-type protein to approximately 70 Gauss in either of the mutant proteins. This value of $2A_{zz}$' in the mutant spectra is close to that expected for a nitroxide near its rigid limit (rotational correlation times longer than about 50 ns) and as seen in Figure 5.7d, the spectrum may be approximated by a simulation of the nitroxide in its rigid-limit where no motional averaging is taking place (dashed trace). This suggests that the label is trapped and effectively fixed relative to BtuB in these Ton box mutants. Using a simple model for motion in a cone[22], the smaller hyperfine splitting observed in the spectrum from the wild-

type protein relative to that for the Ton box mutants can be approximated by rapid motion in a cone that has a half angle of approximately 30 degrees.

In summary, mutations in the Ton box that produce a transport defective phenotype alter the dynamics of TEMPO-CNCbl in its binding site. Taken together, the data in Figures 5.6 and 5.7 provide a clear indication that the energetics and dynamics of the ligand in the substrate binding site of BtuB are coupled to the state of the Ton box on the periplasmic surface.

It should be noted that the mutants L8P, V10P and A5V10C are known to be transport defective[20,21]. In addition, the mutants L8P and V10P lack the ability to bind to TonB with high-affinity[7] and the Ton box in these two mutants appears to be constitutively unfolded[23]. We tested the A5V10C mutant in both a reconstituted and native membrane system and also find that a large fraction of the Ton box is unfolded either in the absence or presence of substrate (Figure 5.9).

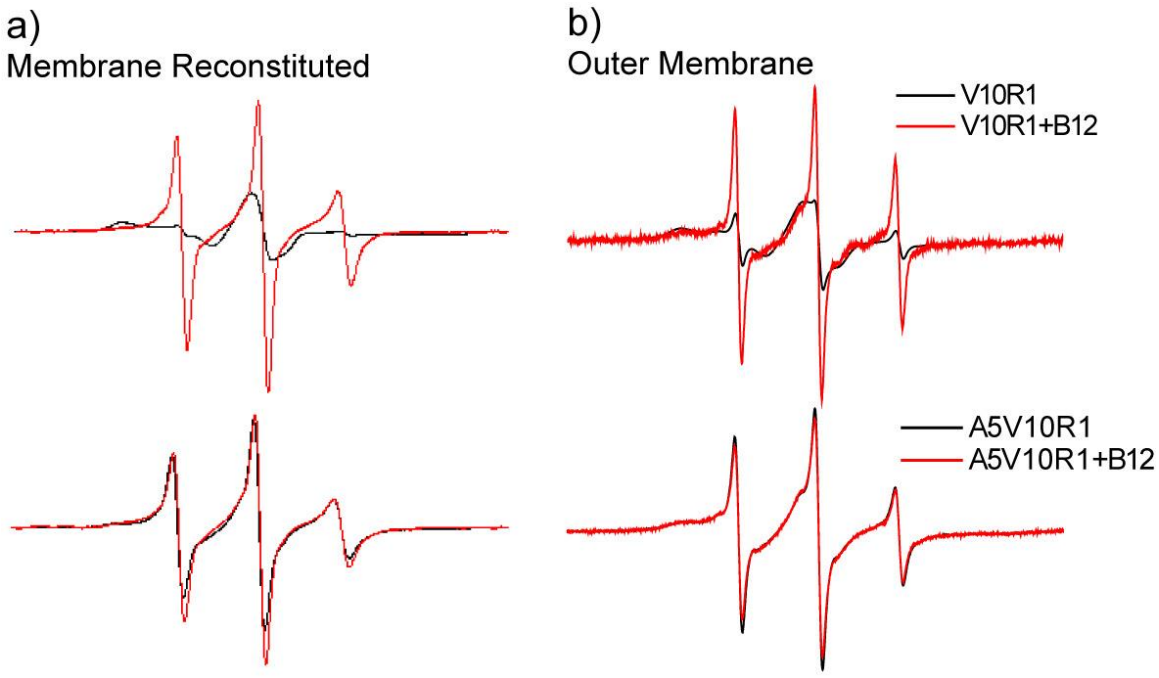

Figure 5.9. The Ton box in transport-defective mutants appears to be constitutively unfolded. Previous work has shown that the Ton box in the transport-defective L8P and V10P mutants appears to be unfolded either in the absence or presence of substrate(S4). Shown in the figure are EPR spectra of the spin-labeled, purified, and reconstituted V10R1 mutant (*top*) and the transport-defective alanine mutant (*bottom*: D6A, T7A, L8A, V9A, V10R1, T11A) in the absence (black trace) and presence (red trace) of vitamin B_{12}.

5.4 Discussion

In the vitamin B_{12} transporter BtuB, substrate binding to the external binding site promotes the unfolding of an energy coupling segment, the Ton box, on the periplasmic surface.[24-26] This transmembrane signaling event increases the affinity of the transporter for TonB[7], and it may help direct TonB to those transporters that are bound to substrate. In the present study, we demonstrate that signaling also takes place from the periplasmic surface to the extracellular surface of BtuB. The binding of a fragment of TonB to the periplasmic Ton

box alters the configuration of the second extracellular loop to produce a more open configuration (Figure 5.5), and TonB binding diminishes the affinity of the transporter for a labeled substrate (Figures 5.6 and 5.7b). Moreover, mutants in the Ton box that produce a transport-defective phenotype, such as V10P or A5V10C, modulate the substrate binding site, and as seen in Figure 5.7d they restrict the dynamics of a spin-label substrate within its binding site.

The data presented here provide clear evidence that the substrate binding site and the Ton box are energetically and structurally linked, which raises interesting questions regarding the mechanism of TonB-dependent transport. In the high-resolution structures of BtuB, there is no obvious pathway for substrate to move through the BtuB barrel; and for transport to occur through BtuB, an unfolding or transient rearrangement of the N-terminal core region must take place. As indicated above, TonB has been proposed to pull[8] or rotate[9] when bound to BtuB in order to promote unfolding or conformational changes in the core necessary to promote transport. However, the allostery that is observed in BtuB suggests that it might not be necessary to pull or rotate the ton box to achieve transport.

Under the conditions used in these experiments, the binding of a fragment of TonB lowers substrate affinity and partially dissociates the TEMPO-CNCbl. We do not presently know whether the dissociated substrate exits the transporter on the exterior surface or is released to the periplasmic surface. If released to the periplasmic interface, one round of transport might be occurring in BtuB simply as a result of TonB binding. In this case, transport could be driven simply by a cycle of attachment and release of TonB from BtuB, where the attachment of TonB to the Ton box alters the population of transient high-energy (or

excited) protein conformational states that are required to mediate substrate movement through the transporter. Such transient states have not been observed in high-resolution structures of TonB-dependent transporters; however, this may simply reflect a failure to populate these states under the conditions used for crystallography.

It was previously suggested that the binding and release of TonB from BtuB might be driven by the conversion of TonB from a monomer to a dimer by the ExbB/ExbB inner membrane proteins[7]. TonB appears to dimerize *in-vivo*[27], and both crystallography and EPR indicate that soluble TonB fragments tend to dimerize[7,28,29]. Since the TonB dimer is observed to convert to a monomer upon interaction with BtuB[7], the conversion of TonB to a dimer would be expected to dissociate TonB from BtuB. Rather than pulling or rotating, the inner-membrane proteins ExbB and ExbD might utilize the inner membrane proton potential to convert TonB from a monomer to a dimer, thereby driving a cycle of attachment and release of TonB from BtuB.

Mutations in the Ton box that are transport-defective, such V10P, were previously found to lack high-affinity binding to TonB[7], and the absence of this high-affinity binding could account, at least in part, for the transport-defective phenotype. However, cold-chase experiments in whole cells indicate that the release of substrate is dramatically slowed in these mutants, presumably as a result of an enhanced affinity of BtuB for substrate[20]. This suggests that these mutants might also fail to transport because the substrate is kinetically or thermodynamically trapped and cannot be released from its binding site. It is interesting that rigid-limit EPR spectra are observed for TEMPO-CNCbl when bound to these

transport-defective mutants (Figure 5.7d), indicating that the substrate is rigidly fixed within its binding site in these mutants.

In BtuB, calcium is known to be a co-ligand for vitamin B_{12} and it is reported to increase the affinity of substrate for the transporter by 1000 fold[15]. Previous work performed at X-band in reconstituted membrane systems indicated that Ca^{2+} acted to order the second extracellular loop and produce slight changes in the position of the loop[29]. The measurements made here at Q-band in intact membrane systems are generally consistent with this result, but they have greater resolution and indicate that the range of structures sampled in the apo state is very large. For example, in Figure 5.2b, distances between labels in loops 2 and 9 vary by more than 20 Å. The addition of Ca^{2+} acts to narrow the distribution and appears to select one of the conformations present in the apo distribution. In this manner, Ca^{2+} binding appears to promote a conformational selection in the second loop[29], leading to an ordering of the loop and the formation of a binding site that is favorable for substrate interaction. Movements in this loop were also examined by molecular dynamics (MD) simulations, and it was also found that Ca^{2+} tended to order the loops[30]; however, the extent of the distance fluctuations seen by MD were much smaller than that seen here, perhaps because of the time-scale of the simulation.

In the BtuB crystal structure, vitamin B_{12} interacts with residues in loops 2, 3, 4, 9, 10, 11. Although we have not sampled loops 3 and 4 or attempted an exhaustive study of the extracellular region, among those sites examined Ca^{2+} produced changes in distance distributions only for labels in loop 2, and vitamin B_{12} appeared to modulate the position

of labels only in loops 2 and 8, with no significant differences in distribution seen for loops 7, 9 and 10. As seen in Figure 5.3b, the loops that did not respond to substrate or Ca^{2+} exhibited very broad distance distributions covering a range of over 30 Å. Unlike loop 2, the predictions from the crystal structures for the other loops match poorly with the experimental distributions, and the longer loops 8 and 10 appear to sample configurations that vary quite dramatically from those in the high-resolution structures. This is not unexpected, since these loops are known to be in conformational exchange[14].

In summary, data obtained from site-directed spin labeling and EPR spectroscopy on a native outer membrane preparation indicate that the binding of TonB to the periplasmic Ton box of BtuB alters the conformation of the extracellular loops and the substrate binding site of this transporter. Mutations in the Ton box that are transport defective also modify the substrate binding site and the state of the substrate. The data indicate that transmembrane signaling travels in both directions in BtuB, a phenomenon that likely plays a critical role in the molecular mechanism of TonB-dependent transport.

5.5 Materials and Methods

Expression and purification of ΔN-TonB.

DNA encoding the *Escherichia coli.* TonB C-terminus (150-239) was transformed into T7 Express lysY/I^q competent cells, and the cells were grown in 2xYT media at 37°C and induced with IPTG at 0.6 OD 600. Cell growth was continued at 20°C until an OD600 of 1.65 was reached, and the cells were then harvested by centrifugation at 4000 *g* for 10 min and resuspended in 25mM Tris, pH 7.5 containing 1 mM 4-(2-aminoethyl)benzenesulfonyl fluoride hydrochloride (AEBSF) (Thermo Fisher Scientific, Pittsburgh, PA), 0.5 mM dithiothreitol (DTT) (Avantor Performance Materials, Inc., Phillipsburg, NJ), 20 units/mL aprotinin (Calbiochem, Darmstadt, Germany), and 100 μM leupeptin (Roche Diagnostics, Indianapolis, IN). The resuspended cells were then lysed using a French press at a pressure of 1300 psi. The clarified lysate was incubated with 10 mL of Ni^{2+}-NTA resin and subserquenly eluted with 25 mM Tris (pH 7.5), 300 mM NaCl, and 250 mM imidazole. The TonB containing fractions were subjected to proTEV plus (Promega, Madison, WI) protease overnight at 4°C to remove the His6 tag. The protein was loaded onto a prepacked 5 mL SP HP anion-exchange column (GE Healthcare, Piscataway, NJ), and a gradient was run from 0.25 M to 1.0 M of NaCl in 25 mM Tris buffer (pH 7.4). Following purification, protein purity was analyzed by SDS-PAGE electrophoresis, and the fractions containing pure TonB were pooled. The protein was dialyzed into 25mM Tris 128mM NaCl (pH 7.5).

Expression and labeling of BtuB in native outer-membranes.

Mutants of BtuB on a pUC8 backbone were engineered using the Agilent Technologies (Santa Clara, CA) QuikChange Site Directed Mutagenesis Kit. The mutant A5V10 was

provided by Prof. Robert Nakamoto (Department of Molecular Physiology, University of Virginia). Wild-type and mutant BtuB were overexpressed in the *E. coli* strain RK5016 (*argH*, *btuB*, *metE*)[21]. Cells were grown for overnight in minimal media containing 100 μg/mL ampicillin and supplemented with 0.24% w/v glucose, 150 μ*M* thiamine, 3 m*M* $MgSO_4$, 300 μ*M* $CaCl_2$, and 0.01% w/v of Met and Arg. Cells were harvested by centrifugation at 4000 *g* for 10 min followed by resuspension in 30 mL 25mM HEPES buffer, pH 6.5. The resuspended cells were then lysed using a French press at a pressure of 1300 psi. To prevent proteolysis of BtuB, AEBSF was added to a final concentration of 400 μg/mL. Following lysis, the solution was centrifuged at 14500 *g* for 10 min. to remove cellular debris. The inner membrane in the supernatant was solubilized by addition of 0.5% sarkosyl, and outer membranes containing BtuB were pelleted by ultracentrifugation at 104,000 *g* for 90 min. Each pellet was resuspended in 4 mL 25mM HEPES.

To spin label free cysteines in BtuB, 100 μL of S-(2,2,5,5-tetramethyl-3-pyrroline-3-yl) methyl methanethiosulfonate (MTSL, Toronto Research Chemicals, North York, ON, Canada) from a 12 mM stock solution in ethanol was added to the resuspended outer-membrane pellet and allowed to react for 2 hours at room temperature. The unreacted spin label was removed by centrifugation at 60,000 rpm for 20 minutes in a Beckman Airfuge (Brea, Ca). Typically, three centrifugation steps were required to remove the unreated label, where the final centrifugation step served to concentrate the sample. The concentration of BtuB in the outer membrane was estimated by titrating the preparation against a sample of known spin labelled substrate (TEMPO-CNCbl) concentration. This was done at sufficiently high substrate concentrations that virtually no free ligand was present until a 1:1 stoichiometry had been reached. To determine the affinity of TEMPO-

CNCbl for BtuB, the concentration of TEMPO-CnCbl was held constant at 10 or 20uM while BtuB was titrated into the sample. In these titrations, final protein concentrations ranged from 5uM to 80uM.

Reconstitution of BtuB.

For measurements on BtuB in proteoliposomes, the outer membrane preparations were solubilized by addition of 0.6g/L *n*-octyl-β-D-glucopyranoside (OG), ANAGRADE (Anatrace, Marmee, OH) in 100 mM Tris buffer (pH 8.05), containing a final concentration of 8 mM EDTA. After a 2 h incubation the detergent complex was ultracentrifugated at 90,000 *g* for 1 h to remove non-soluble material. The protein in the supernatant was then spin-labeled by adding 200 μL of 12 mM MTSL, and the reaction was allowed to proceed for 1 h at room temperature. The protein was then loaded onto a prepacked 5 mL Q-sepharose high-performance anion-exchange column (Amersham Biosciences, Piscataway, NJ), and a gradient was run from 0.25 M to 1.0 M of LiCl in 25 mM BisTris buffer containing 17 mM OG (pH 7.0). Following purification, protein purity was analyzed by SDS-PAGE electrophoresis, and the fractions containing pure BtuB were pooled. A solution of 4:1 OG/1-palmitoyl-2-oleoylphosphatidylcholine (POPC) mixed micelles was produced by sonication for 15 minutes (Branson Danbury, CT) the pure BtuB was then added to this mixture. Dialysis to remove the OG was performed with 6 exchanges of 4 liters each containing 150 mM NaCl and 10 mM HEPES at pH 6.5 with 1 mM NaN_3 and 100 nM EDTA. The dialyzed protein was pelleted by centrifugation at 10,000 g and solubilized in ~1mL dialysis buffer. Samples were subsequently concentrated for EPR spectroscopy using a Beckman Airfuge (Brea, Ca). Final lipid concentration was

determined using a phosphate assay and ranged from 20-60mM. Final protein concertation was determined using a amido black assay and range from 90-200 uM.

Synthesis of TEMPO-CNCbl.

The spin labelled substrate, TEMPO-CNCbl, was synthesized as described previously[12]. Briefly, the ribose-5'-hydroxyl was activated with 1,1′-Carbonyl-di-(1,2,4-triazole) (CDT, Sigma) followed by reaction with with 4-amino TEMPO in DMSO. This reaction was carried out under argon and the TEMPO-CNCbl product was precipitated by the addition of a 1:1 mixture of acetone and diethylether. The crude reaction product was subsequently purified by HPLC on a C18 reverse phase column and the product confirmed by mass spectrometry.

Continuous Wave EPR.

For continuous wave EPR, 4uL of sample was loaded into glass capillaries with a 0.6mm inner diameter and a 0.84mm outer diameter (VitroCom, Mountain Lakes, NJ). Continuous-wave (CW) EPR measurements were recorded at X-band using a Bruker EMX spectrometer fitted with a room temperature ER 4123D dielectric resonator (Bruker Biospin, Billerica, MA). Unless otherwise noted, EPR spectra were 100 Gauss scans, using a modulation amplitude of 1 Gauss and a microwave power of 2 mW. The spectra were baseline corrected and normalized to the total spin number using LabVIEW software provided by Dr. Christain Altenbach (University of California, Los Angeles).

To estimate the binding affinity of TEMPO-CNCbl to BtuB, the normalized amplitude (A) of the central ($m_{I=0}$) nitroxide resonance was measured and plotted versus the BtuB concentration. Since the EPR spectrum is a linear combination of the aqueous and bound

TEMPO-CNCbl spectra, the amplitude A may be given as: $A = f_f A_f - f_b A_b$, where f_f and f_b are the fractions of aqueous and bound label and A_f and A_b are the intrinsic normalized amplitudes of the aqueous and bound label, respectively. The values of A_f and A_b were independently determined from bound and aqueous EPR spectra, and the amplitude versus [BtuB] data were then fit using a standard expressions for 1:1 binding[31] to generate a dissociation constant K_d using the non-linear least squares fitting method implemented in Mathematica (Wolfram Scientific, Champaign, IL).

Pulsed EPR measurements.

Samples for double electron-electron resonance (DEER) contained approximately 15-20 μL of double labeled outer membrane BtuB preparations in 15% deuterated glycerol. The samples were placed into quartz sample tubes having a 1.5mm inner diameter 1.8 mm outer diameter (VitroCom, Mountain Lakes, NJ) and then rapidly frozen in isopropanol cooled with dry ice. The data were recorded at 80 K on a dedicated Q-band Bruker E580 spectrometer fitted with an EN5107D2 dielectric resonator. For DEER experiments, the dead-time free four-pulse sequence with phase-cycled π/2-pulse was used[32]. Typical pulse lengths were 16 ns for π/2 and 32 ns for π the observer pulses and 20 ns π for the pump pulse. The pump pulse was set to the maximum of the echo-detected field swept spectrum and the observer pulses were set 60 MHz lower. The deuterium modulations were averaged by increasing the first interpulse delay by 16 ns for 8 steps. To obtain distance distributions, the normalized primary DEER data $V(t)/V(0)$ were processed to remove the background function from intermolecular interactions and the resulting form factors $F(t)/F(0)$ were fitted with a model-free Tikhonov regularization to distance distributions with

DeerAnalysis2013 software package[33]. The error ranges shown in the distance distributions are based upon variation in the background form factors that produce fits within 15% RMSD of the best fits. Predictions of the expected distance distributions based upon published crystal structures were made using the program MMM[16]. In this program, we used a rotamer library for the R1 side-chain that was determined using density functional theory and consistent with available crystal structures[34]. Structures were visualized using PyMOL Molecular Graphics System, Version 1.7.4 (Schrodinger, LLC).

5.6 References

1. Braun, V. Energy transfer between biological membranes. *ACS Chem Biol* **1**, 352-354 (2006).

2. Noinaj, N., Guillier, M., Barnard, T.J. & Buchanan, S.K. TonB-dependent transporters: regulation, structure, and function. *Annu Rev Microbiol* **64**, 43-60 (2010).

3. Postle, K. & Kadner, R. Touch and go: Tying TonB to transport. *Mol. Microbiol.* **49**, 869-82 (2003).

4. Postle, K. & Larsen, R.A. TonB-dependent energy transduction between outer and cytoplasmic membranes. *Biometals* **20**, 453-65 (2007).

5. Freed, D.M., Horanyi, P.S., Wiener, M.C. & Cafiso, D.S. Conformational exchange in a membrane transport protein is altered in protein crystals. *Biophys J* **99**, 1604-10 (2010).

6. Xu, Q., Ellena, J.F., Kim. M. & Cafiso, D.S. Substrate-dependent unfolding of the energy coupling motif of a membrane transport protein determined by double electron-electron resonance. *Biochemistry* **45**,10847-54 (2006).

7. Freed, D.M., Lukasik, S.M., Sikora, A., Mokdad, A., & Cafiso D.S. Monomeric TonB and the ton box are required for the formation of a high-affinity transporter-TonB complex. *Biochemistry.* **52**, 2638-48 (2013).

8. Gumbart, J., Wiener, M. C. & Tajkhorshid, E. Mechanisms of force propagation in TonB-dependent outer membrane transport. *Biophys. J.* **93**, 496-504 (2007).

9. Klebba, P.E. ROSET Model of TonB Action in Gram-negative Bacterial Iron Acquisition. *J Bacteriol* (2016).

10. Pawelek, P.D., Croteau, N., Ng-Thow-Hing, C., Khursigara, C. M., Moiseeva, N., Allaire, M. & Coulton, J. W. Structure of TonB in complex with FhuA, E-coli outer membrane receptor. *Science.* **312**, 1399-1402 (2006).

11. Shultis, D. D., Purdy, M. D., Banchs, C. N & Wiener, M. C. Outer membrane active transport: structure of the BtuB:TonB complex. *Science.* **312,** 1396-9 (2006).

12. Joseph, B., Sikora, A., Bordington, E., Jeschke, G., Cafiso, D., Prisner, T. Distance Measurement on an Endogenous Membrane Transporter in *E. coli* Cells and Native Membranes Using EPR Spectroscopy. *Angew. Chem. Int. Ed. Engl.* **54**, 6196-99 (2015).

13. Joseph B., Sikora A. & Cafiso D.S. Ligand induced conformational changes of a membrane transporter in *E. coli* cells with PELDOR/DEER. *JACS*. **6**, 1844-47 (2016).

14. Kim, M., Xu, Q., Murray, D. & Cafiso, D. S. Solutes alter the onformation of the ligand binding loops in outer membrane transporters. *Biochemistry*. **47**, 670-9 (2008).

15. Cadieux, N., Barekzi, N. & Bradbeer, C. (2007) Observations on the calcium dependence and reversibility of cobalamin transport across the outer membrane of Escherichia coli. *J Biol Chem* **282**, 34921-28 (2007).

16. Polyhach, Y., Bordignon, E. & Jeschke, G. Rotamer libraries of spin labelled cysteines for protein studies. *Phys. Chem. Chem. Phys.* **13**, 2356-66 (2011).

17. Chimento, D. P., Mohanty, A. K., Kadner, R. J. & Wiener, M. C. Substrate-induced transmembrane sgnaling in the cobalamin transporter, BtuB. *Nat. Struct. Biol*. **10**, 394-401 (2003).

18. Cherezov V, *et al.* In meso structure of the cobalamin transporter, BtuB, at 1.95 A resolution. *J Mol Biol* **364**, 716-34 (2006).

19. James, K.J., Hancock. M.A., Moreau, V., Molina. F. & Coulton. J.W. TonB induces conformational changes in surface-exposed loops of FhuA, outer membrane receptor of Escherichia coli. *Protein Sci* **17**,1679-88 (2008).

20. Barekzi, N. Ph. D. Thesis Mutational analysis of the proteins BtuB and TonB: their roles in cobalamin transport. (University of Virginia, Charlottesville, Virginia 2009).

21. Gudmundsdottir, A., Bell, P. E., Lundrigan, M. D., Bradbeer, C. & Kadner, R. J. Point mutations in a conserved region (TonB box) of *Escherichia coli* outer membrane protein BtuB affect vitamin B12 transport. *J. Bacteriol.* **171**, 6526-33 (1989).

22. Van, S.P., Birrell, G.B. & Griffith, O.H. Rapid Anisotropic Motion of Spin Labels - Models for Motion Averaging of ESR Parameters. *J Magn Reson* **15**, 444-59 (1974).

23. Coggshall, K.A., Cadieux, N., Piedmont, C., Kadner, R. & Cafiso, D.S. Transport-defective mutations alter the conformation of the energy-coupling motif of an outer membrane transporter. *Biochemistry* **40**, 13946-71 (2001).

24. Cadieux, N. & Kadner, R.J. Site-directed disulfide bonding reveals an interaction site between energy-coupling protein TonB and BtuB, the outer membrane cobalamin transporter. *Proc Natl Acad Sci USA* **96**, 10673-78 (1999).

25. Fanucci, G. E., Coggshall, K. A., Cadieux, N., Kim, M., Kadner, R. J. & Cafiso D. S. Substrate-induced conformational changes of the periplasmic N-terminus of an outer-membrane ttransporter by site-directed spin labeling. *Biochemistry*. **42**, 1391-1400 (2003).

26. Merianos, H. J.,Cadieux, H., Lin, C. H., Kadner, R. J. & Cafiso, D. S. Sunstrate-induced exposure of an energy-coupled motif of a membrane transporter. *Nat. Struct. Biol.* **7**, 205-9 (2000).

27. Sauter, A., Howard, S.P. & Braun, V. In vivo evidence for TonB dimerization. *J Bacteriol* **185**, 5747-54 (2003).

28. Chang, C., Mooser, A., Pluckthun, A. & Wlodawer, A. Crystal structure of the dimeric C-terminal domain of TonB reveals a novel fold. *J. Biol. Chem.* **276**, 27535-40 (2001).

29. Koedding, J., Howard, P., Kaufmann, L., Polzer, P., Lustig, A. & Welte, W. Dimerization of TonB is not essential for its binding to the outer membrane siderophore receptor FhuA of Escherichia coli. *J. Biol. Chem.* **279**, 9978-86 (2004).

30. Csermely, P., Palotai, R. & Nussinov, R. Induced fit, conformational selection and independent dynamic segments: an extended view of binding events. *Trends Biochem Sci* **35**, 539-546 (2010).

31. Gumbart, J., Wiener, M. C. & Tajkhorshid, E. Coupling of calcium and substrate binding through loop alignment in the outer-membrane transporter BtuB. *J. Mol Biol.* **393**, 496-504 (2009).

32. Swillens, S. Interpretation of binding curves obtained with high receptor concentrations: practical aid for computer analysis. *Mol Pharmacol* **47**,1197-1203 (1995).

33. Pannier, M., Viet, S., Godt, A., Jeschke, G. & Spiess, H. W. Dead-time free measurement of dipole-dipole interactions between electron spins. *J. Magn. Reson.* **142**, 331-40 (2000).

34. Jeschke, G., Chechik, V., Ionita, P., Godt, A., Zimmermann, H., Banham, J., Timmel, C. R., Hilger, D. & Jung, H. DeerAnalysis2006 – a comprehensive software package for analyzing pulsed ELDOR data. *Appl. Magn. Reson.* **Vol. 30**, 473-498 (2006).

35. Warshaviak, D.T., Serbulea, L., Houk, K.N. & Hubbell, W.L. Conformational analysis of a nitroxide side chain in an alpha-helix with density functional theory. *J Phys Chem B* **115**, 397-405 (2011).

Chapter 6: Urea denaturation of the BtuB hatch domain

6.1 Introduction:

All TBDTs are proteins are comprised of three domains; the 22-stranded β-barrel, a hatch or plug domain and the TonB interacting domain or Ton Box. The plug domain is comprised of 130-150 resides comprised of both α-sheets and β-sheets. The motions of this plug have long been a source of study.[1,2] A major hurdle to elucidating the transport cycle of TBDTs has been proving the mechanism of substrate passage across the membrane which must involve plug domain changes. However molecular dynamics simulations have failed to produce a water channel large enough to facilitate substrate passage, indicating large structural rearrangements of the hatch are necessary.[3] None of the crystal structures, even with substrate and/or TonB bound show plug displacement great enough to allow for substrate passage.[1,4,5] Previously obtained experimental data suggests two possible mechanisms for the creating of this water filled channel. The first mechanism has a significant portion of the plug domain unfolding into the periplasmic space. Steered molecular dynamics simulations have been able to unfold enough of the N-terminal portion of the plug to form a cavity big enough for substrate passage.[6] A cysteine accessibility study suggests that large portions of the hatch domain become solvated upon substrate binding, possibly by denaturation into the periplasm.[7] The second mechanism involves the substrate passing between sequential binding sites as it is transported. Molecular dynamics simulations show a large number of water molecules at the interface of the barrel and plug in several TBDTs, proving the plug is highly solvated.[8] Thermal denaturation studies show

that the hatch and barrel act as independent domains[9] and low urea concentrations are needed to reversibly form a pore.[10] These experiments point to a pore that is small with a low energetic cost of formation.

Urea has long been used as a protein denaturant.[11,12] The unfolded state exposes the interior hydrophobic residues to water, creating a water-swollen state with a smaller volume, optimizing free energy of the macromolecule.[13,14] Studies conducted on both soluble and membrane bound proteins clearly show reversible denaturation and a linear relationship between denaturant concentration and free energy changes.[15,16]

A resulting linear extrapolation model (LEM) has been widely used for these measurements, $\Delta G^{Urea} = \Delta G^{Water} - m[\mathrm{C}]$. The m value or slope of this fit is a measure of protein surface area exposed to solvent during denaturation and so correlated to protein stability when exposed to urea.[17]

In order to better understand which theory more closely resembles the actual TBDT transport strategy a previous study out of the Cafiso lab utilized urea denaturation in combination with SDSL-EPR to obtain thermodynamic data on the BtuB hatch domain. The data presented in Flores Jimenez & Cafiso[18] indicate that the hatch domain does not unfold as a whole. These data are represented in Table 6.1.

Table 6.1 Previously obtained thermodynamics data from the hatch domain of BtuB

Mutant	$\Delta G_U^o \left(\frac{kcal}{mol}\right)$	$m \left(\frac{kcal}{mol\ M}\right)$	C_0 (M)
V10R1	3.01 ± 0.24	0.93 ± 0.06	3.25 ± 0.13
T30R1	3.33 ± 0.12	1.00 ± 0.04	3.32 ± 0.04
V78R1	2.12 ± 0.05	0.29 ± 0.00	7.23 ± 0.13
N128R1	2.53 ± 0.08	0.36 ± 0.01	6.95 ± 0.12

This table reports the denaturation data of the hatch domain residues tested. The ΔG_U^o is free energy for unfolding in the absence or denaturant. The *m* parameter is a measure of solvent accessible protein surface area exposed to solution upon denaturation. C_0 is the concentration of urea that represent the midpoint of the denaturation. These parameters were obtained from the EPR line shapes as described in the methods section. Table adapted from Flores Jimenez & Cafiso, 2012[18].

The *m* and C_0 values obtained as part of that study paint a clear picture, the *m* values for V10 and T30 are much higher than any other part of the hatch and the C_0 values for these two residues are lower. These two parameters both point to this segment unfolding to expose more protein surface area at a lower urea concentration. The authors concluded that a segment including residues V10 and T30 but not V78 or further unfolds at low urea concentrations.

Molecular dynamics simulations were performed to better understand the size a potential pore needed to be in order to facilitate the transport of CNCbl. Figure 6.1 depicts the pore formed by the removal of residues 6-65.

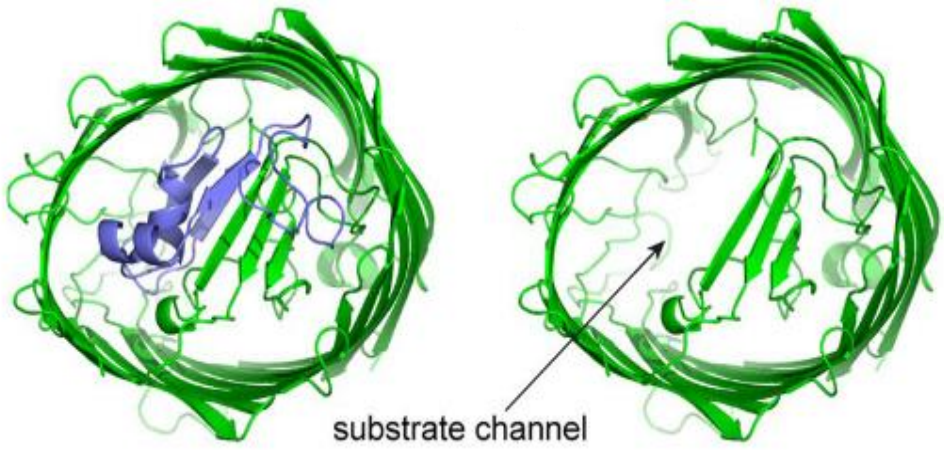

Figure 6.1 Possible B_{12} substrate channel formed when residues 6-65 are removed. Here a section of the BtuB hatch domain (residues 6-65, depicted in blue) are removed to reveal a pore large enough to accommodate CNCbl transport. A similar pore was observed during a steered molecular dynamics simulation in which the ton box was pulled and portions of the hatch were denatured. There is no data to indicate whether such a pore is opened during transport in any TBDT. Taken from Flores Jimenez & Cafiso, 2012[18]

Building on these experiments we set to probe similar energetic parameters for residues between T30 and V78 in an attempt to narrow down the residues participating in the pore and whether the denatured cooperatively, similar to V10 and T30 or independently. The data indicated that the hatch between T30 and V78 does not unfold in one step and points to a transient pore mechanism.

6.2 Results and Discussion:

Using the procedure described in the materials and methods section five mutants of the BtuB hatch domain were created. These mutants; L46, D53, N57, I66 and S74 were grown and purified then subjected to increasing urea concentrations. The mutants were chosen to represent a variety of hatch positions specifically on putative substrate binding loops 1 (N57) and 2 (S74) as well as on the two β-sheets (D53 and I66) and α-helix (L46) not tested in the previous study. These residues are modeled in figure 6.2.

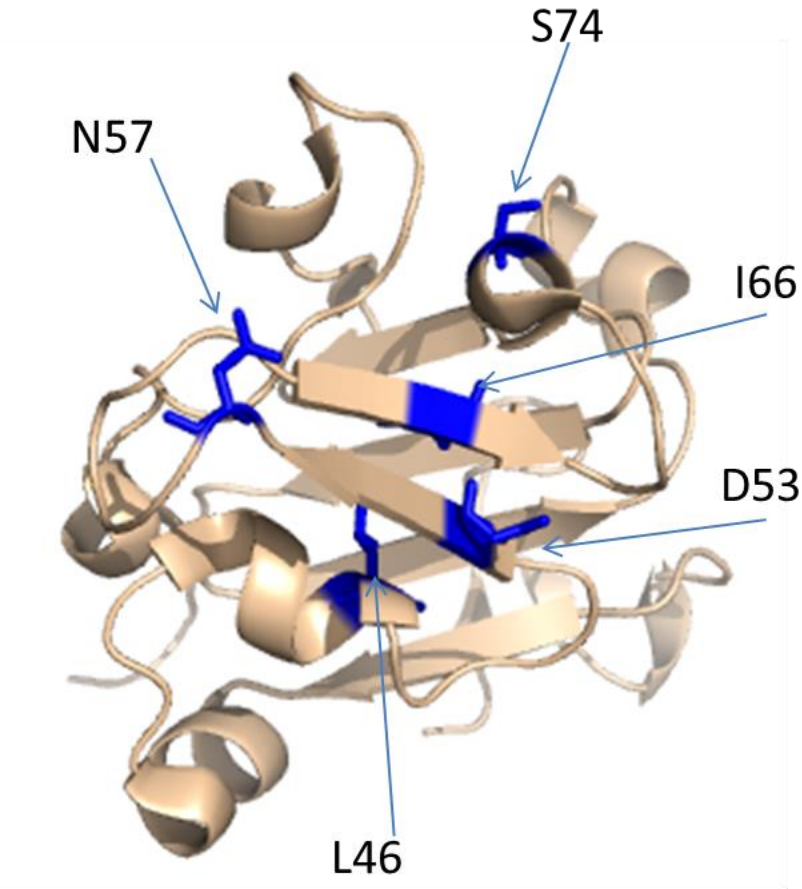

Figure 6.2 Model of BtuB hatch domain residues. The hatch domain of the high resolution BtuB crystal structure (PDB 1NQE) with the residues used in this study depicted as ball and stick models in blue.

Each residue notably had fairly immobile line shapes when urea was absent with the exception of N57. (Figure 6.3) These restricted line shapes indicate that the residues studied are folded normally and are likely unperturbed by the mutagenesis and subsequent spin labeling. This is very important especially for these sites because they are buried in the hatch and such a location would produce a very immobile line shape. An analysis of residue N57 using the simulation program MMM produced two predicted rotamers for the MTSL spin label.[19] This indicates that the N57 CW spectrum shows an unexpectedly high degree of mobility, this is most likely due to its location on a solvent exposed substrate binding

loop that is unnaturally ordered in the crystal structure. Further studies of the substrate binding loops in the absence of crystallization buffers may provide more insight to their specific functions.

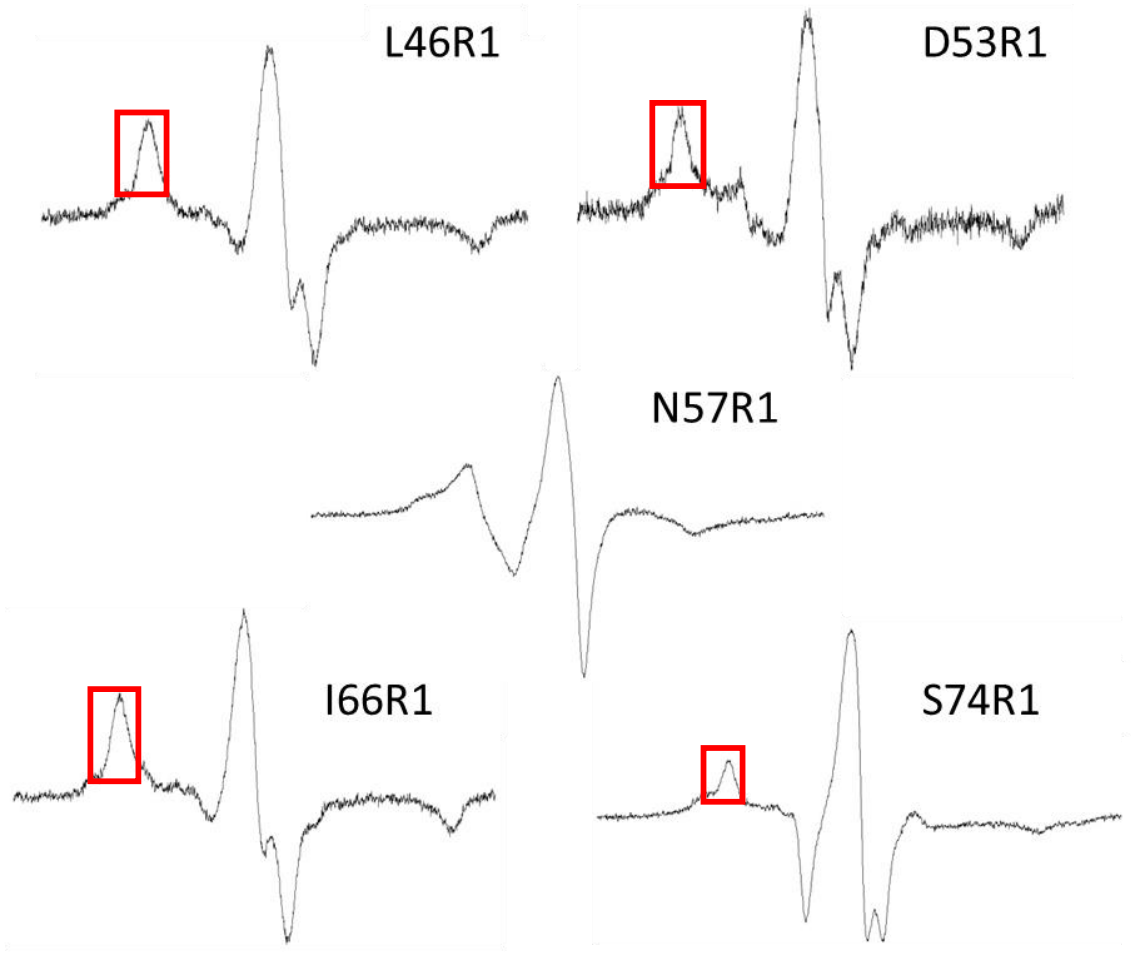

Figure 6.3 Line shapes of BtuB hatch domain residues in the absence of urea. Here the position of the low field hyperfine extreme indicated with a red box. This hyperfine extreme is where tertiary contact is seen in a CW-EPR spectrum. The nitroxide hyperfine extrema, A_{zz}, was measured for each spectrum shown above. All residues with the exception of N57 have A_{zz} values that are between 34.35 and 35.35 G. These values are consistent with predicted rigid limit simulation value of 37G[20] and experimental A_{zz} values for the most restricted MTSL in lipid of 35.98[21]. The A_{zz} value measured for N57 is considerably lower at 26.84 ± 0.89 G, indicating that this residue is much more mobile than other hatch positions. This mobility is most likely due to the position of N57 on a hatch domain loop putatively described as substrate binding loop 2.

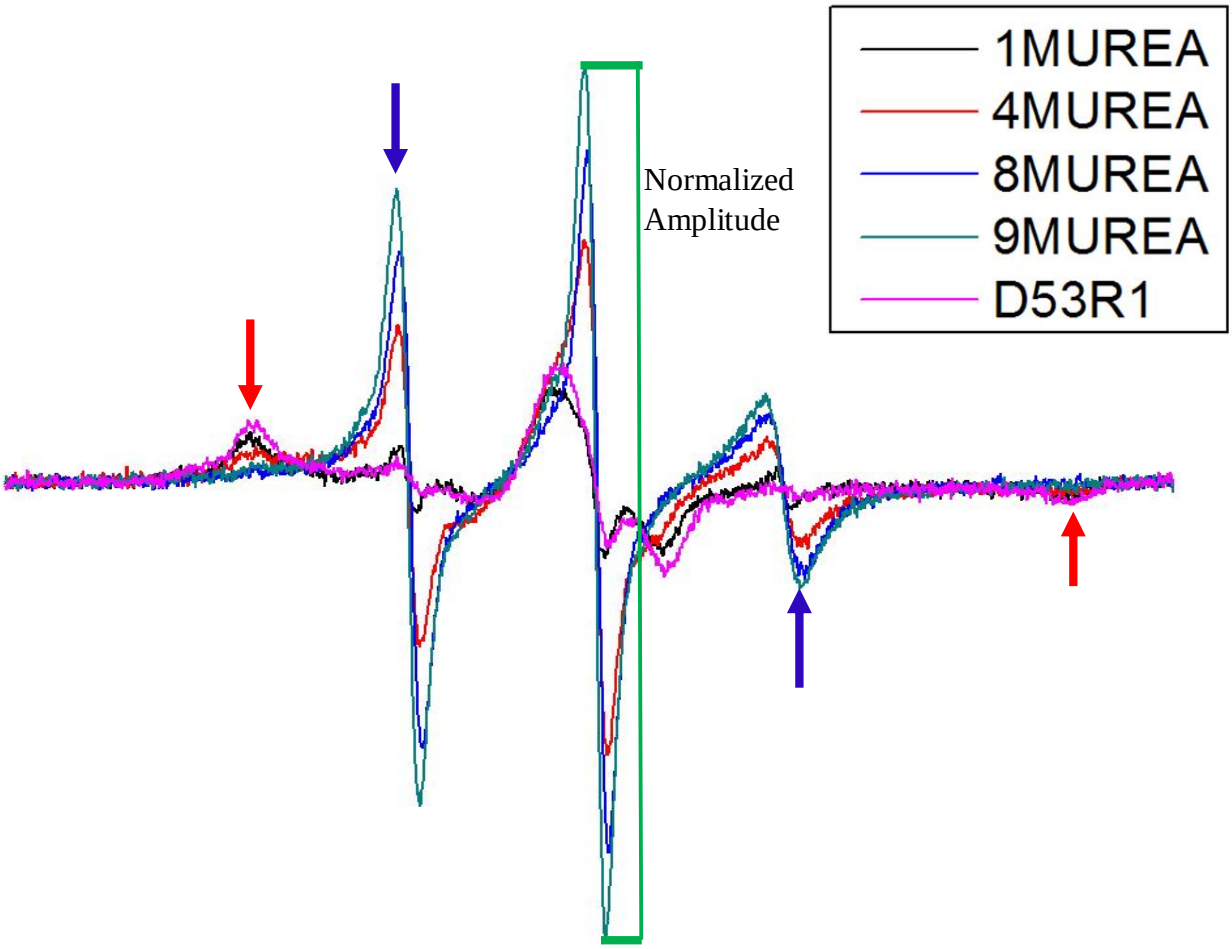

Figure 6.4 Representative spectra of D53R1 from 0 to 9M urea. As urea concentration increases the broad spectral components decrease (red arrows) and the narrow spectral components increase (blue arrows). These features highlighted here on the high and low field line are also present in the mid field line. Narrow line features are a result of fast spin label motions and will increase as the denaturation progresses while broad line features are a result of slow moving or frozen spin labels and are expected to decrease. The distance between peaks in the mid field line of the normalized CW-EPR spectrum is the normalized amplitude.

Upon exposure to increasing concentration of urea, ranging from 0-7 (L46R1) to 0 -12 (S74R1 and I66R1) all line shapes exhibited increased mobility. This change occurs when secondary and tertiary structure is lost allowing backbone dynamics to increase. An example of the lineshapes seen during this type of denaturation experiment is shown in Figure 6.4. The highest concentration of urea tested varied but always represented a line

shape at which the unfolding transition is complete and that did not change with increasing urea. A line shape that did not exhibit change with increasing urea represented a fully denatured state for the local residue. Interestingly, some mutants (D53, I66 and S74) releveled residual protein structure at these highest urea concentrations. Existence of slower motional components in high urea concentrations have been reported in BtuB[11] and FepA[22] and is most likely due to variation in the unfolded structure of the protein at these sites. It is also consistent with previous work that finds nativelike protein structure can be found even in high denaturant concentrations[23] and with the hypothesis that denatured states are more complex than just a random coil[24].

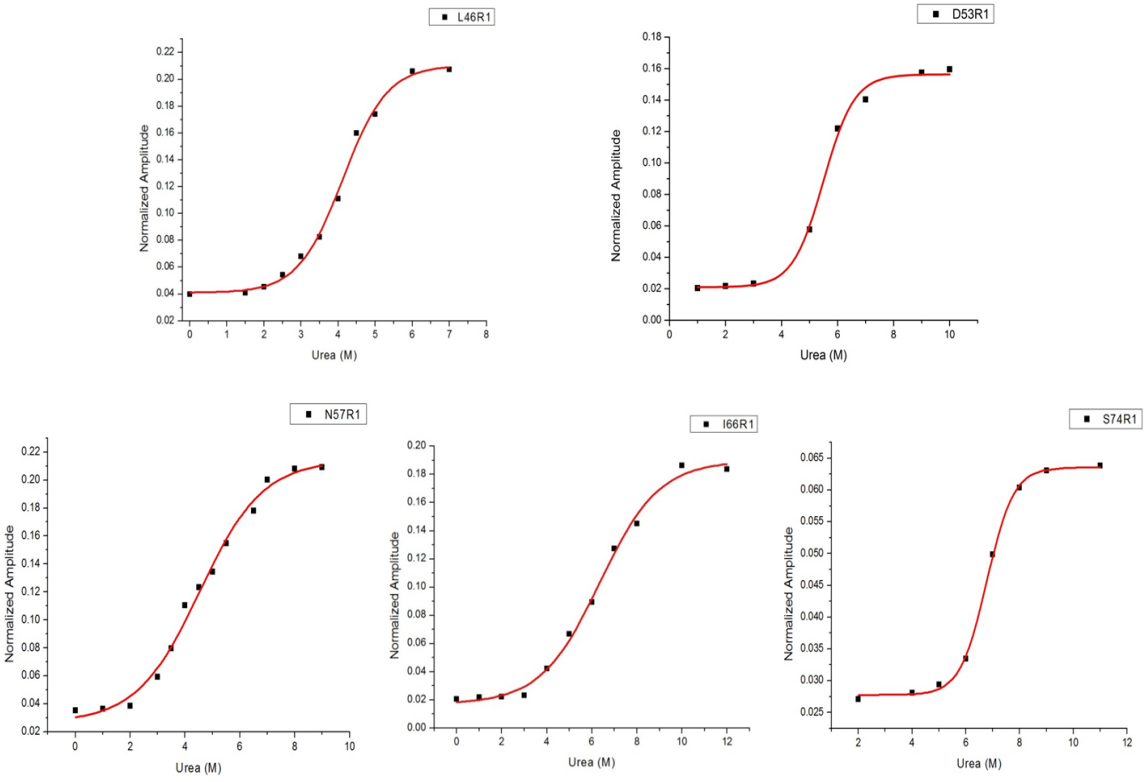

Figure 6.5 Plots of the normalized amplitudes from the five hatch mutants as a function of the urea concentration. The normalized amplitude is linearly related to the fraction of unfolded protein. The red fit lines were obtained by fitting the data point to equation 6.1 (see Materials and methods). Here we assume a two state model in which the protein exists in either a folded or unfolded state.

Figure 6.5 depicts the plots and fits of the normalized amplitude versus urea concentration. The parameters obtained from the fit (see equation 1, Materials and Methods) were then applied to Equation 6.2 to obtain the parameter *m* and to equation 6.3 to obtain ΔG_U°. All the thermodynamic data are listed in Table 6.2. The *m* parameter, which is a measure of the surface area exposed upon denaturation varies widely but is unaffected by the addition of CNCbl with the notable exception of N57. The *m* parameter data for L46R1, I66R1 and S74R1 is reflective of previous work. In Flores & Cafiso[18] denaturation at sites V10 and T30 produced a *m* value very close to 1. These two residues are closer to the N terminus of

BtuB and are close to L46. On the other side of the hatch, I66 and S74 exhibit *m* values that are identical within error to previously studied sites on the C-terminus of the hatch domain; E108, N128. The *m* values of D53 and N57 are intermediate between these two extremes and do exhibit increases upon CNCbl binding. The CNCbl mediated *m* value increases for these two residues indicates that the substrate is changing the unfolding event by causing an increase in the surface area of protein that is unfolded.

Next we examine the C_0 values; in these data, we observe a trend of increasing C_0 from N to C terminus with the exception of N57. Also in almost every case the addition of CNCbl decreases that value significantly. Since the C_0 value indicates the urea concentration required to denature half of the protein population, these data show that substrate binding promotes hatch instability. Notably the I66 C_0 value increases over 1.5 M when B_{12} binds, indicating this may not be a global hatch destabilization event.

Interestingly the free energy of unfolding does not change very significantly as the hatch is scanned. This is consistent with the previous study[18] but the values of ΔG_U° should be viewed cautiously as they have been known to be substantially affected by the SDSL process, especially when sites of significant tertiary contact are probed.[25] $\Delta\Delta G_U^\circ$ on the other hand directly measures the difference between spin labeled sites when the protein is in the apo or substrate free state and after CNCbl is added. These data show that the magnitude and sign of the free energy varies widely between positions in the hatch. The change in free energy that is due to the CNCbl binding event seems to stabilize portions of the hatch and destabilize other portions.

Table 6.2: Urea denaturation curves for BtuB hatch domain mutants.

BtuB Mutant	m (Kcal mol^{-1} M^{-1})	C_0 (M)	ΔG_U° (Kcal mol^{-1})	$\Delta\Delta G_U^\circ$ (Kcal mol^{-1})
L46R1 Apo	1.03 ± .04	4.39 ± .05	4.52 ± .18	1.30
L46R1 CNCbl	1.10 ± .05	2.93 ± .03	3.22 ± .35	
D53R1 Apo	.615 ± .05	5.02 ± .08	3.09 ± .25	0.03
D53R1 CNCbl	.696 ± .05	4.40 ± .07	3.06 ± .23	
N57R1 Apo	.534 ± .12	6.72 ± .03	3.59 ± .08	-1.00
N57R1 CNCbl	.877 ± .08	5.24 ± .07	4.59 ± .41	
I66R1 Apo	.411 ± .07	5.59 ± .23	2.30 ± .39	-0.53
I66R1 CNCbl	.399 ± .05	7.10 ± .17	2.83 ± .33	
S74R1 Apo	.403 ± .06	8.14 ± .35	3.28 ± .05	0.99
S74R1 CNCbl	.395 ± .06	5.81 ± .26	2.29 ± .35	

Physical parameters derived using equations described in materials and methods section. C_0 corresponds to the concentration of urea that results in half the protein being denatured, m is related to the solvent accessible protein surface area exposed to solvent upon denaturation. ΔG_U° is the free energy of unfolding a specific residue. $\Delta\Delta G_U^\circ$ is a good measure of substrate induced stability changes at a specific residue. Errors calculated using the procedure given in the materials and methods section.

6.3 Conclusions:

The lack of a trend in the *m* data for the hatch domain indicates that a single unfolding event of the entire N-terminus to about residues 60-65 allowing substrate passage, as had been previously hypothesised[18], is unlikely. If a major section of the hatch left the barrel, the free energy of unfolding might be expected to decrease for the entire domain upon substrate addition. Instead, it supports the hypothesis that the hatch domain rearranges in small chunks to allow for substrate passage. This type of rearrangement is seen in alpha-helical transporters[23] and would cause certain sections of the hatch domain to destabilize ($+\Delta\Delta Gu^{\circ}$) and others to stabilize ($-\Delta\Delta Gu^{\circ}$) when substrate is bound. In the context of the pervious BtuB work, a possible region of lower stability that would be involved in substrate passage can be better identified. L46 exhibits thermodynamic parameters clearly resembling those of V10 and T30 while I66 and S74 fall into the group of S74 and residues not part of the hatch (see table 6.1). Interestingly, S74 and I66 m values are not as small as previously reported values for more C-terminal residues. The two residues that don't fall into either group, D53 and N57, are likely very critical for substrate passage. N57 is discussed in more detail below. Based on these data, residues up to I66 participate in the passage of CNCbl but do not unfold cooperatively as seen in figure 6.1. A transient pore mechanism of alternating small openings that allow for CNCbl contact with conserved sites[8] in the hatch and barrel is more likely. The thermodynamic data strongly indicate that the addition of substrate destabilizes the entire hatch region in BtuB. Previous work shows that certain residues C-terminal for T30 show some retained structure in their "fully denatured" state.[18] I66R1 and S74R1 also display some secondary structure in their fully denatured state, usually 12M urea, further indicating that this region behaves similarly to

protein regions further C-terminal in the protein that are not thought to unfold during transport. This transient pore would not require a large energy contribution to form and would refold quickly.

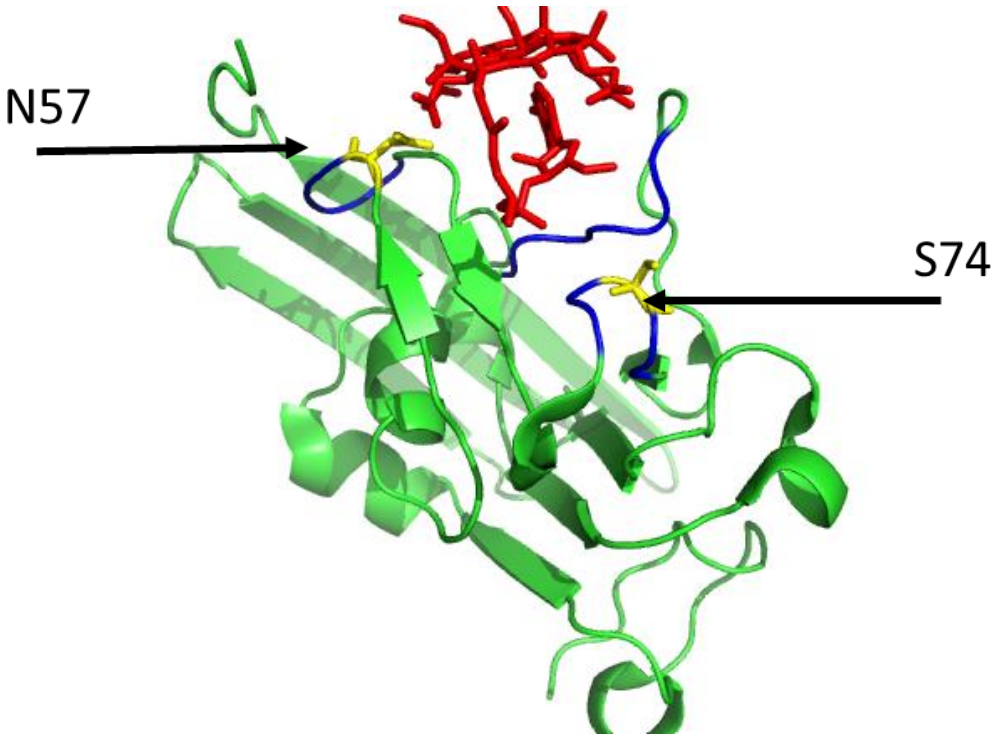

Figure 6.6 The hatch domain of BtuB with CNCbl bound. The hatch domain and 3 strands of the β-barrel taken from BtuB (PDB 1NQH) shown in green with the three putative substrate binding loops highlighted in blue[8]. The CNCbl molecule is shown as a stick model in red. N57 and S74 are shown in yellow. Both of these residues lie close to the substrate and may behave differently from other hatch domain residues due to direct substrate interactions.

These data also show that N57 is denatured to a greater extent and at a lower urea concentration than expected based on its location in the crystal structure, leading us to believe that this residue behaves differently in the presence of substrate. N57 is on a loop

region that is part of the hatch domain but resides fully inside the barrel. This residue has the largest change in solvent exposed surface area when substrate is bound, while at the same time exhibiting a large negative shift in unfolding transition midpoint. While not definitive proof of this area's involvement in transport these data show large changes in N57 that may be relevant to transport. S74 also shows a large substrate mediated change. This mutant has a large reduction in the midpoint of the folding transition (C_0) when B_{12} is bound. Previous crystallography data show that in the apo state, S74 is part of an alpha helix but in the substrate bound state this region (72-76) loses secondary structure. The substrate bound crystal structure also shows the B_{12} molecule in proximity to the N57 and S74 containing turns. A third turn, residues 85-96 slows considerably, and shows root mean squared difference (rmsd) greater than 6Å (Figure 6.6). These data, taken together, agree with previous work hypothesizing that these three turns participate in B_{12} binding[8]. One or more of these turns may make direct contact with the substrate; they may also participate in the alternating access method of transport by blocking access to the extracellular space during transport.

6.4 Materials and Methods:

Primer Design and Experimental Mutagenesis

Primers were designed such that annealing temperature (T_m) is greater than or equal to 78^{o}C using the equation T_m= 81.5 + 0.41(%GC) - 675/N, where %GC is the percentage of guanine and cytosine and N is the number of residues. Cysteine mutations were introduced into the BtuB wild-type plasmid (pAG1) using the Quick-Change site-directed mutagenesis kit (Stratagene, La Jolla, CA). Plasmids were sent out for sequencing (GENEWIZ, South Plainfield, NJ) to ensure the desired mutations were present. The mutants were then transformed into the *Escherichia coli* strain RK5016.

Growth, Solubilization, Spin labeling, Purification, and Reconstitution

For overexpression, cells were grown in minimal "A" media, 0.1 M Phosphate buffer, 8 mM $(NH_4)_2SO_4$ and .02 M sodium citrate. After autoclaving, the media was supplemented with 0.2% glucose, 3 mM $MgSO_4$, 300 μM $CaCl_2$, 0.01% Methionine and Arginine and 0.1mg/L Ampicillin. Cells were harvested by centrifugation at 4000 *g* for 10 min followed by resuspension in 30 mL HEPES buffer, pH 6.5. The resuspended cells were then lysed using a French press at a pressure of 1300 psi. To prevent proteolysis of BtuB, AEBSF was added to a final concentration of 400 μg/mL. Following lysis, the solution was centrifuged at 14500 *g* for 10 min. to remove cellular debris. The inner membranes in the supernatant were solubilized by addition of 0.5% sarkosyl, and the outer membranes containing BtuB were pelleted by ultracentrifugation at 104,000 *g* for 90 min. Each pellet was resuspended in 4 mL HEPES buffer. Addition of 0.6g/L *n*-octyl-β-D-glucopyranoside

(OG), ANAGRADE (Anatrace, Marmee, OH) in 100 mM Tris buffer (pH 8.05), containing a final concentration of 8 mM EDTA, was used to solubilize the outer membrane. After a 2 h incubation the detergent complex is ultracentrifugated at 90,000 *g* for 1 h, the solubilized protein in OG micelles remained in the supernatant. The protein was then spin-labeled by adding 200 µL of 12 mM of 1-oxyl-2,2,5,5-tetramethyl-3-pyrroline-3-methyl methanethiosulfonate (MTSL, Toronto Research Chemicals, North York, ON, Canada) The reaction to generate side chain R1 was allowed to proceed for 2 h at 42^{o}C in order to label mutants deep in the barrel. The protein was loaded onto a prepacked 5 mL Q-sepharose high-performance anion-exchange column (Amersham Biosciences, Piscataway, NJ), and a gradient was run from 0.25 M to 1.0 M of LiCl in 25 mM BisTris buffer containing 17 mM OG (pH 7.0). Following purification, protein purity was analyzed by SDS-PAGE electrophoresis, and the fractions containing pure BtuB were pooled. The pure BtuB was reconstituted into 1-palmitoyl-2-oleoylphosphatidylcholine (POPC) by dialysis. A solution of mixed POPC/OG mixed micelles were sonicated to solubilize the lipid, then added to the purified protein. Dialysis was performed over 3-4 d in 150 mM NaCl and 10 mM HEPES at pH 6.5 with 1 mM NaN_3 and 100 nM EDTA added, to remove all the OG molecules. The dialyzed protein was pelleted by centrifugation at 10,000 g and solubilized in ~ 1mL dialysis buffer. A Beckman airfuge was used to concentrate the protein to a final concentration ranging from 100-200µM. For experiments in which CNCbl was present the CNCbl was added to a final concentration of 250µM to insure complete saturation of available protein.

Urea denaturation and CW-EPR measurements

Urea was added to 0.65 mL tubes to get specific urea concentration using the equation y = 0.7332x + 0.2643 where y is the goal final [urea] and x is the original [urea]. X is obtained using the equation x= v(4/stock[urea]) where v is the volume in µL of stock urea added. The urea was then dried O/N using a lyophilizer. 4µL of protein or protein with CNCbl was added and three freeze thaw cycles were performed in order to evenly distribute the denaturant within the vesicle. The sample was then loaded into glass capillaries with 0.60 mm i.d. x 0.84 mm o.d. (VitroCom, Mountain Lakes, NJ). Spectra were obtained using a Varian E-line 102 series X-band spectrometer with a loop-gap resonator (Medical Advances, Milwaukee, WI). All spectra were taken at 2 mW incident microwave power and 1 G modulation amplitude, and were baseline subtracted and normalized based on the area under the absorption curve.

Denaturation Data Analysis

The values of normalized amplitude of the EPR spectra as a function of urea concentration are plotted in OriginPro (Origin Lab Northhampton, MA) and fit to equation 6.1.

$$A = \frac{A_f - A_u}{1 + e^{(C - C_0)/dC}} + A_u \tag{6.1}$$

A two state model is assumed in which the protein is exists in either the folded or unfolded state, represented by A_f and A_U respectively. C_0 is the urea concentration that is represents the midpoint of the denaturation. dC is a measure of the width in C at the point of the largest change in A and it is used in equation 6.2 when calculating *m*.

$$m = RT/dC \quad (6.2)$$

Here R is the universal gas constant and T is the kelvin temperature of the sample. The value of RT is taken to be 0.596 kcal/mol with an uncertainty of 1%.[27] This method is then used to get the free energy of unfolding in the absence of urea using equation 6.3.

$$\Delta G_U^\circ = mC_0 \quad (6.3)$$

Error values on C_0 are determined by the quality of the initial fit of the dHpp data to equation 6.1. Errors on m and ΔG_U° were calculated with the proper error propagation equations.

6.5 References:

1. Shultis, D.D., Purdy, M.D., Banchs, C.N. & Wiener, M.C. Outer membrane active transport: structure of the BtuB:TonB complex. *Science.* **312**, 1396-9 (2006).

2. Pawelek, P.D., Croteau, N., Ng-Thow-Hing, C., Khursigara, C. M., Moiseeva, N., Allaire, M. & Coulton, J. W. Structure of TonB in complex with FhuA, E-coli outer membrane receptor. *Science.* **312**, 1399-1402 (2006).

3. Faraldo-Gomez, J. D., Smith, G. R. & Samson, M. S. Molecular dynamics simulations of the bacterial outer membrane protein FhuA: A comparative study of the ferrichrome-free and bound states. *Biophys. J.* **85**, 1406-20 (2003).

4. Chimento, D. P., Mohanty, A. K., Kadner, R. J. & Wiener, M. C. Substrate-induced transmembrane signaling in the cobalamin transporter BtuB. *Nat. Struct. Biol.* **10**, 394-401 (2003).

5. Cherezov, V., Yamashita, E., Lui, W., Zhalnina, M., Cramer, W. A. & Caffrey, M. In meso structure of the cobalamin transporter, BtuB, at 1.95 Å resolution. *J. Mol. Biol.* **364**, 716-734 (2006).

6. Gumbart, J., Wiener, M. C. & Tajkhorshid, E. Mechanisms of force propagation in TonB-dependent outer membrane transport. *Biophys. J.* **93**, 496-504 (2007).

7. Ma. L., Kaserer. W., Annamalai. R., Scott. D. C., Jin. B., Jiang, X. X., Xiao, Q. B., Maymani, H., Massis, L. M., Ferreira, L. C., Newton, S. C. & Klebba, P.E. Evidence of ball-and-chain transport of ferric enterobactin through FepA. *JBC.* **282**, 397-406 (2007).

8. Chimento D., Kadner R. & Wiener M. Comparative structural analysis of TonB-dependent outer membrane transporters: implications for the transport cycle. *Proteins*: *Struct, Funct, Bioinf* **59**, 240-51 (2005).

9. Bonhivers, M., Desmadril, M., Moeck, G. S., Boulanger, P., Colomer-Pallas, A. & Finkelstein, A. Stability studies of FhuA, a two-domain outer membrane protein from *Escherichia coli*. *Biochemistry.* **40**, 2606-13 (2001).

10. Udho, E., Jakes, K. S., Buchanan, S. K., James, K. J., Jiang, X., Klebba, P. E. & Finkelstein, A. Reconstitution of bacterial outer TonB-dependent transport in planar lipid bilayer membranes. *Proc. Natl. Acad. Sci. U.S.A.* **106**, 21990-5 (2009).

11. Kauzmann, W. Some factors in the interpretation of protein denaturation. *Adv. Protein. Chem.* **14**, 1-63 (1959).

12. Street, S. O., Courtemanche, N. & Barrick, D. Protein folding and stability using denaturants. *Meth. Cell Biol.* **84**, 295-325 (2008).

13. Roche, J., Caro. J., Norberto. D., Barthe. P., & Roumestand. C. Cavaties determine the pressure unfolding of proteins. *Proc. Natl. Acad. Sci. USA*. **109**, 6945-50 (2012).

14. Saruoria, S., Ghosh, T., Garcia, A., & Garde, S. Studying presssure denaturation of a protein by molecular dynamics simulations. *Proteins.* **78**, 1641-51 (2010).

15. Harris, N. J., & Booth, P. J. Folding and stability of membrane transport proteins *in vitro*. *Biochim. Biophys. Acta.* **1818**, 1055-66 (2012).

16. Booth, P. J., & Curnow, P. Folding scene investigation: membrane proteins. *Struc. Biol.* **19**, 8-13 (2009).

17. Makhatadze, G. I. Thermodynamics of protein interactions with urea and guanidinium chloride. *J. Phys. Chem. B.* **103**, 4781-85 (1999).

18. Flores Jiménez, R. H. & Cafiso, D. S. The N-terminal domain of a TonB-dependent transporter undergoes a reversible stepwise denaturation. *Biochemistry*. **51**, 3642-50 (2012).

19. Polyhach, Y., Bordignon, E. & Jeschke, G. Rotamer libraries of spin labelled cysteines for protein studies. *Phys. Chem. Chem. Phys.* **13**, 2356-66 (2011).

20. Columbus, L. Ph. D. Thesis. University of California Los Angeles, California (2001).

21. Voinov, M. A., Rivera, I & Smirnov, A. I. Surface Electrostatics of Lipid Bilayers by EPR of a pH-Sensitive Spin-Labeled Lipid. *Biophys. J.* **104**, 106-16 (2013).

22. Klug, C. S. & Feix, J. B. Guanidine hydrochloride unfolding of a β-strand in FepA using site-directed spin labeling. *Protein Sci.* **7**, 1469-76 (1998).

23. Shortle, D. & Ackerman, M. S. Persistence of nativelike topology in a denatured protein in 8 M urea. *Science.* **293**, 487−89 (2001).

24. Dill, K. A. Dominant forces in protein folding. *Biochemistry*. **29**, 7133−55 (1998).

25. Radestock, S. & Forrest, L.R. The alternating-access mechanism of MFS transporters arises for inverted-topology repeats. *J. Mol. Biol.* **407**, 698-715 (2011).

26. McHaourab, H. S., Lietzow, M. A., Hideg, K. & Hubbell, W. L. Motion of spin-labeled side chains in T4 lysozyme. Correlation with protein structure and dynamics. *Biochemistry*. **35**, 7692−7704 (1996).

27. Hong, H. D., Park, S., Jimenez, R., Rinehart, D. & Tamm, L.K. Role of aromatic side chains in the folding and thermodynamic stability of integral membrane proteins. *JACS.* **129**, 8320-27 (2007).

Chapter 7: Conclusions and Future Directions

SDSL-EPR has long been used to study membrane proteins[1]. DEER specifically has provided many unique insights into membrane protein structure and function[2-4]. This work details the development, optimization and utilization of this powerful technique into native systems. Using DEER in whole cells and intact outer membranes has already produced insights into the TBDT transport cycle. However, in order to reach its maximum potential, we must continue to learn more about the outer membrane and how it may influence the proteins inside it.

Chapter 3 describes the development of the first whole cell DEER measurements and describes how this technique compares to other membrane systems. It details the development of a technique that is sure to be utilized by many researchers in the future to get high resolution structural data on membrane proteins in the whole cell environment. Currently, this technique is not being used to examine other membrane proteins or cell systems. The current protocol has only been applied to BtuB, but preliminary experiments indicate it may be useful for other outer-membrane proteins. The next experiments in this project will focus on performing DEER measurements in the closely related TBDTs, FhuA and FecA. These proteins have been the subject of extensive study and have shown promising signs of specific labeling in outer membranes. Initial attempts have not been successful at producing DEER signals in whole cells. This is most likely due to the need for IPTG induction and the resulting large inclusion bodies that are formed when expressing these two transporters. These inclusion bodies have not been a problem when these proteins are studied in OM and reconstituted systems because they are removed via

centrifugation but they would remain in the whole cell system. Inclusion bodies do remain in the cytosol of the cell but may constitute upwards of 90% of the mass of the cell. These inclusion bodies stretch and strain the cell, they also may change the environment of protein in the outer membrane by compressing the periplasmic space and increasing membrane stress. If a protocol to limit the inclusion bodies were devised, by optimizing the IPTG concentration and time/temperature of induction, the whole cell DEER protocol should be easily applied to FhuA and FecA. The next steps after that might be development of labeling the periplasmic sections of the protein such as the ton box and periplasmic turns. We have found that the MTSL does not produce a signal for periplasmic sites in whole cells. Probing these sites would be very useful because better understanding of the Ton box motions and distances in whole cells may provide insights into the transport mechanism.

In chapter 4 the whole cell DEER technique is shown to be sensitive to ligands. The calcium and CNCbl mediated changes to distance distribution clearly reflect OM and lipid vesicle samples. This leads the way for studies of other ligand effects on BtuB and other membrane transporters. Characterizing the OM preparation as well as better understanding effects this system has on protein structure and function is a very important future goal of this work. Currently the only work done towards characterization of the OM has been a few cryo EM images that show a large amount of heterogeneity in vesicle shape and size. Beyond that the OM preparation has not been well characterized and further studies with the goal of understanding protein environment would be useful. It is also very useful to understand the specific effects, if any, that the OM environment has on BtuB. The effects that are most interesting are ones that may not exist or be different in reconstituted systems. Direct comparison experiments between the artificial reconstituted systems and native

systems have shown very similar data for loop 2 mutants (see figure 3.7 and 4.8). This is unsurprising, because as a proof of concept we choose experiments that were likely to not be affected by lipid environment. Experiments done at other sites in BtuB do show a marked difference from crystal structure data. However, the whole cell DEER technique was developed in order to study protein conformations and populations that would not be accessible in lipid or detergent vesicles. Therefore a very important set of future experiments would focus on elucidating the power and scope of native membrane DEER. Understanding the specific benefits of native membranes over artificial lipids will make the technique more promising and attractive to future researchers.

In addition to further native system DEER and CW method development a very important future experiment involves using the loop DEER constraints to construct a map of loop movements. Using the distance distributions that have been taken between the outer loops of BtuB in a variety of ligand conditions as constraints, a molecular dynamics simulation could provide a map of the motions of these loops. The outer loops of BtuB and other TBDTs have long been the source of studies but very little is known about their exact function or how their positions change during the various stages of transport. DEER data were obtained on nine double loop mutants of BtuB. The data obtained from these experiments have been very useful, but in order to paint a clear picture of loop motions a MD simulation using all the distance distributions is needed. A few methods exist to use EPR based constraints in combination with crystal structures to sample protein conformations using MD. The lab of Benoît Roux has developed the MDDS and re-MD techniques to use DEER data for just this purpose.[5,6] Another technique, RosettaEPR, out

of Vanderbilt University, also relies on EPR data to elucidate structural information not easily obtainable by other means.[7]

Chapter 5 builds upon the developed method of native system DEER and utilizes the TEMPO-CNCbl substrate analog to describe the effects of TonB binding on the outer loops of BtuB and its CNCbl binding affinity. These experiments clearly show that TonB binding causes an allosteric effect that leads both to an explanation of how TonB mediates transport through BtuB and how the loops are influenced when transport occurs. This reduction in BtuB's CNCbl affinity upon TonB binding is not seen in mutants that are known to be transport deficient, further supporting the hypothesis that the role of TonB may simply be a passive weight on the ton box. The energy step in TonB dependent transport would then shift from the TonB-Ton box interaction to the dissociation and dimerization of TonB that happens before or after transport. This finding is supported by previous work that suggests a dimer-monomer conversion is very important for transport in this system.[8]

These experiments showing TonB binding causes release of bound CNCbl raise the important question of sidedness. Does binding of the C terminus of TonB facilitate one round of transport or does the CNCbl simply dissociate and leave the transporter binding site? In order to solve this complex problem, BtuB would be solubilized into lipid vesicles, TonB C-terminal fragments would be added and cycles of freeze thaw would insure the TonB is present on both sides of the membrane. A paramagnetic relaxation agent such as nickel ethylenediamine-N,N'-diacetic acid (NiEDDA) would then be added to the buffer in contact with the outer leaflet. Upon addition of TEMPO-CNCbl, a CW-EPR signal would only be detectable if the substrate was transported inside the vesicle where NiEDDA was

absent. This experiment would require many controls but would shed definitive light on the directionality of substrate release, providing a key piece of the molecular mechanism of TonB mediated transport.

Finally Chapter 6 describes work that aims to better understand the energetics of BtuB hatch changes during transport. Building on previous work[9], denaturation of the BtuB hatch domain provides data on stability and extent of change as a function of residue position. These data show that there is no general trend in hatch stability or change in stability upon addition of CNCbl; pointing to a transient pore mechanism for CNCbl transport. This mechanism proposes that the substrate passes through the transporter using multiple contact points on the barrel and hatch domain, thus creating a pore that opens sequentially using low energy steps. This is in contrast to experiments that point to a large portion of the hatch rearranging and the formation of a water filled cavity large enough for substrate passage[10,11]. In order to strengthen the argument for the transient pore, more data points are required. Future experiments in this direction will involve more residues so a better trend emerges. Currently the exact residues involved in the transient pore are not known. Getting energetic measurements for more sites in the hatch will give us a better picture of the nature of the pore. Another future direction involves identifying the barrel substrate contacts that only exist during transport. One possible method of doing this involves studying ion pairs that are found to be in proximity in BtuB crystals. One such pair involves R14 and D316; the distance between these two resides increases from 4.3Å to 7.5Å when CNCbl binds. Furthermore the bactericidal protein colicin has the opposite effect; this lead the authors to conclude that this ion pair may be involved in the transport cycle.[12] This and similar ion pairs may be vital contact points for substrate passage.

References

1. Altenbach, C., Flitsch, S.L., Khorana, H.G. & Hubbell, W.L. Structural Studies on Transmembrane Proteins .2. Spin Labeling of Bacteriorhodopsin Mutants at Unique Cysteines. *Biochemistry* **28**, 7806-7812 (1989).

2. Borbat PP, Mchaourab HS, Freed JH. Protein structure determination using long-distance constraints from double-quantum coherence ESR: study of T4 lysozyme. *J. Am. Chem. Soc.* **124**, 5304–14 (2007)

3. Bennati M, Weber A, Antonic J, Perlstein DL, Robblee J, Stubbe J. Pulsed ELDOR spectroscopy measures the distance between the two tyrosyl radicals in the R2 subunit of the *E. coli* ribonucleotide reductase. *J. Am. Chem. Soc.* **125**, 14988–89 (2003).

4. Jeschke G, Wegener C, Nietschke M, Jung H, Steinhoff H. Interresidual distance determination by four-pulse double electron-electron resonance in an integral membrane protein: the Na+/proline transporter PutP of *Escherichia coli*. *Biophys. J.* **86**, 2551–57 (2004).

5. Roux, B. & Islam, S. M. Restrained-ensemble molecular dynamics based on distance histograms from double electron-electron resonance spectroscopy. *J. Phys. Chem. B.* **117**, 4722-39 (2013).

6. Islam, S. M. & Roux, B. Simulating the distance distribution between spin-labels attached to proteins. *J. Phys. Chem. B.* **119**, 3901-11 (2015).

7. Hirst, S. J., Alexander, N., Mchaorab, H. S. & Meiler, J. RosettaEPR: An integrated tool for protein structure determination from sparse EPR data. *J. Struct. Biol.* **173**, 506-14 (2011).

8. Freed, D.M., Lukasik, S.M., Sikora, A., Mokdad, A., & Cafiso D.S. Monomeric TonB and the ton box are required for the formation of a high-affinity transporter-TonB complex. *Biochemistry.* **52**, 2638-48 (2013).

9. Flores Jiménez, R. H. & Cafiso, D. S. The N-terminal domain of a TonB-dependent transporter undergoes a reversible stepwise denaturation. *Biochemistry*. **51**, 3642-50 (2012).

10. Gumbart, J., Wiener, M. C. & Tajkhorshid, E. Mechanisms of force propagation in TonB-dependent outer membrane transport. *Biophys. J.* **93**, 496-504 (2007).

11. Chimento, D. P., Mohanty, A. K., Kadner, R. J. & Wiener, M. C. Substrate-induced transmembrane sgnaling in the cobalamin transporter, BtuB. *Nat. Struct. Biol.* **10**, 394-401 (2003).

12. Lukasik, S.M., Ho, D. & Cafiso, D. S. Molecular basis for substrate-dependent transmembrne signaling in an outer-membrane transporter. *JMB*. **370**, 807-11 (2007).